

A MATHEMATICAL MODEL FOR CEMENT KILNS

By

PIROOZ DARABI

B.Sc., Sharif University of Technology, Iran, 2004

A THESIS SUBMITTED IN PARTIAL FULFILLMENT OF
THE REQUIREMENT FOR THE DEGREE OF
MASTER OF APPLIED SCIENCE

in

THE FACULTY OF GRADUATE STUDIES

(Mechanical Engineering)

The University of British Columbia

January 2007

© Pirooz Darabi, 2006

ABSTRACT

Rotary kilns have numerous industrial applications including cement production. Frequent operational problems such as low thermal efficiency, refractory failure, and poor product quality have prompted extensive efforts to improve and optimize their design. Mathematical modeling and Computational Fluid Dynamics constitute effective tools recently used for these purposes.

A cement kiln consists of three major parts: the hot flow, the bed, and the wall. A CFD code which had the capability of simulating the hot gas was developed further to simulate the kiln. In the present work, two 1-D mathematical models are proposed and implemented in the existing CFD code. The first model consists of the steady-state solution for the material and temperature evolution within the bed. The second one simulates tire combustion in the kiln. The tire burning model assumes that tire combustion occurs in two major successive steps, devolatilization and char combustion. For the devolatilization model, external heat and mass transfer, three parallel reactions, and enthalpy effects are considered the dominant phenomena. The char combustion model considers the enthalpy effect and the external mass transfer.

With the aid of the developed model, full-scale industrial cement kilns under steady-state and realistic operational conditions are simulated. In addition, cement kilns with combustion of full scrap tires in the middle of them are mathematically modeled. The limits and feasibility of tire combustion are further explored by running numerical simulations with different tire flow rates and different injector locations. The flow field, temperature distribution and species distribution are presented. Analysis of the results indicates that, with the help of the proposed model, a better understanding of the important processes within cement kilns can be obtained. The model can be used for addressing operational problems and optimizing designs. It is also concluded that successful firing of tires can lead to a cheaper, longer lasting, and less polluting kiln.

TABLE OF CONTENTS

Abstract	ii
Table of Contents	iii
List of Tables	viii
List of Figures	xi
Nomenclature	xiii
Acknowledgements	xvii
Dedication	xviii
Chapter 1. Introduction	1
1.1. Cement Production Process	1
1.2. Process of Cement Rotary Kilns	5
1.3. Operational Problems of Cement Rotary Kilns	6
1.4. Multi-Dimensional Modeling	9
1.5. Motivation for this Work	14
1.6. Objectives	16
Chapter 2. Physical Model and Governing Equations	18

2.1.	Hot Flow Model.....	19
2.1.1.	<i>Conservation Equations</i>	19
2.1.2.	<i>Solution Methodology</i>	21
2.1.3.	<i>Boundary Conditions</i>	22
2.2.	Wall/Refractories Model.....	27
2.2.1.	<i>Governing Equation</i>	27
2.2.2.	<i>Solution Methodology</i>	27
2.2.3.	<i>Boundary Conditions</i>	30
2.3.	Other Models	31
2.4.	Post-Processing.....	31
Chapter 3.	Clinker Formation in Cement Kilns	33
3.1.	Introduction.....	33
3.2.	Clinker Formation Process.....	34
3.3.	Objectives	36
3.4.	Literature Survey	36
3.5.	Mathematical Model	38
3.5.1.	<i>Clinker Formation Model</i>	39
3.5.2.	<i>Formation of Thermal NO_x</i>	49
3.5.3.	<i>Modified Parent Code</i>	50

3.6.	Grid Generation	52
3.6.1.	<i>Geometry and Refractory Lining Details for Kiln #1</i>	52
3.6.2.	<i>Geometry and Refractory Lining Details for Kiln #2</i>	54
3.7.	Boundary Conditions	55
3.8.	Solution Methodology	61
3.9.	Results and Discussion	62
3.9.1.	<i>Validation on Clinker Formation Model</i>	63
3.9.2.	<i>Mass and Energy Balance</i>	66
3.9.3.	<i>Clinker Temperature and Composition</i>	68
3.9.4.	<i>Gas Temperature Distribution</i>	70
3.9.5.	<i>NO_x Emissions</i>	75
3.9.6.	<i>Refractory Temperature Distribution</i>	76
3.10.	Summary and Conclusions	77
3.11.	Future Work	79
Chapter 4.	Mid-Kiln Firing of Tires in Cement Kilns	80
4.1.	Introduction.....	80
4.2.	Objectives	83
4.3.	Literature Survey	84
4.4.	Physical Model.....	86

4.4.1.	<i>Assumptions</i>	86
4.5.	Mathematical Model	87
4.5.1.	<i>Tire Combustion Model</i>	87
4.5.2.	<i>Formation of Thermal NO_x</i>	92
4.5.3.	<i>Modified Parent Code</i>	92
4.6.	Grid and Boundary Conditions	95
4.6.1.	<i>Test Kiln</i>	95
4.6.2.	<i>Tire Combustion Model</i>	99
4.7.	Solution Methodology	100
4.8.	Results and Discussion	100
4.8.1.	<i>Mass and Energy Balance</i>	101
4.8.2.	<i>Clinker Temperature and Composition</i>	103
4.8.3.	<i>Gas Temperature Distribution</i>	105
4.8.4.	<i>Refractory Temperature Distribution</i>	106
4.8.5.	<i>NO_x Emissions</i>	107
4.8.6.	<i>Overall Impact of Mid-Kiln Firing of Tires on Kiln Performance</i>	108
4.8.7.	<i>Sensitivity Analysis</i>	110
4.9.	Summary and Conclusions	117
Chapter 5.	Summary, Conclusions, and Recommendations	120

Bibliography 125

Appendix A 131

LIST OF TABLES

Table 2-1: Components of equation (2-1).....	20
Table 2-2: Curve fit data for thermal conductivities of refractory layers	29
Table 3-1: Raw material components	33
Table 3-2: Clinker phases	34
Table 3-3: Clinker formation process	34
Table 3-4: Clinker formation reactions [3]	34
Table 3-5: Simplified clinker formation reactions.....	41
Table 3-6: Thermal data for clinker formation reactions.....	43
Table 3-7: Summary of production rates	44
Table 3-8: Summary of reaction rates.....	45
Table 3-9: Summary of the pre-exponential factors and activation energies for clinker formation reactions	45
Table 3-10: Material information for Kiln #1	57
Table 3-11: Fuel input information for Kiln #1	57
Table 3-12: Air input information for Kiln #1.....	58
Table 3-13: Material information for Kiln #2.....	60
Table 3-14: Fuel input information for Kiln #2	60

Table 3-15: Air input information for Kiln #2.....	61
Table 3-16: Loss-free composition of Kiln #1.....	64
Table 3-17: Loss-free composition of Kiln #2.....	64
Table 3-18: Comparison between the model prediction and Bogue calculation for Kiln #1.....	65
Table 3-19: Comparison between the model prediction and Bogue calculation for Kiln #2.....	65
Table 3-20: Mass and energy balance for Kiln #1.....	66
Table 3-21: Mass and energy balance for Kiln #2.....	67
Table 3-22: Clinker temperature at the kiln exit.....	70
Table 3-23: Summary of the average gas and clinker temperature at the exit and the peak.....	72
Table 3-24: Dust information for Kiln #1.....	74
Table 4-1: Composition and kinetic parameters.....	90
Table 4-2: Proximate, ultimate analysis and lower heating value for the tire rubber [39].....	91
Table 4-3: Material information for test kiln.....	97
Table 4-4: Fuel input information for test kiln.....	97
Table 4-5: Air input information for test kiln.....	98
Table 4-6: Input data for tire combustion sub-model for the case with 20% co-combustion.....	99
Table 4-7: Mass and energy balance: without co-combustion of tire.....	101
Table 4-8: Mass and energy balance: with 10% co-combustion of tire.....	102

Table 4-9: Mass and energy balance: with 20% co-combustion of tire.....	102
Table 4-10: Summary of important parameters with tire injection at $x=50$ m and different tire flow rates	109
Table 4-11: Summary of important parameters with 20% co-combustion of tire and different tire injection points.....	114
Table 4-12: Summary of results for three different grids	116

LIST OF FIGURES

Figure 1-1: Cement production line (reproduced form [1]).....	4
Figure 1-2: The kiln system	8
Figure 1-3: Heat transfer paths (taken from [2]).....	8
Figure 2-1: Coupling of the models (taken from [2])	18
Figure 2-2: Boundary conditions of the hot flow.....	26
Figure 2-3: Refractory lining details.....	29
Figure 3-1: Kiln hood details of Kiln #1.....	53
Figure 3-2: Refractory lining details of Kiln #1	53
Figure 3-3: Kiln hood details of Kiln #2.....	54
Figure 3-4: Refractory lining details of Kiln #2	55
Figure 3-5: Boundary conditions for Kiln #1	56
Figure 3-6: Boundary conditions for Kiln #2	59
Figure 3-7: Axial profile of species in Kiln #1	69
Figure 3-8: Axial profile of species in Kiln #2.....	69
Figure 3-9: Gas temperature distribution in Kiln #1.....	71
Figure 3-10: Gas temperature distribution in Kiln #2.....	71

Figure 3-11: NO distribution in Kiln #1	75
Figure 3-12: NO distribution in Kiln #2	76
Figure 3-13: Refractory temperature distribution in Kiln #1	77
Figure 3-14: Refractory temperature distribution in Kiln #2	77
Figure 4-1: Boundary conditions for test kiln.....	96
Figure 4-2: Axial profile of species: without co-combustion of tire.....	104
Figure 4-3: Axial profile of species: with 10% co-combustion of tire	104
Figure 4-4: Axial profile of species: with 20% co-combustion of tire	105
Figure 4-5: Gas temperature distribution.....	106
Figure 4-6: Refractory temperature distribution	106
Figure 4-7: NO concentration distribution.....	108
Figure 4-8: Axial profile of species: with 50% co-combustion of tire	111
Figure 4-9: Gas temperature distribution: with 50% co-combustion of tire	112
Figure 4-10: NO distribution: with 50% co-combustion of tire.....	112
Figure 4-11: Axial profile of species: 20% co-combustion of tire with tire injection point $x=80$ m.....	115
Figure 4-12: Axial gas temperature profile for three different grids	117

NOMENCLATURE

A	area, m ²
A	pre-exponential factor, 1/s
\vec{B}	body force vector per unit volume, N/m ³
c	molecular concentration, mol/m ³
C_1	Constant in $k - \varepsilon$ turbulence model
C_2	Constant in $k - \varepsilon$ turbulence model
C_3	Constant in $k - \varepsilon$ turbulence model
C_p	specific heat capacity, J/(kg.K)
C_μ	Constant in $k - \varepsilon$ turbulence model
d	kiln diameter, m
E	activation energy, J/mol
F_t	tire flow rate, 1/s
\vec{F}_{visc}	additional viscous term vector due to the turbulence, N/m ³
G	turbulent energy generation rate, kg/(m.s ³)
h	enthalpy, J/kg
h_c	convective heat transfer coefficient, W/(m ² .K)
k	thermal conductivity, W/(m.K)
k	turbulent kinetic energy per unit mass, m ² /s ²

k	rate constant , 1/s
l_t	turbulent length scale, m
L	kiln length, m
L_{fus}	latent heat of fusion, J/kg
m	mass, kg
\dot{m}	mass flow rate, kg/s
m_i	mass fraction of species, wt%
M	molecular weight, kg
N_t	tire flow rate, tire/revolution
P	pressure, N/m ²
Pr_t	Constant in $k - \varepsilon$ turbulence model
q	heat flux, W/m ²
\dot{q}	heat flow rate per unit volume, W/m ³
\dot{Q}	heat flow rate, W
r	reaction rate, 1/s
r	kiln radius, m
R	universal gas constant, J/(kg.K)
R	production rate, mol/(m ³ .s)
R	thermal heat resistance, K/W
Sm_t	Constant in $k - \varepsilon$ turbulence model

S_{ξ}	source terms in equation 1-1
t	time, s
T	temperature, K
u	velocity in coordinate direction x, m/s
\bar{U}	mean velocity, m/s
v	velocity, m/s
v	velocity in coordinate direction y, m/s
v_{sto}	stoichiometric matrix
V	reactor volume, m ³
\vec{V}	fluid velocity vector
\vec{V}_t	additional viscous term vector due to the turbulence, N/m ³
w	velocity in coordinate direction z, m/s
W	weight, kg
x	axial position, m
x	mass fraction, wt%
Y	mass fraction, wt%

Greek:

Γ_{ξ}	diffusion coefficients in equation 1-1
ΔH	reaction heat per unit mass, J/kg
$\Delta \hat{H}$	reaction heat per unit volume, J/m ³
θ	bed angle, degree
ε	turbulent energy dissipation rate per unit mass, m ² /s ³
ε	emissivity
κ	Von-Karman constant
μ_{eff}	effective viscosity, kg/(m.s)
μ_l	laminar viscosity, kg/(m.s)
μ_t	turbulent viscosity, kg/(m.s)
ξ	unknown in equation 1-1
ρ	density, kg/m ³
σ	Stephan-Boltzmann constant, W/(m ² .K ⁴)
σ_k	Constant in $k - \varepsilon$ turbulence model
σ_{ε}	Constant in $k - \varepsilon$ turbulence model
ω	kiln rotational speed, rpm

ACKNOWLEDGEMENTS

I would not have completed this thesis without the significant help of many great people who have made my life at UBC a pleasant and productive experience.

First and foremost, I would like to express my sincere gratitude to my outstanding supervisors, Dr. Martha Salcudean and Dr. Ian Gartshore, for their continuous support and patience during my stay at UBC. I consider myself very fortunate for having the opportunity to work with them. I would also like to thank my co-supervisor, Dr. Steven Rogak, for his guidance.

For their unlimited technical support, I gratefully acknowledge, Dr. Jerry Yuan, who always had time for discussion no matter how busy he was and without whom I could not have accomplished this work, and Dr. David Stropky, who generated the complex grids with the software developed by him. I am very glad to have had the chance to work and collaborate with great companies such as Process Simulations Ltd. (PSL) and Lafarge, through PSL. I would also like to thank Maureen Phillips for all her help and support.

To my wonderful friends at UBC, I send a special thank you, especially Niussha Javid, Hassan Rivaz, Alireza Forghani, Ali Asadkarami, Amir Nejat, Bijan Azadi, Massimo Diciano, Ali Kashani, Amin Karami, Hamed Mahmudi, Mohammad Sepasi, Ali Soltanzade, and Tingwen Li. They have all contributed to my happy and memorable life in Vancouver.

Finally, this work is dedicated to my wonderful parents and my dear sisters for all their love and support. I always felt them near me, even though they were living far away during my period of study in Canada. They have been my main motivation throughout my studies.

To my parents

Chapter 1. INTRODUCTION

Kilns are often regarded as the heart of cement manufacturing plants. Plant profits are affected by the efficiency of these machines. One of the most important phases of cement production takes place in kilns. In order to produce cement with acceptable quality, it is important to make sure that the material has been properly burned. For these reasons, the utmost importance has been given to kiln operation, and efforts have been made to improve their design in order to get high-quality products with the lowest cost.

Rotary kilns, due to having the capability of handling varied feedstock and long residence time, are widely employed by industry in processes such as calcination of limestone and production of cement. Similar to many other industrial processes their operation is not free of problems, among which dust generation, emission of pollutants, low thermal efficiency, low product quality, and refractory failure are considered as the most important ones.

This chapter starts with a brief introduction to the cement production process and cement kilns; next, the problems associated with the operation of cement kilns and the need for modeling are addressed. Then there is a literature survey on the models available for rotary kilns, and the motivations leading to the present work are described. At the end, the objectives of this work are presented.

1.1. CEMENT PRODUCTION PROCESS

Cement is a fine, gray substance and is made from a mixture of natural elements such as limestone, clay, sand, and/or shale. Cement is the final product of a cement plant, and is packed and shipped for further usage. Most commonly, cement is used to produce concrete. When cement is mixed with

water, it can form a hard, solid material called concrete. Concrete is inert, waterproof, fire resistant, and is the most common construction material in the world.

The production of cement, schematically shown in Figure 1-1, consists of three fundamental stages:

1. Preparation of the raw material
2. Production of the clinker
3. Preparation of the cement

The first step in the cement manufacturing process is the preparation of the raw materials. Generally, the raw mixture for cement production consists of limestone (the major ingredient), shale, clay, sand, and iron ore. After being quarried from local rocks, the material is loaded into trucks for transportation to the crushing plant. Through a series of crushers and screens, the raw materials are reduced to an acceptable size for clinker production. Then the raw materials are mixed to meet a desired composition and are fed into a mill where the raw materials are ground. The material exiting the mill is called kiln feed and is stored in silos until required for further processing in the plant.

After being prepared, the raw mixture goes into the pyroprocessing system. This system either consists of a preheater tower, a calciner, and a dry rotary kiln or only a wet process kiln. In either of them, the same chemical reactions take place: evaporation of the moisture content of the raw mixture, calcination of the limestone, and the reactions between the calcium oxide with the other materials. This results in a final nodular product known as "clinker". The hot clinker will be discharged into a clinker cooler where some of the heat is recovered. The recovered heat will be returned to the pyroprocessing system; this, to some extent, reduces the fuel consumption and improves the energy efficiency of the system.

The cooled clinker, which can now be handled on standard conveying equipments, will be stored in clinker silos until needed for cement production. Clinker, with some gypsum and other additives, will be ground together to form cement. Cement will be stored in cement silos and ready for distribution. It will be shipped in bulk or in bags and distributed to customers.

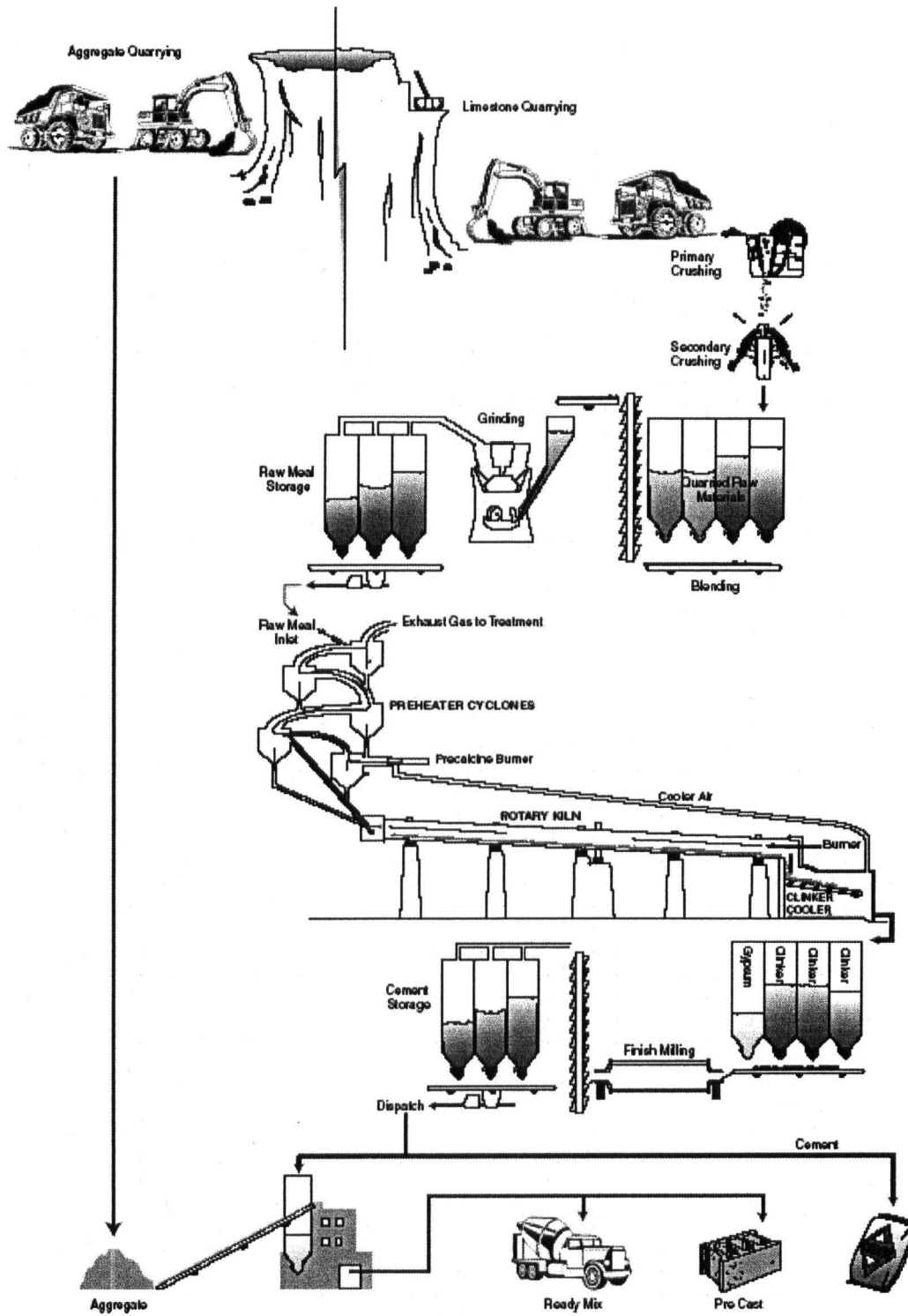


Figure 1-1: Cement production line (reproduced form [1])

1.2. PROCESS OF CEMENT ROTARY KILNS

Rotary kilns are usually considered to be the most important part of any cement manufacturing plant. They are used by industry to heat the solid material to the point where a required chemical reaction(s) can take place. This heating process needs efficient timing. The residence time of the solid material in the kiln is an important design component and is set by factors such as diameter, length, rotational speed, and slope.

A rotary cement kiln, as shown in Figure 1-2, is a very large rotating sloped cylinder 3-5 meters in diameter and 45-165 meters in length, depending on the type of process and production rate. The raw material is fed from the elevated cold end and, due to rotation and gravity, moves down to the far end of the kiln. The other end, also known as fire-end, is hot whose temperature is maintained by combustion of fuel. In the hot zone of a cement rotary kiln, the temperature of the solid material can go up to or beyond 1480 °C.

Physical/chemical phenomena that occur inside a rotary kiln include three-dimensional turbulent flow with fuel combustion in the gas phase, three-dimensional flow plus the chemical evolution of species in the bed of material (mud) along with three modes of heat transfer (radiative, convective and conductive) between and within the three components of the kiln, i.e. the hot gas, the mud and the rotating wall. In addition, the hot wall loses some of heat via radiation and convection (either free or forced) to its surroundings. All the above-mentioned heat transfer paths are schematically depicted in Figure 1-3.

There are two distinct flow phases within a cement rotary kiln: the hot gas and the solid material. The overall flow of the solid material is simple; it enters the kiln from the cold end and flows downward

to the other end. On the other hand, the flow within the hot gas is very complex and usually more than one source of air flow exists in the kiln system. Typically, there are three sources for the air inside a kiln system (primary, secondary and in-leakage) and one for the fuel. As mentioned before, at the fire-end of the kiln, fuel combustion occurs where fuel reacts with the oxygen in the air and burns. Fuel is usually delivered via the burner system, which can be a simple pipe or a more sophisticated system; the primary air is also supplied through the burner system. The secondary air comes from the bottom of the cooler which after recovering the energy of hot clinker and passing through the kiln hood, enters the flame area. The third one is the in-leakage air which mostly comes through the air gaps in the kiln hood.

1.3. OPERATIONAL PROBLEMS OF CEMENT ROTARY KILNS

Cement production is an energy intensive process; it requires high temperatures and large energy amounts. In addition, the cement industry operates at low thermal efficiencies [1] and due to having very high-temperature environment (especially in the kiln system) emits NO_x . This suggests the need to seek opportunities to improve energy efficiency and reduce the emissions of a cement plant. Pyroprocessing is the main step for cement production, during which the necessary reactions leading to cement formation occur. The pyroprocessing step dominates the energy consumption and environmental impacts related to the cement industry, and accounts for approximately 75% of the energy consumption of the plant [1]. Therefore, by improving the pyroprocessing step and more specifically the cement rotary kiln, the greatest reductions in the energy consumption and pollutant emissions of the cement industry can be achieved.

As mentioned above, the high temperature and chemical processes that take place in kilns lead to formation of pollutants such as NO_x. The emission of these pollutants and keeping them under certain limits (imposed by regulations) are among the important issues for cement kilns operators.

Refractory failure is another issue related to rotary kilns, primarily due to the expense of replacing bricks. In addition for replacing brick, the kiln system and plant production, will be shut down and this leads to loss of production.

Dust generation from the raw material is an important problem associated with these machines. However, by applying new technologies such as bag filters and special add-ons, the dust particles are continuously collected and recirculated into the kiln system. This allows for a more effective control on this issue.

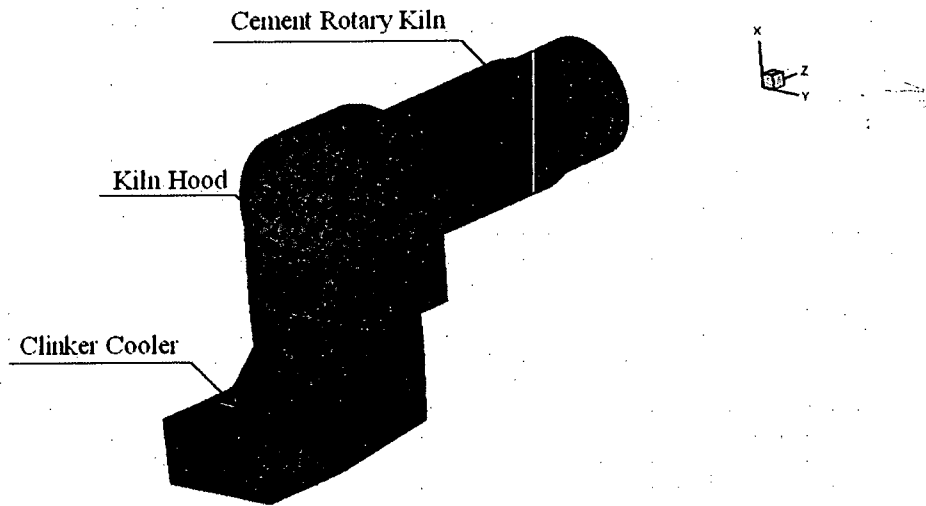
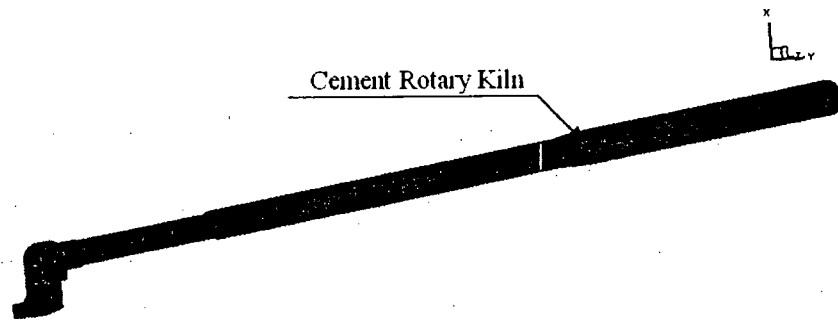


Figure 1-2: The kiln system

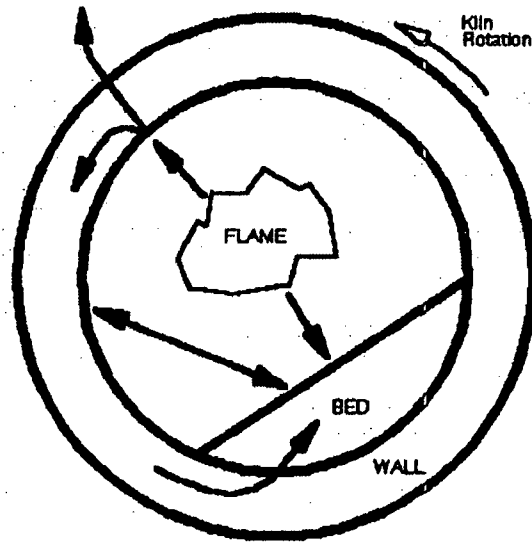


Figure 1-3: Heat transfer paths (taken from [2])

1.4. MULTI-DIMENSIONAL MODELING

The physical/chemical processes inside a rotary kiln are complicated and poorly characterized and understood. In addition, the operation of rotary kilns is accompanied by problems such as low thermal efficiency, poor product quality and emission of pollutants. Based on the source and the nature of the problem, some of them are easily fixed while the other are sophisticated and require additional investigations. The existence of such problems brings the need for having a good understanding and a good physical basis for the effective control and optimization of the system. In addition, it will be very helpful to develop a tool that can predict the kiln performance with a new firing system, and assess the effects of changes in different parameters on the process, etc.

In order to obtain a better understanding of the processes inside a kiln and reach enhanced operational conditions and designs, numerous studies have been performed. These studies have been conducted in two general paths: experimental/empirical and mathematical/analytical.

As mentioned earlier, rotary kilns are very large high-temperature cylinders in which complex processes occur. These aspects produce technical and economical difficulties for conducting experiments on full-scale rotary kilns. For instance, it will not be easy or inexpensive to obtain measurement data; in addition, they are often limited. Moreover, the measurement data come with some extent of uncertainty and error. These data are associated with certain operational conditions which will reduce their applicability range. Testing new burners or new operating conditions is generally costly and risks compromising the production that is expected from the kiln. Therefore, it

would be very useful to have a computational model with predictive capabilities to guide the experiments, reduce their number, and diminish the risk associated with them.

There are some empirical or semi-empirical studies conducted on rotary kiln. With the aid of these studies, the operational condition of a rotary kiln (most generally, the heat and mass balance) or the impact of one key element on the overall process, such as the relation between the kiln rotational speed and residence time of the material can be obtained, see [4] for more detail. However, as with all empirical or semi-empirical correlations, they are limited to certain geometries and process parameters and their extrapolation outside the range used to establish them is risky.

Besides experimental and empirical studies, analytical and computational methods can be useful in understanding the design and operation of industrial systems such as rotary kilns. Rotary kilns, due to the complexity of the processes within them, do not lend themselves to analytical solutions. Therefore, the governing equations of the process have been solved numerically using computational methods. Computational fluid dynamics (CFD) is one of these tools and is mainly employed to simulate the processes associated with fluid flow. For this purpose, initially the governing partial differential equations (PDE) of the system are established and then with the aid of a CFD code, are numerically solved. In addition to CFD, mathematical modeling has been found to be a feasible approach to understanding and optimizing complex systems such as cement rotary kilns.

In a cement rotary kiln, in addition to the fluid flow, other phenomena such as heat transfer, turbulence and chemical evolution should be taken into account as well. After modeling a problem using CFD, detailed useful information, such as velocity, temperature, and species concentration distributions are obtained. Analysis of the CFD results can increase our insight and understanding

over the investigated process; lead us to improved designs with better operational conditions and product qualities and, even increase the speed of the required modifications, if any, made on the process and design of the system. It is important to validate a CFD model (as much as possible) in order to ascertain that it is a reasonably good representation of the system.

It is also important to mention that many of the problems related to the kiln operation, such as poor product quality and refractory failure can be associated with the operation and design of the burner which can be improved by a better understanding of the combustion process in the flame area. Therefore, it will be crucial to simulate the fluid flow and fuel combustion in the flame area as detailed and reliable as possible.

Over the past years, the physical components of rotary kilns have been separately investigated leading to an improved understanding of the processes occurring in kilns. For instance, the heat transfer [5-8] and the bed motion [9-12] have been the subject of many numerical and experimental studies. There can be many different reasons for conducting separate investigations of only one component of a rotary kiln. The lack of understanding of the other process components and the impossibility of representing and solving the governing equations for the whole system can be considered as the most important reasons for this matter. However, as time passed, numerical tools and methods for simulating such complicated systems became available and hence the understanding of the process within rotary kilns was improved. In addition, the components in a rotary kiln (the hot flow, the bed and the wall) act together. Therefore, in order to develop a complete model for rotary kilns, all the interactions between the components including all the important phenomena have to be considered. This goal can be achieved by developing a fully-coupled model including all the important components of a rotary kiln.

One-dimensional models can be useful for obtaining a better understanding and improving the kiln operation and design. This goal has been achieved by studying the impact of key variables such as kiln speed or production rate on the kiln operation. However, such models have never been suitable for detailed investigation. For example, they do not have the capability to optimize the burner design. This deficiency is mainly because of the assumption made in one-dimensional models which is the uniform distribution of any parameter in the cross-sections. Although these models do not provide detailed information and lack some essential capabilities, they represent a considerable progress over previous completely empirical practices.

M. A. Martins et al. [13], for example, developed a 1-D mathematical model for the simulation of petroleum coke calcination in rotary kilns. They predicted the axial temperature and composition profiles within the bed and the gas and showed better agreement with measured data in comparison to other simulations in the literature.

H. A. Spang [14] developed a 1-D dynamic model for cement kilns in which the axial temperature and material evolution within the gas and solid phase were obtained. He indicated that with the applied approach the qualitative behavior of an actual kiln could be simulated well. He was also able to model the impact of chain section on the heat transfer between the solid material and the gas. However, he predicted a too high peak temperature in the burning zone, which is mainly caused by the instability associated with the positive feedback from the endothermic reactions during the formation of clinker in the solid material. In addition, the mass transfer between the solid and the gas as well as the liquid formation within the bed is missing in this work. Similar to other 1-D models, no detailed description regarding the burner area and flame shape can be obtained from this work.

In addition to one-dimensional models, a number of multi-dimensional models have been developed for rotary furnaces. For instance, F. Marias [15] has simulated an incinerator consisting of a 1-D model for the burning bed of solid waste and a 3-D model for the gas phase. He has been able to predict the combustion of the volatile matter within the incinerator as well as the thermal and chemical species evolutions. However, the wall is not included in the model and this, in fact, reduces the accuracy of this work. It should be stressed that, although investigating the quantitative results of this or similar works can improve the understanding on the flow and heat transfer behavior within rotary kilns, multi-dimensional models with more emphasis on clinker formation in the bed or similar processes are still required.

In 1995, Bui et al. [16] developed a mathematical model for coke calcining kilns which includes 3-D calculations of material transport along with the fuel combustion in the gas phase. In addition, a 3-D model is proposed for the bed motion assuming two layers of material in the bed: active layer and plug flow layer. Both layers are assumed to behave like Newtonian fluids. However, since the bed chemistry of a cement kiln makes it different from coke calcining kilns, models with cement bed characteristics are still required.

Lime and cement kilns, to some extent, have similar bed behaviours. They both have the calcination step in common. But the chemical reactions occurring in the bed of cement kilns are more complicated than lime kilns. M. Georgallis [2] recently developed a three-dimensional steady-state model to predict the flow and heat transfer in the pre-heat and calcination zones of rotary lime kilns. His model consists of three full-coupled sub-models: the hot flow, the bed, and the rotary wall. Similar to Bui's work, his bed model consists of two Newtonian regions in which the calcination

reaction is modeled and is assumed to be dominated by heat transfer. The model is validated against some experimental data and shows the potential for optimizing the process and operation of a lime kiln. However, the author points out that for solving the equations related to the bed motion, a better computational scheme is needed. He also suggests a 1-D approach for solving the wall model in order to reduce the computation time. In addition, the preheating zone of the lime kiln is missing in his work and this, in fact, reduces the applicability range of the proposed model. His work was related to lime kilns and not cement kilns.

The most complete and recent work on cement kilns, to the author's knowledge, was done by Mastorakos et al. [17] in which a 2-D axisymmetric gas model is coupled with 1-D models of the wall and the bed. They claim that clinker chemistry, shell temperature, and the composition of the exhaust gas are well predicted. In the bed model of this work, the clinker chemistry is included and this makes the model different from lime kilns. Similar to any other model their work had uncertainties such as insufficient information given in the heat and temperature range of clinkering reaction, and reaction rates that were set by trial and error to match the expected composition at the exit.

1.5. MOTIVATION FOR THIS WORK

The literature review revealed the capability of modeling for complex system such as cement rotary kilns. However, all the above models on cement kilns had some shortcomings; for example, Spang had simulated the whole cement kiln in 1-D and had missed some important aspects of the system such as liquid formation and mass transfer between the bed and the gas. In the other article, Mastorakos et al. proposed a model with insufficient information on its clinker formation model. The proposed clinker model in this work is a combination of what was achieved by Spang [14] and Mastorakos et al. [17]. The information regarding the clinker formation reactions such as heat of

reaction, reaction rates, and specific heat of bed material were taken from Spang's work while the liquid formation model, which was missing in Spang's work, was completely inspired by the other work.

Another important aspect related to hot furnaces such as cement rotary kilns is the formation of NO_x , which was also missing in the above studies. Cement kilns are expensive to run and emit pollutants especially nitrogen oxides. These two negative aspects of them led researchers and plant operators to try alternative fuels, such as waste derived fuels, to save energy and reduce the emissions of pollutants. A literature survey revealed that no mathematical studies on the combustion of scrap tires in cement kilns have been performed before. In this work, combustion of full scrap tires in the middle of the kiln is numerically simulated and analyzed for the first time.

Refractory failure is another important problem associated with rotary kilns, and has to be avoided as much as possible. Flame impingement on the wall is one of the major causes. Therefore, by detailed investigation of the processes in a cement kiln, especially in the flame area, an improved understanding of the characteristics of the hot flow and its impact on the refractory lining of the kiln can be obtained.

The primary goal of this work was to develop a model to simulate cement rotary kilns, including the clinker formation process and formation of NO_x . Flexibility and completeness can be considered the major advantages of the present work over the previous ones. With the aid of this study, the important processes within a cement rotary kiln are quantitatively simulated. Co-combustion of tire in the middle of cement kilns along with its impacts on NO_x emissions and product quality are investigated as well.

Three different industrial kilns are targeted for the simulations carried out in this work: Kiln #1, Kiln #2 and test kiln. Kilns #1 and #2 are used for the simulation related to the clinker production and test kiln, which is basically the cylindrical section of Kiln #1, is used for mid-kiln firing of tires. These kilns were investigated through collaboration with PSL and Lafarge. For this work, essential information for full-scale models consisting of geometry details and boundary conditions were extracted and developed by Jerry Yuan. Based on these details, complex grids were generated by David Stropky, using a grid generation software developed by him.

1.6. OBJECTIVES

The need for development of a fully-coupled three-dimensional cement rotary kiln was described earlier. It was also mentioned that emissions of pollutants, low thermal efficiency, and high operational costs are the major concerns associated with cement rotary kilns. The overall objective of this work is to model mathematically cement rotary kilns to provide a scientific tool for obtaining an improved understanding and ultimately use this mathematical model as a tool to optimize their design and operation. The objectives of the current research can be summarized as,

1. To develop a fully-coupled model capable of simulating the production of clinker in cement rotary kilns
2. To validate the developed CFD model against available plant data
3. To obtain a better understanding of the important phenomena within cement rotary kilns
4. To investigate tire combustion in the middle of cement kilns in order to achieve a better understanding of its possibilities and limitations

Chapter 2 describes the CFD code developed in our research group and used for the simulations in this work. In Chapter 3, full-scale cement rotary kilns are modeled and investigated. The combustion of full scrap tires inside the cement kilns is modeled in Chapter 4. The summary of this work, along with its conclusions and recommendations, are presented in Chapter 5.

Chapter 2. PHYSICAL MODEL AND GOVERNING EQUATIONS

The model for cement rotary kilns must include the hot flow in the gas, the process within the bed of material, and the wall. In order to develop a fully-coupled model, these three models should be coupled by exchanging the necessary information such as temperature, heat flux, and flow rate of CO_2 release from the bed, as shown in Figure 2-1. This coupling is essential and cannot be ignored because the gas flow and temperature computations need the inner wall and the bed surface temperatures as boundary conditions. Similarly the heat flux from the gas is applied as a boundary condition for the bed and the wall.

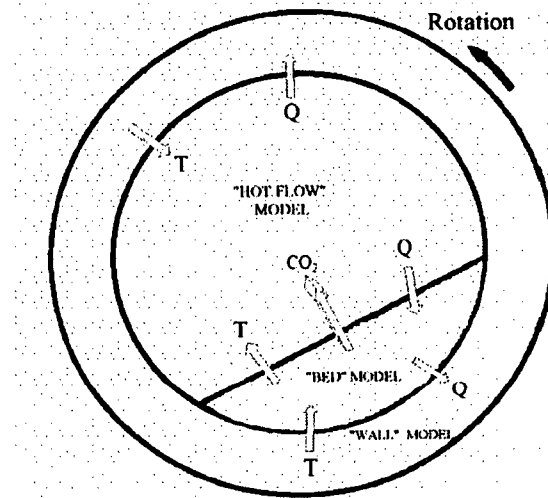


Figure 2-1: Coupling of the models (taken from [2])

In the present work, a steady-state model to simulate the physical/chemical processes inside a cement rotary kiln is presented. The temperature distribution and species concentrations inside the cement kiln at different operating conditions are visualized and/or tabulated. Analysis of these results can

lead to a better understanding of the processes inside cement rotary kilns and can, in fact, aid us in obtaining improved design and operating conditions for a given cement kiln.

In this chapter, the governing equations, the solution methodology, and the boundary conditions the gas and the wall are described. The model for the bed of material will be explained in Chapter 3.

2.1. HOT FLOW MODEL

In order to simulate the gas, the governing conservation equations for the fluid flow, heat transfer, and chemical evolutions are written and solved.

2.1.1. Conservation Equations

All the simulations in this work were basically performed with a CFD solver originally developed by Dr. Nowak in our research group at the University of British Columbia [18] and developed further by Jerry Yuan for lime kilns [19]. The model is based on steady-state assumptions for incompressible fluids which, in addition to solving for Navier-Stokes equations, includes the thermal energy, the turbulent energy and its dissipation ($k-\varepsilon$ model), and the conservation equations for the mass fractions of chemical species. In addition to the laminar and turbulent steady-state flows, more complex flows, including buoyancy effects and fuel combustion, can also be simulated with this code. The general steady-state conservation equation for the flow under consideration can be written as

$$\nabla \cdot [\rho \xi \vec{V} - \Gamma_{\xi} \nabla \xi] = S_{\xi} \quad (2-1)$$

where ξ are the unknowns, Γ_{ξ} are the diffusion coefficients and S_{ξ} are the source terms of 17 partial differential equations, as given in Table 2-1.

Table 2-1: Components of equation (2-1)

Equation	ξ	Γ_ξ	S_ξ
Continuity	1	0	0
Momentum (3)	\vec{V}	μ_{eff}	$-\nabla P + B + F_{visc}$
Energy	h	$\frac{\mu_{eff}}{Pr_t}$	S_h
Turbulent kinetic energy	k	$\frac{\mu_{eff}}{\sigma_k}$	$G - \rho\varepsilon$
Dissipation rate of turbulent energy	ε	$\frac{\mu_{eff}}{\sigma_\varepsilon}$	$C_1 \frac{\varepsilon}{k} G - C_2 \rho \frac{\varepsilon^2}{k} + C_3 \rho \varepsilon \nabla \cdot (\vec{V})$
Species (10)	m_i	$\frac{\mu_{eff}}{Sm_i}$	S_{m_i}

where $\vec{V} = (u, v, w)$ is the fluid velocity vector (m/s), ρ is the fluid density (kg/m^3), μ_{eff} is the effective viscosity (kg/m.s), P is the pressure (N/m^2), $B = (B_x, B_y, B_z)$ is the body force vector per unit volume (N/m^3), $F_{visc} = (F_{v,x}, F_{v,y}, F_{v,z})$ is the additional viscous terms due to the turbulence per unit volume (N/m^3), h is the enthalpy (J/kg), k is the kinetic energy of turbulence per unit mass (m^2/s^2), ε is the dissipation rate of turbulence per unit mass (m^2/s^3), G is the turbulence energy generation rate (kg/m.s^3) and m_i is the mass fraction of species (wt%).

The species considered in the transport equations consists of seven elementary, whose transport equations are always solved (O₂, CH₄, CO₂, CO, H₂O, H₂ and N₂) and three secondary species (NO, NH₃ and HCN) which are considered only for NO concentrations.

The effective viscosity (μ_{eff}) is given by

$$\mu_{eff} = \mu_t + \mu_l \quad (2-2)$$

where μ_l is the laminar viscosity and μ_t is the turbulent viscosity evaluated from the relation

$$\mu_t = \rho C_\mu k^2 / \varepsilon.$$

In addition, the turbulence energy generation rate (G) is given by

$$G = \mu \left\{ 2 \left[\left(\frac{\partial u}{\partial x} \right)^2 + \left(\frac{\partial v}{\partial y} \right)^2 + \left(\frac{\partial w}{\partial z} \right)^2 \right] + \left(\frac{\partial u}{\partial y} + \frac{\partial v}{\partial x} \right)^2 + \left(\frac{\partial w}{\partial x} + \frac{\partial u}{\partial z} \right)^2 + \left(\frac{\partial v}{\partial z} + \frac{\partial w}{\partial y} \right)^2 \right\} - \frac{2}{3} (\mu \nabla \cdot \vec{V} + \rho k) \nabla \cdot \vec{V} \quad (2-3)$$

The usual values of the constants are: $C_1 = 1.44$, $C_2 = 1.92$, $C_3 = 1.0$, $C_\mu = 0.09$, $\sigma_k = 1.0$, $\sigma_\varepsilon = \kappa^2 / [(C_2 - C_1) C_\mu^{1/2}] = 1.22$ (where $\kappa = 0.42$ is the Von Karman constant), $Pr_t = 1.0$ and $Sm_t = 1.0$.

2.1.2. Solution Methodology

The conservation equations are discretized by the first order Hybrid scheme [20] and are solved with a CFD code based on a finite volume method [21]. In addition, pressure-correction and multisegment techniques are applied. Applying these techniques results in an efficient code, that has the capability

to calculate the steady-state flows in complex three-dimensional regions. All the codes are written in FORTRAN algorithmic language.

In the pressure-correction method (for incompressible problems), a time derivative of pressure is added to the continuity equation, which tightly couples the continuity and momentum equations. This coupling makes the system of equations easier to solve. Furthermore, the strategy of dividing the domain into segments results in the capability of local refinement of the mesh to capture the important interactions and processes with more detail and with better numerical efficiency. The code has been validated through a number of problems with complex geometries and has proven to be a reliable solver [22].

2.1.3. Boundary Conditions

The code allows for dividing the boundary conditions into patches. This patching system allows for separating different boundary conditions from each other. The boundary conditions of the hot gas for a cement rotary kiln are shown in Figure 2-2. In addition to the cylindrical section, the kiln hood, the burner, and the cooler are also depicted in this figure. Boundary conditions for various patches are described as below:

aa) Flow rate condition: This condition allows for setting convective flow rates and sets the diffusive terms to zero.

For primary air, secondary air, in-leakage air, and the fuel, a mass flow rate condition is imposed. This condition allows for prescribing the uniform distribution of the normal component of velocity on that patch, according to the following formula:

$$v_n = \dot{m}/(\rho A) \quad (2-4)$$

where v_n is the normal component of velocity (m/s), \dot{m} is the mass flow rate (kg/s), ρ is the density (kg/m³) and A is the area of the patch (m²).

The fuel is assumed to be a combination of coke and coal and the air is assumed to be consisting of 23.13% oxygen, 76.15% nitrogen, and the rest moisture.

In addition to the above conditions for the inlets, the values of the turbulent energy and its dissipation rate are calculated with the following equations

$$k = 1.5\bar{U}^2 \left(\frac{u'}{\bar{U}} \right)^2 \quad (2-5)$$

$$\varepsilon = C_\mu^{3/4} \frac{k^{3/2}}{l_t} \quad (2-6)$$

where k is the turbulent kinetic energy, \bar{U} is the mean velocity at the inlet, $\frac{u'}{\bar{U}}$ is the turbulence intensity (set to 5%), ε is the dissipation rate of turbulent energy, C_μ is constant (set to 0.09) and l_t is the turbulent length scale and is set to 10% of a characteristic geometric length.

bb) Wall condition: different types of wall conditions are used for this work: regular wall, refractory, and bed of material.

For regular walls, no-slip and no-penetration conditions are used. A no-slip boundary condition says that the fluid in contact with a wall will have the same velocity as the velocity of the wall. A no-penetration boundary condition means no fluid flow, either convective or diffusive, is allowed through the wall. A regular wall condition is set for the hood and cooler wall. In addition, in order to avoid heat loss and concentrate on the process within the cylindrical section of the model, the wall temperature of these two regions is set to the temperature of the secondary air, and therefore no heat transfer is allowed through them.

Two other types of wall conditions are used: the bed of material and the refractory which are both employed for the rotary kiln (see Figure 2-2). For refractory, similar to regular walls, no-slip and no-penetration conditions are set. However, in order to calculate for the heat losses, conduction is allowed through it. In addition, due to having negligible rotation speeds in comparison to the velocities in the flow field, the velocity of the rotary wall is set to zero.

For the bed of material, again a no-slip condition is assumed. However, because of the chemical evolution within the bed and the release of CO_2 and H_2O , a no-penetration condition can no longer be used. The mass flow rate of these two components is set as a source term for their transport equations in the gas region close to the surface of the bed. In addition, similar to the refractory wall, the bed has energy interaction with the hot flow, i.e. it is assumed that the hot gas is the heat source of the bed.

For all the walls, the tangential stress and the values of k and ε are imposed according to the wall function method proposed by Launder and Spalding [23].

The emissivity of the refractory and the bed surface, for radiation calculation, is set to a default value of 0.8.

cc) Outlet condition: it is assumed that the kiln exit is sufficiently far away and not affected by the downstream conditions; therefore, a zero-gradient boundary condition, for velocity and scalars, is imposed at the exit.

$$\frac{\partial v_n}{\partial n} = 0 \quad (2-7)$$

$$\frac{\partial \phi}{\partial n} = 0 \quad (2-8)$$

In addition to the above boundary conditions, a constant laminar viscosity of $\mu_l = 2 \times 10^{-5} \text{ kg/(m.s)}$ is considered in the calculations; turbulent Prandtl and Schmidt numbers are also assumed to be constant and equal to 1.0 throughout the whole field.

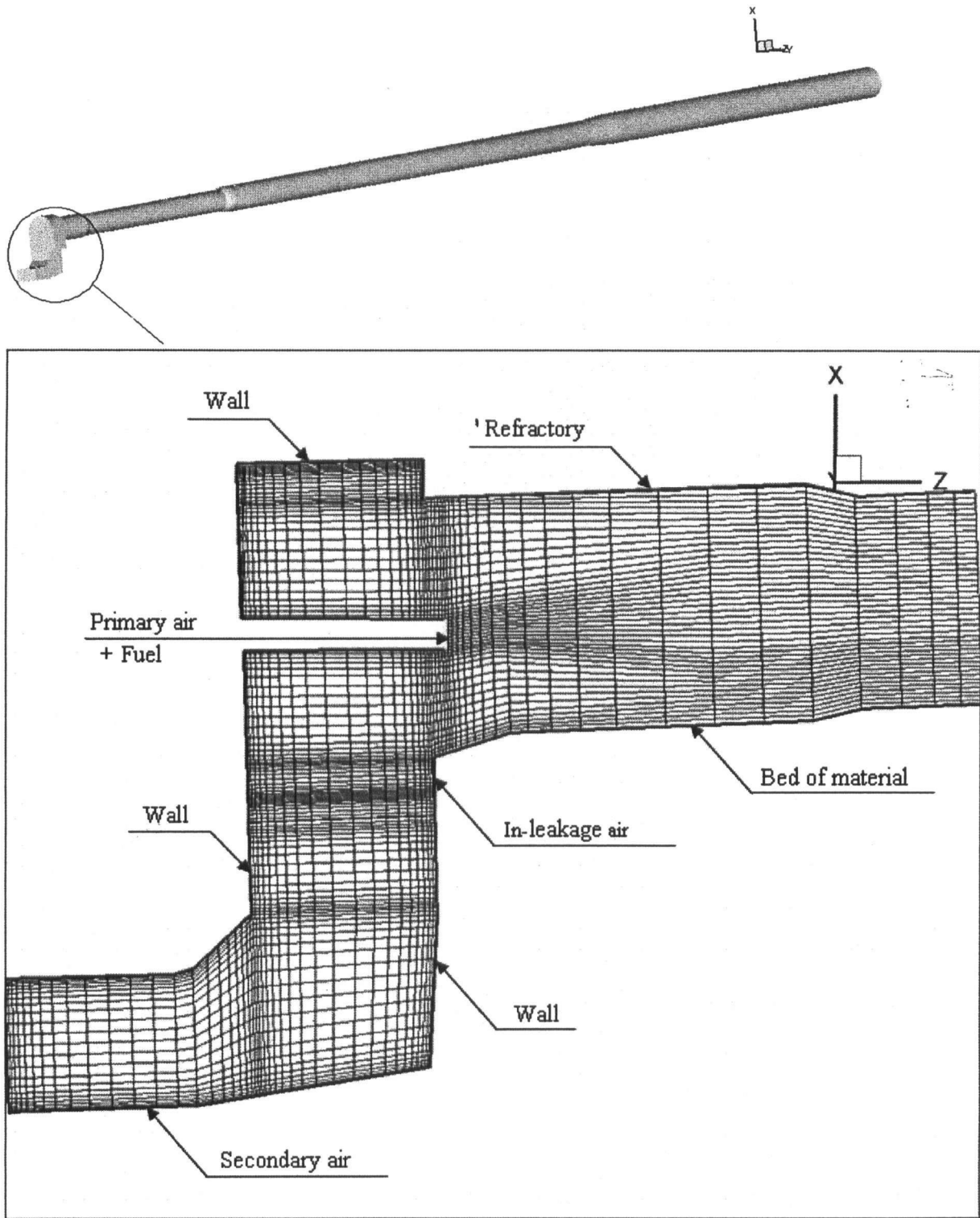


Figure 2-2: Boundary conditions of the hot flow

2.2. WALL/REFRACTORIES MODEL

In addition to the model for the hot gas, the existing CFD code includes the wall model. The wall model is coupled with the hot flow model in order to calculate the inner wall temperature as a boundary condition for the hot flow and also to get the heat loss through the refractory wall.

2.2.1. Governing Equation

The conduction equation in cylindrical coordinates is written as follows [24]

$$\frac{1}{r} \frac{\partial}{\partial r} \left(kr \frac{\partial T}{\partial r} \right) + \frac{1}{r^2} \frac{\partial}{\partial \theta} \left(k \frac{\partial T}{\partial \theta} \right) + \frac{\partial}{\partial x} \left(k \frac{\partial T}{\partial x} \right) = 0 \quad (2-9)$$

Comparing the order of magnitude of the temperature gradients in the radial direction with those in the angular and axial direction and considering the values of the kiln length and diameter, by performing a simple order of magnitude analysis, it can be concluded that, the angular and axial terms can be neglected. Therefore, the above equation is reduced to the following equation

$$\frac{1}{r} \frac{\partial}{\partial r} \left(kr \frac{\partial T}{\partial r} \right) = 0 \quad (2-10)$$

2.2.2. Solution Methodology

The wall of rotary kilns is usually multi-layered with the following arrangement, from inside to outside: coating, brick and steel shell. Therefore, the 1-D conduction equation for the multi-layered refractory wall is written as follows

$$Q_{cond} = \frac{T_{W,in} - T_{W,out}}{R_i} \quad (2-11)$$

where Q_{cond} is the conductive heat flow rate (W), $T_{W,in}$ is the inner temperature of the wall (K), $T_{W,out}$ is the outer temperature of the wall and R_i is the heat resistance of the i^{th} layer (K/W), which is calculated as follows [24]

$$R_i = \frac{\ln\left(\frac{r_{out,i}}{r_{in,i}}\right)}{2\pi k_i L} \quad (2-12)$$

where $r_{out,i}$ is the outer radius of the i^{th} layer (m), $r_{in,i}$ is the inside radius of the i^{th} layer (m), L is the height of the cylinder (m) and k_i is the thermal conductivity of the i^{th} layer (W/m.K).

The refractory detail of kiln #1, for instance, is shown in Figure 2-3. As illustrated in this figure, at each cross-section the wall of this kiln consists of three different layers, which are specified by different names and have different thicknesses and thermal conductivities. The conductivity of each refractory layer varies with its temperature; this effect is included in the model by writing the thermal conductivity in the form of

$$k_i = a_i + b_i T + c_i T^2 \quad (2-13)$$

where a_i , b_i and c_i are constants and can be derived by fitting the thermal conductivity data (provided by the manufacturer) in curves. Table 2-2 summarises the value of these constants for all the refractory layers in this work.

Table 2-2: Curve fit data for thermal conductivities of refractory layers

Type	a_i [W/(m.K)]	b_i [W/(m.K ²)]	c_i [W/(m.K ³)]
Stainless Steel	14.7	0.016	-0.504x10 ⁻⁵
Magnel RS	5.23	-0.0019	-
Aladin 80	2.00	-	-
Magnel RSV	5.23	-0.0019	-
TZ 40	3.06	-0.0003	-
Z_Dol	3.06	-0.0003	-
PERMAL7	5.23	-0.0019	-
Alumina	2.00	-	-
RT 150	0.4	-	-
Castable MC22	1.00	-	-
Coating	4.13	-0.00458	0.154x10 ⁻⁵
Kricon 32	1.10	-	-
AS90S	3.60	-0.001	-

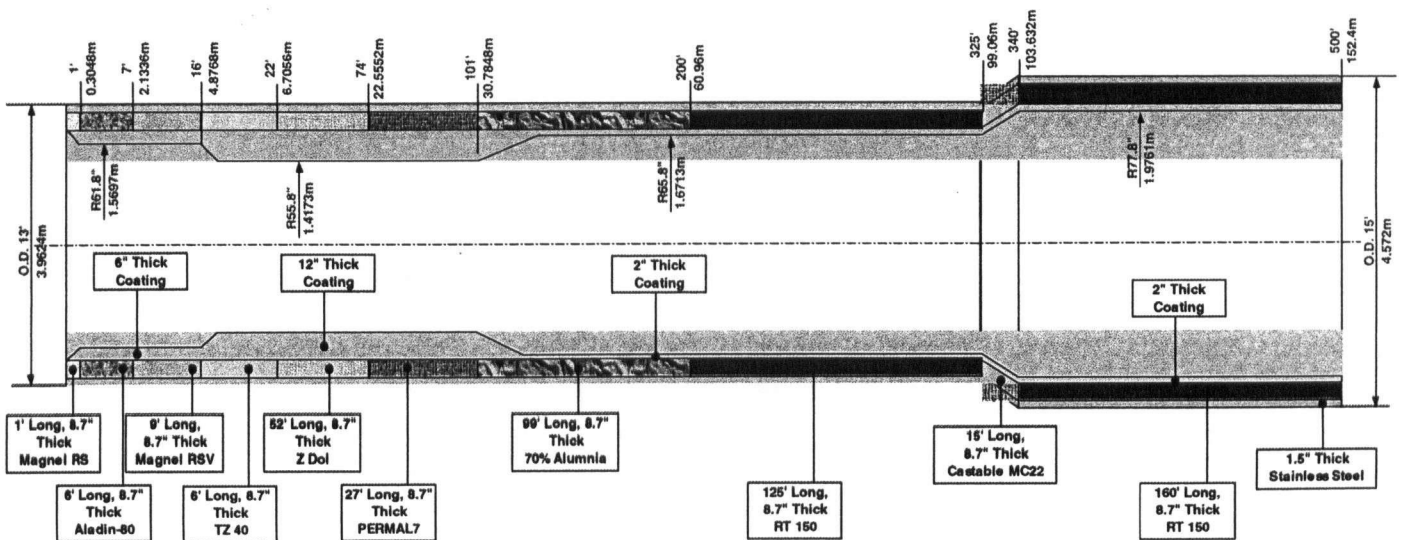


Figure 2-3: Refractory lining details

2.2.3. Boundary Conditions

Two different boundary conditions are considered for the wall model: one as a net heat flux on the inner side and the other one as a heat loss on the outer side.

For the inner wall, a net heat flux is calculated and then imposed on each control volume of the refractory, according to the following equation. This net heat flux consists of three parts: convection from the hot gas to the inner wall, radiation from the hot gas to the inner wall, and radiation from the wall to the hot gas. The first two parts are provided by the CFD code and are accounted for by the first term on the right hand side of this equation; while the third part is a function of the inner wall temperature.

$$q_{net} = q_{in} - \sigma \epsilon_{in} T_{W,in}^4 \quad (2-14)$$

where q_{net} is the net heat flux passing through the wall (W/m^2), q_{in} is the sum of convective and radiative heat flux taken from the hot gas (W/m^2), σ is Stefan-Boltzmann constant ($\sigma = 5.67 \times 10^{-8} W/(m^2.K^4)$), ϵ_{in} is the emissivity of the inner wall (which is set to 0.8 as default) and $T_{W,in}$ is the temperature of the inner wall (K).

As mentioned before, the outer wall shell loses heat to the ambient air through convection and radiation, which can be formulated as follows

$$q_{out} = h_c (T_{W,out} - T_{am}) + \sigma \epsilon_{out} (T_{W,out}^4 - T_{am}^4) \quad (2-15)$$

where q_{out} is the heat flux lost from the shell to the ambient air (W/m^2), h_c is the convective heat transfer coefficient ($\text{W}/\text{m}^2\cdot\text{K}$), $T_{w,out}$ is the outer wall temperature (K), T_{am} is the ambient temperature (K), and ε_{out} is the emissivity of the outside wall (which is also set to 0.8 as default).

It is assumed that the kiln shell loses heat by free convection. This heat transfer coefficient, for turbulent cases ($Gr_f Pr_f > 10^9$), is calculated with the following equation [24]

$$h_c = c(T_w - T_{am})^{1/3} \quad (2-16)$$

where h_c is the convective heat transfer coefficient ($\text{W}/\text{m}^2\cdot\text{K}$), T_w is the kiln shell temperature (K), T_{am} is the ambient temperature (K), and constant c is equal to 1.24 for horizontal cylinders ($\text{W}/\text{m}^2\cdot\text{K}^{4/3}$).

2.3. OTHER MODELS

All the above equations are the general conservation equations for the hot flow and the wall, and are solved by the original CFD code. However, whenever a new process is added to the model, such as clinker formation (Chapter 3) or tire combustion (Chapter 4), the code is modified accordingly. All the necessary modifications, such as solution of the new conservation equations and coupling considerations are explained in their relevant chapters and were not included in this chapter.

2.4. POST-PROCESSING

After solving the model equations with the fully-coupled CFD code, the results are written in a series of data and diagnostic files. The diagnostic files are usually investigated to make sure the code has

reached a satisfactory convergence and the data files are used for analysis and post-processing purposes.

Chapter 3. CLINKER FORMATION IN CEMENT KILNS

3.1. INTRODUCTION

Cement kilns are utilized by industries to produce clinker. In order to produce clinker, a raw material with a specific mixture is fed into the kiln, and after a series of chemical reactions, known as “clinkering reactions”, clinker is formed. The whole process leading to the production of clinker is called “clinker formation” [25]. The hot clinker leaves the kiln and is subjected to a series of post-processes until cement is produced. These processes are summarized as follows: the hot clinker after being cooled down, partially crunched and homogenized is thrown into the cement mill for final grinding. During the grinding, a small amount of additives (gypsum and limestone) is combined with the clinker, and finally cement with the desired composition is produced. Clinker is different from cement, and these two terms cannot be interchangeably used. Cement is the final product of a cement plant while clinker is the final product of a cement kiln.

The raw material of cement kilns, as shown in Table 3-1, is mainly a mixture of calcium carbonate, silicon dioxide and aluminium, and iron oxides [25]. Due to the chemical reactions taking place within cement kilns, the chemical composition of clinker is different from that of the raw material (see Table 3-2).

Table 3-1: Raw material components

Chemical Formula	Name
$CaCO_3$	Calcium Carbonate
SiO_2	Silicon dioxide (Silica)
Al_2O_3	Aluminium oxide (shale)
Fe_2O_3	Iron oxide

Table 3-2: Clinker phases

Name	Shorthand formula	Typical percentage
Tricalcium silicate (Alite)	$C_3S (3CaO.SiO_2)$	45-65
Dicalcium silicate (Belite)	$C_2S (2CaO.SiO_2)$	10-25
Tricalcium aluminate	$C_3A (3CaO.Al_2O_3)$	7-12
Tetracalcium aluminoferrite	$C_4AF (4CaO.Al_2O_3.Fe_2O_3)$	5-11

3.2. CLINKER FORMATION PROCESS

In a cement rotary kiln, the solid material with the aid of a 3-4 degree inclination and the rotational motion of the kiln (with an approximate speed of 1-5 rpm), flows toward the burner end. Simultaneously, the hot gas flows above the solid material in the opposite direction. The hot gas is the major heat source for the bed of material. As the solid material flows, it gains heat, and its temperature increases. After a certain temperature, a complex series of exothermic and endothermic chemical reactions (as summarized in Table 3-3 and Table 3-4) occur.

Table 3-3: Clinker formation process

Temperature [°C]	Process
100	Evaporation of free water
900 - 1200	Reaction between calcium carbonate or calcium oxide and alumino-silicates
1250 - 1280	Beginning of liquid formation
> 1280	Further liquid formation & completion of formation of compounds

Table 3-4: Clinker formation reactions [3]

No.	Reaction	Standard enthalpy of reaction [kJ/kg]
1	$CaCO_3 \rightarrow CaO + CO_2 \uparrow$	+1780
2	$MgCO_3 \rightarrow MgO + CO_2$	+1395
3	$CaO + Al_2O_3 \rightarrow CA$	-100
4	$2CaO + Fe_2O_3 \rightarrow C_2F$	-114

5	$2CaO + SiO_2 \rightarrow C_2S$	-732
6	$CA + C_2F + CaO \rightarrow C_4AF$	+25
7	$CA + 2CaO \rightarrow C_3A$	+25
8	$C_2S + CaO \rightarrow C_3S$	+59

The length of a rotary kiln depends mainly on the amount of time required to heat up the raw material to a certain temperature. In cement kilns, based on Table 3-3, the objective is to reach a very high bed temperature, at least $1280^{\circ}C$. The kiln length is also dependent on the type of the kiln process: wet and dry. In wet kilns the feed material has high moisture content and therefore, longer kilns are needed. Dry kilns have a preheater tower installed before them. The preheating towers dry and partially calcinate the solid material and as a result, dry kilns are much shorter than wet ones. The highly endothermic reaction of $CaCO_3 \rightarrow CaO + CO_2 \uparrow$, the first step in clinker formation, is called calcination. Partially calcinated raw material means that the calcium carbonate, to some extent but not completely, has been decomposed into CaO and CO₂.

A cement kiln consists of three distinct temperature zones: the preheating zone, the calcining zone and the burning zone. Each zone is named based on its process. These zones are bounded by the temperature range and the chemical reactions taking place within them [25]. In the preheating zone, the solid material is dried and heated to the point that calcination can begin ($900^{\circ}C$). The calcination zone is self-explanatory; in this zone calcination is initiated and completed. During calcination the CO₂ content of the bed is released and transferred to the hot gas. Because of this, the solid mass flow rate will gradually decrease. The end of calcination is the beginning of the burning zone. The burning zone is the hottest part of the kiln, where the temperature of the bed may exceed $1280^{\circ}C$. In this zone, the solid material is melted and liquid is formed. The liquid is principally composed of alumina and iron oxides. It acts as flux in the formation of the calcium silicates of clinker, C₃S and C₂S. The amount of the molten phase is sufficient enough to cause the material to cohere into small balls of

clinker. Finally, the clinker consisting of C_3S and C_2S crystals embedded in a matrix of the aluminates and ferrites (C_3A and C_4AF) is formed.

This chapter is organized as follows: first, the objectives are mentioned and it is followed by a discussion on the literature related to this work. Then, a 1-D bed model, including the governing material and energy balance equations, and the coupling with the existing CFD code is described. After that, the grids for two full-scale cement kilns including their boundary conditions are presented. Then, the simulations results are analyzed and validated against limited plant data. Finally, summary, conclusions, and future recommendations are presented.

3.3. OBJECTIVES

The primary objectives of this work are to develop a scientific tool for simulating cement rotary kilns and to obtain an improved understanding of the important processes inside them. In order to fulfill the above objectives, a simplified one-dimensional model based on the ODEs describing the axial evolution of the temperature and material composition inside the bed was developed. Then, this model was implemented in an existing UBC CFD code developed in our research group [18, 21]. With the aid of this code, two full-scale cement kilns were simulated and limited available plant data were used for validation.

3.4. LITERATURE SURVEY

For this work detailed studies on simulation of cement rotary kilns were required. Unfortunately, a literature survey revealed that only a few papers were available. The scarcity of literature is possibly

exacerbated by the desire of the companies engaged in this research area to keep their data and experience confidential and therefore gain a competitive advantage.

An earlier paper was written by H. A. Spang [14] in which a dynamic model of cement kilns was developed. In this work, a coupled 1-D mathematical model for coal/oil-fired cement kilns including the gas, the solid, and the wall was developed and investigated through a series of plots. The author concluded that with the aid of the proposed model, qualitative behaviour of actual cement kilns can be predicted properly. Although modeling the cement kilns in only one dimension can be too much of a simplification, but this work was a good starting point for future work. In particular, Spang showed that the two exothermic reactions of clinker formation make the numerical solution unstable and, in fact, no truly steady-state solution was obtained by him. This instability was one of the main deficiencies of Spang's work.

Many years later, E. Mastorakos *et al.* [17] simulated a coal-fired rotary cement kiln. Similar to Spang's work, the bed equations were solved in a one-dimensional domain. However, in this work, the flow field, the temperature and mass distribution in the hot gas along with the wall temperature were obtained in 3-D. They revealed satisfactory predictions compared to both the limited measurements in a full-scale cement kiln, and the trends based on experience. However, their clinker model was not complete; for instance, some major thermo-chemical data, such as temperature ranges and the heat of clinker formation reactions were missing. The kinetics data (pre-exponential factors and activation energies) were significantly different from that of Spang [14]. As a matter of fact, E. Mastorakos *et al.* have mentioned that the pre-exponential factors and the activation energies were chosen by trial and error to get the expected clinker composition at the kiln exit. This, of course, limits predictive capabilities of the model. Despite some deficiencies, the introduction of a closure equation for the liquid formation, based on physical insight, was one of the important contributions of

their work and was used in our model. A similar equation for the liquid formation was written by G. Locher [3].

In this work, a 1-D steady-state mathematical model, including the axial material and temperature evolution within the bed, was developed and then implemented in the existing code. It is important to mention that the bed model in this work is a combination of E. Mastorakos *et al.* and Spang's work. To be specific, the original clinker formation model was based on Spang's model and it was further developed by including the liquid formation model, inspired by what was achieved by E. Mastorakos *et al.*, and the mass transfer between the gas and the bed.

The major advantages of the developed bed model in the present work lie in its flexibility and completeness. With the aid of the developed code, industrial-size cement rotary kilns are simulated and analyzed. Based on the quantitative and qualitative analysis of the results, it is ultimately concluded that significant progress has been achieved in the development of a predictive scientific tool for the simulation of cement rotary kilns. Also, the developed model can be used to address operational problems and optimize the design and operation of these complicated machines.

3.5. MATHEMATICAL MODEL

The formulation and coding of the mathematical model consists of two separate steps: the development of the bed model including the clinker formation process, and its implementation in the existing code.

3.5.1. Clinker Formation Model

Initially a set of assumptions and simplifications used in the development of the model are described.

Then, the conservation equations for the mass and energy of the bed are derived.

3.5.1.1. *Assumptions and Simplifications*

As mentioned earlier, a cement kiln is a counter-current system in which the solid material flows in one direction and the gas flows in the opposite direction. The CFD code used for the simulations in this work already had the capability of calculating the steady-state flows in complex three-dimensional geometries. Therefore, no additional considerations were required for the gas phase.

The clinker formation process is complicated and it is not possible to model in all details. So efforts were made to develop a simple model for the clinker formation process, while the essential characteristics and features were maintained. The solid material of the bed flows by a combination of the gravity and rotational forces, both leading to a flow with diffusive and convective movement of particles. Mathematical equations for the particular motions inside the bed are complex [9-11] and are beyond the scope of this work. Therefore, the flow of the solid material required significant simplification. For example, all the mixing and gravity effects were neglected and, similar to the previous works [14, 17], it was assumed that the movement of the solid material is governed by the plug flow rules. A constant axial velocity was chosen for the plug flow of the bed.

In addition to this, the bed chemistry was significantly simplified. In reality, chemical reactions in the solid phase take place at the interface between crystals and are limited by both diffusion and kinetics. However, due to the high extent of mixing in the bed and following the path of other researchers, the chemical reactions within the bed were assumed to be only limited by kinetics [14, 17]. Furthermore,

the reaction rates were determined by Arrhenius' law. Heats of clinkering reactions, specific heat and latent heat of the solid material were assumed to be constant. It was also assumed that the bed temperature was controlled by the external heat transfer from the hot gas, the heat released due to the clinkering reactions and convection and conduction with the wall. However, the heat transfer between the solid material and the wall was neglected in this work.

For a real kiln, due to the mixing of particles and rotation of the wall, the bed surface is not flat and can have different irregular shapes [9]. In addition, the bed height is not necessarily constant throughout the whole kiln. However, for simplicity and avoiding grid generation difficulties, the bed height was assumed to be constant throughout the whole kiln and the bed surface was assumed to be flat.

For modeling the clinker formation process, all the reactions listed in Table 3-4 should be considered. This will not be an easy task because it needs dealing with 14 components and eight reactions for which eight rate constants - i.e. eight activation energies and pre-exponential factors - are to be known. These eight rate constants (k_i) should be derived either experimentally or by trial and error, which is difficult and time-consuming. However, H. A. Spang [14] proposed a simpler model with five arbitrary reactions. In this system only the main components of the clinker formation process, both from the raw material mixture and the clinker phases, are involved and are summarized in Table 3-5. This simplified system of reactions is the base for our clinker formation model.

Table 3-5: Simplified clinker formation reactions

No.	Reaction	Rate constant
1	$CaCO_3 \rightarrow CaO + CO_2$	k_1
2	$2CaO + SiO_2 \rightarrow C_2S$	k_2
3	$C_2S + CaO \rightarrow C_3S$	k_3
4	$3CaO + Al_2O_3 \rightarrow C_3A$	k_4
5	$4CaO + Al_2O_3 + Fe_2O_3 \rightarrow C_4AF$	k_5

3.5.1.2. Energy Balance Equations

For rotary kilns, heat transfer plays an important role and therefore efforts have been directed to improving its understanding [8]. It consists of radiation and convection between the hot gas, the bed, and the refractory wall, particle-particle conduction and radiation among bed material particles, conduction through the wall and convection and radiation between the kiln shell and the ambient air. In this work, all the above listed terms are accounted for except the particle-particle conduction and radiation in the bed (that are accounted for in a global way in the one-dimensional approximation and are not individually evaluated) and heat transfer between the wall and the bed. The heat transfer mechanisms between and within the gas and the wall were already included in the existing code. However, for coupling the code the ones related to the bed needed to be taken care of.

There are two main heat transfer/generation mechanisms for the bed: the first one is the heat transfer between the hot gas and the bed, which occurs through a combination of convection and radiation. The second one is the summation of the heat of the clinkering reactions. The final temperature of the bed depends on the total amount of heat transferred and/or generated via the above mechanisms. The energy balance equation, assuming plug flow condition for the bed and neglecting pressure losses, can be written as

$$\dot{m}C_p \frac{dT}{dV} = -\sum_i \Delta \hat{H}_r r_i + \dot{q} \quad (3-1)$$

Two equations, equations (3-2) and (3-3), were derived from the above equation

$$\dot{m}C_p \Delta T = \dot{Q} \quad (3-2)$$

$$vC_p \frac{dT}{dx} = -\sum_i \Delta H_r r_i \quad (3-3)$$

where \dot{m} is the mass flow rate of material (kg/s), C_p is the specific heat of the bed material ($C_p = 1088 \text{ J/kg.K}$) [14], v is the axial velocity of the bed material (m/s), T is the temperature of the bed (K), \dot{Q} is the net heat flow to the bed (W), ΔH_r is the heat of reaction (J/kg) and r_i is the rate of reaction (1/s).

In our modeling, the following strategy was applied to get the bed temperature: first, the net amount of heat flux (radiation and convection) from the gas to the bed was found and multiplied by the area of the bed in each control volume to get the net heat flow. Then, based on the amount of this heat, with equation (3-2) the bed temperature at the exit of the control volume was calculated. The average temperature of that control volume was calculated and, then reaction rates and the total heat generated due to clinkering were calculated. With the aid of equation (3-3), the bed temperature was updated. If the temperature difference between the new one, calculated by equation (3-3), and the old one, calculated by equation (3-2), was less than one degree, it was acceptable; if not, the new temperature was considered an old temperature, and the above procedure was repeated until the above mentioned temperature difference went under one degree in that control volume.

It should be mentioned that each clinkering reaction can take place only in a given range of temperature, out of which it is ignored. Table 3-6 contains a summary of the temperature ranges and standard enthalpies of the clinkering reactions, taken from [3].

Table 3-6: Thermal data for clinker formation reactions

No.	Reaction	Temperature range [K]	Standard enthalpy of the reaction ¹
1	$CaCO_3 \rightarrow CaO + CO_2 \uparrow$	823 to 1233	+1.782e6 [J/kg CaO]
2	$2CaO + SiO_2 \rightarrow C_2S$	873 to 1573	-1.124e6 [J/kg CaO]
3	$C_2S + CaO \rightarrow C_3S$	1473 to 1553	+8.01e4 [J/kg CaO]
4	$3CaO + Al_2O_3 \rightarrow C_3A$	1473 to 1553	-4.34e4 [J/kg CaO]
5	$4CaO + Al_2O_3 + Fe_2O_3 \rightarrow C_4AF$	1473 to 1553	-2.278e5 [J/kg CaO]
6	$Clinker_{sol.} \rightarrow Clinker_{liq.}$	> 1553	+6.00e5 [J/kg]

¹Positive sign indicates an endothermic reaction and vice versa.

3.5.1.3. Material Balance Equations

As mentioned earlier, a cement rotary kiln behaves approximately like a plug flow reactor, where the bed material moves with a constant axial velocity and there is no axial diffusion. Therefore, the general plug flow reactor formula is used for the material balance in the bed:

$$\frac{\partial c_j}{\partial t} = -\frac{\partial(c_j v)}{\partial x} + R_j \quad (3-4)$$

Assuming a constant axial velocity (v) and steady-state condition, the above equation is reduced to

$$v \frac{\partial c_j}{\partial x} = R_j \quad (3-5)$$

where C_j represents the concentration of component j with production rate R_j .

The above equation was separately written and solved for each species involved in the simplified clinker formation reactions (as in Table 3-5) excepting for CO_2 . In order to complete the material balance equations, the production rate (R_j) of each species is required. The production rate matrix (R) can be determined by the equation (3-6) and are summarized in Table 3-7.

$$R = v_{sto}^T r \quad (3-6)$$

Table 3-7: Summary of production rates

Component	Production rate
$CaCO_3$	$R_1 = -r_1$
CaO	$R_2 = r_1 - r_2 - r_3 - r_4 - r_5$
SiO_2	$R_3 = -r_2$
C_2S	$R_4 = r_2 - r_3$
C_3S	$R_5 = r_3$
Al_2O_3	$R_6 = -r_4 - r_5$
C_3A	$R_7 = r_4$
Fe_2O_3	$R_8 = -r_5$
C_4AF	$R_9 = r_5$

According to Table 3-7, the production rate of each component is a function of reaction rates. Therefore, for calculating the production rates, reaction rates should be determined. Reaction rates can be written in different forms such as $r_i = K_i C_{j,1}^{\alpha_1} C_{j,2}^{\alpha_2} \dots$ or $r_i = k_i Y_{j,1}^{\beta_1} Y_{j,2}^{\beta_2} \dots$ (where Y_j represents the mass fraction of component j). Based on Spang's work, the reaction rates were written in the latter form and are summarized in Table 3-8.

Table 3-8: Summary of reaction rates

No.	Reaction	Reaction rate
1	$CaCO_3 \rightarrow CaO + CO_2 \uparrow$	$r_1 = k_1 Y_{CaCO_3}$
2	$2CaO + SiO_2 \rightarrow C_2S$	$r_2 = k_2 Y_{SiO_2} Y_{CaO}^2$
3	$C_2S + CaO \rightarrow C_3S$	$r_3 = k_3 Y_{CaO} Y_{C_2S}$
4	$3CaO + Al_2O_3 \rightarrow C_3A$	$r_4 = k_4 Y_{CaO}^3 Y_{Al_2O_3}$
5	$4CaO + Al_2O_3 + Fe_2O_3 \rightarrow C_4AF$	$r_5 = k_5 Y_{CaO}^4 Y_{Al_2O_3} Y_{Fe_2O_3}$

As mentioned earlier, the reaction rates are determined by Arrhenius' law; therefore, the reaction constants can be written as below

$$k_i = A_i \exp(-E_i / RT) \quad (3-7)$$

where A_i is the pre-exponential factor (1/s), E_i is the activation energy (J/mol) and R is the universal gas constant and is equal to $R = 8.314 \text{ (J/g.mol.K)} = 1.9872 \text{ (Cal/g.mol.R)}$. The values of A_i and E_i were taken from Spang [14] and are summarized in Table 3-9.

Table 3-9: Summary of the pre-exponential factors and activation energies for clinker formation reactions

Rate constant	Pre-exponential factor [1/s] (A_i)	Activation energy [J/mol] (E_i)
k_1	4.55e31	7.81e5
k_2	4.11e5	1.93e5
k_3	1.33e5	2.56e5
k_4	8.33e6	1.94e5
k_5	8.33e8	1.85e5

Finally, the production rates were plugged into equation (3-5) and nine ordinary differential equations (normalized with respect to the mass of CaO) for the axial evolution of the components involved in clinker formation, excepting for CO_2 , were obtained and are as follows

$$v \frac{dY_{CaCO_3}}{dx} = - \frac{M_{CaCO_3}}{M_{CaO}} k_1 Y_{CaCO_3} \quad (3-8)$$

$$v \frac{dY_{CaO}}{dx} = k_1 Y_{CaCO_3} - k_2 Y_{SiO_2} Y_{CaO}^2 - k_3 Y_{CaO} Y_{C_2S} - k_4 Y_{CaO}^3 Y_{Al_2O_3} - k_5 Y_{CaO}^4 Y_{Al_2O_3} Y_{Fe_2O_3} \quad (3-9)$$

$$v \frac{dY_{SiO_2}}{dx} = - \frac{M_{SiO_2}}{2M_{CaO}} k_2 Y_{SiO_2} Y_{CaO}^2 \quad (3-10)$$

$$v \frac{dY_{Al_2O_3}}{dx} = - \frac{M_{Al_2O_3}}{3M_{CaO}} k_4 Y_{CaO}^3 Y_{Al_2O_3} - \frac{M_{Al_2O_3}}{4M_{CaO}} k_5 Y_{CaO}^4 Y_{Al_2O_3} Y_{Fe_2O_3} \quad (3-11)$$

$$v \frac{dY_{Fe_2O_3}}{dx} = - \frac{M_{Fe_2O_3}}{4M_{CaO}} k_5 Y_{CaO}^4 Y_{Al_2O_3} Y_{Fe_2O_3} \quad (3-12)$$

$$v \frac{dY_{C_2S}}{dx} = \frac{M_{C_2S}}{2M_{CaO}} k_2 Y_{SiO_2} Y_{CaO}^2 - \frac{M_{C_2S}}{M_{CaO}} k_3 Y_{CaO} Y_{C_2S} \quad (3-13)$$

$$v \frac{dY_{C_3S}}{dx} = \frac{M_{C_3S}}{M_{CaO}} k_3 Y_{CaO} Y_{C_2S} \quad (3-14)$$

$$v \frac{dY_{C_3A}}{dx} = \frac{M_{C_3A}}{3M_{CaO}} k_4 Y_{CaO}^3 Y_{Al_2O_3} \quad (3-15)$$

$$v \frac{dY_{C_4AF}}{dx} = \frac{M_{C_4AF}}{4M_{CaO}} k_5 Y_{CaO}^4 Y_{Al_2O_3} Y_{Fe_2O_3} \quad (3-16)$$

where M_i is the molecular weight.

The amount of CO_2 , being released into the gas phase, was determined by writing a proportional equation between the calcium carbonate and the carbon dioxide and is as follows

$$\dot{m}_{CO_2} = \frac{M_{CO_2}}{M_{CaCO_3}} \dot{m}_{CaCO_3} \quad (3-17)$$

Equations (3-8) to (3-17) mathematically describe the axial evolution of the composition inside the bed of solid material and were solved to simulate the clinker formation process.

3.5.1.4. Closure Equations and Parameters

In addition to the mass and energy balance equations, there are some additional process aspects, such as liquid formation, and parameters, such as the specific heat of solid material, bed angle etc., that should be addressed.

Reaction III (C_3S formation), which is the final step in the clinker formation, occurs only in the presence of liquid phase. In this work, the involvement of reaction III was judged according to the

availability of liquid; if liquid was available, reaction III was taken into account and the fraction of the related components were updated accordingly. Otherwise, the rate of this reaction was set to zero.

The liquid melting inside the bed was modeled by including an additional equation taking into account a new parameter, liquid fraction (Y_{fus}). If the bed temperature exceeded a temperature (called the fusion temperature $T_{fus} = 1553 K$ [3]), based on the excess amount of heat and the latent heat of fusion $L_{fus} = 600 kJ/kg$ [3], the fusion fraction was calculated; Otherwise, no liquid was formed. An upper limit of $Y_{fus} = 0.3$ [3] was set, above which the fusion was neglected. Fusion fractions more than zero meant the liquid was available and C_3S was forming.

It was assumed that the solid material flows with a constant velocity, which was set as $v = 0.0127 m/s$ [14] for all the cases regardless of the size of the kiln. In addition, the specific heat of the solid material was assumed to be constant ($C_p = 1088 J/kg.K$ [14]) for all the cases.

The bed angle (θ) was another important parameter, which cannot be measured and because of its direct impact on the heat flow to the bed was required to be chosen carefully. The higher the bed angle, the bigger the bed surface area will be. The surface area is multiplied by the heat flux from the gas phase, and any increase in its value will increase the heat flow to the bed of material. In summary, by increasing the bed angle, the solid phase temperature increases; this relationship was one of the main challenges we encountered in the modeling procedure.

In literature [14, 17], a bed angle of 90 degrees was chosen; however, we noticed that not all kilns can have the same bed angles. This conclusion was reached after very high clinker temperatures were

obtained for kilns with bed angle of $\theta = \pi/2$. This problem was addressed by repetitive adjustment of the bed angle until relatively good results (considering the clinker temperature, composition and exhaust gas temperature) were achieved. Not only was this task hard but also time-consuming; each time the bed angle was changed, the whole grid was regenerated and the entire code execution process, which usually takes at least a few days, was repeated. For instance, for simulating Kiln #1, a Pentium III computer with a 1.3 GHz CPU and 2.1 GB of RAM was used. First, the cold flow was computed in 18 hours (2000 iterations). Then, the hot flow including the bed model was obtained in 130 hours (after 10000 iterations). Finally, the post-processing code for NO_x calculations was executed and was completed in 6.5 hours. In total, the simulation of Kiln #1 one was completed in 154.5 hours (6.4 days).

The issue of bed angle and its influence on the process remains a difficult issue and constitutes a limitation for the model predictive capabilities. For existing kilns there is information available on gas temperature at the exit, clinker composition and temperature at the exit that one can use to tune the model. It is necessary to perform a mass and energy balance together with the detailed CFD computations to make sure that the assumptions made are reasonable.

3.5.2. Formation of Thermal NO_x

“Nitrogen oxides” (NO_x) is a general term used for gases which contain nitrogen and oxygen in varying amounts. Thermal NO_x refers to the nitrogen oxides formed at very high temperatures, usually above 2200° F, and is the dominant formation mechanism in hot furnaces such as cement kilns. The formation rate of thermal NO_x is primarily a function of temperature and the residence time of nitrogen at that temperature, which can mathematically be predicted by the following equation.

$$\frac{d[NO]}{dt} = 2[O] \frac{(k_1 k_2 [O_2] [N_2] - k_{-1} k_{-2} [NO]^2)}{(k_2 [O_2] + k_{-1} [NO])} \quad (gmol / m^3 .s) \quad (3-18)$$

For the simulations in this chapter, the rate data (k_i) were selected from the work done by Hanson and Salimian and the partial equilibrium approach was used for determining the concentration of oxygen radicals (see Appendix A for more detail). The source term, due to the formation of thermal NO_x , is calculated with following equation

$$S_{th,NO} = M_{w,NO} \frac{d[NO]}{dt} \quad kg / (m^3 .s) \quad (3-19)$$

where $M_{w,NO}$ is the molecular weight of NO, and $\frac{d[NO]}{dt}$, the formation rate, is computed as mentioned above.

3.5.3. Modified Parent Code

It is apparent that no clinker formation model can be sufficient on its own and should be incorporated in a model consisting of the gas and the wall as well. This is because the wall, the gas, and the clinker model all interact and impact on each other. For instance, the gas temperature depends on the wall temperature and the clinker temperature. The solid phase absorbs energy from the gas and the wall, and its temperature will depend on the local temperature of both of them. These interactions are important and have to be included in final model.

The existing CFD code had the capability of 3-D simulation of the hot flow, and the multi-layered wall. However, a model for the bed was missing. Therefore, the developed bed model was implemented in the existing code. For coupling the interactions between the hot flow and the bed, the

mass and heat transfer between the existing code and the bed model were considered. This will also result in the conservation of the mass and energy of the whole system.

For including the energy interactions, only one modification was required. This was done by considering the heat transfer between the hot gas and the bed. The heat flux equation, equation (3-20), was written such that a portion of the heat flux was absorbed by the bed and the rest was reflected back to the hot gas.

$$q_{net} = q_{in} - \sigma \epsilon_{in} T_{b,in}^4 \quad (3-20)$$

where q_{net} is the net heat flux into the bed (W/m^2), q_{in} is the sum of convective and radiative heat flux taken from the hot gas (W/m^2), σ is Stefan-Boltzmann constant ($\sigma = 5.67 \times 10^{-8} W/(m^2 \cdot K^4)$), ϵ_{in} is the emissivity of the bed (which is set to 0.8 as default) and $T_{b,in}$ is the temperature of the bed (K).

For conserving the mass of the system, the mass transfer from the bed to the gas was taken into account. It consisted of two parts: release of H_2O during drying and release of CO_2 during the calcination. The amount of H_2O and CO_2 (in the form of mass flow rate) was treated as an additional source term in the transport equation of these components in the gas flow field.

For a real kiln, in addition to the release of these two components, the solid material constantly generates dust. The dust particles will eventually become a part of the gas phase; they will drift and leave the kiln at the exit. Including dust circulation is complicated and needs some basic knowledge. Unfortunately, in the literature no discussions were available on this matter. Modeling dust formation was beyond the scope of this thesis and therefore it was neglected.

3.6. GRID GENERATION

First, the grid for two full-scale cement kilns, including the rotary kiln, the hood, and a length of the cooler, was generated. Then, the boundary conditions were imposed. In addition, the wall of each kiln was implemented according to the refractory lining details provided by the plant. Kiln characteristic data for two industrial kilns were extracted and supplied by Dr. Jerry Yuan. The grids including the proper boundary conditions were generated with a special software developed by Dr. David Stropky.

3.6.1. Geometry and Refractory Lining Details for Kiln #1

The smaller kiln, referred to as Kiln #1, had a cylindrical section with a length of $L_1=154.65$ m and a diameter of $d_1 = 3.1394$ m . All the geometry details were extracted from the related AutoCAD files of this kiln and are depicted in Figure 3-1. In addition, the refractory details of this kiln are exhibited in Figure 3-2. The grid for Kiln #1 was generated based on the given dimensions and considering a bed angle of $\theta = 78^\circ$.

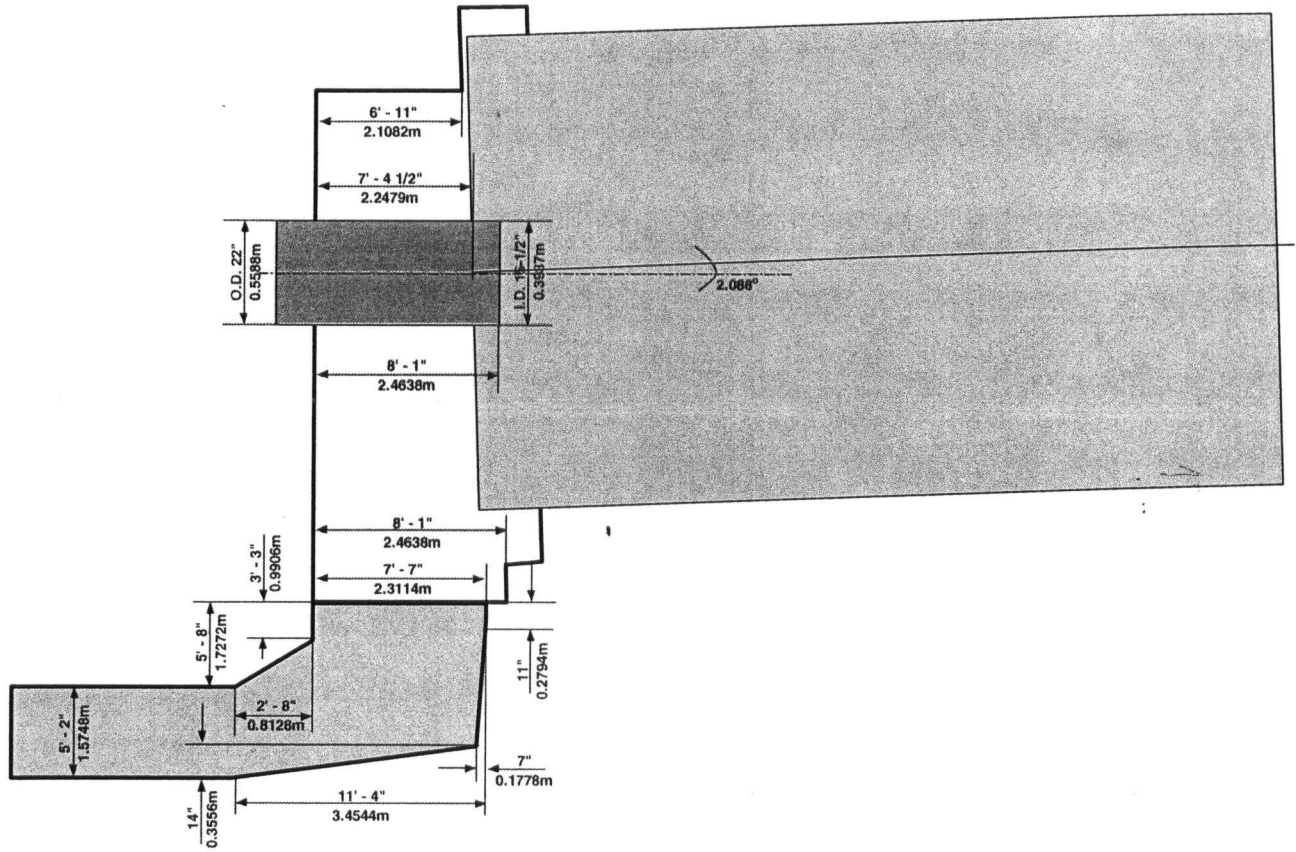


Figure 3-1: Kiln hood details of Kiln #1

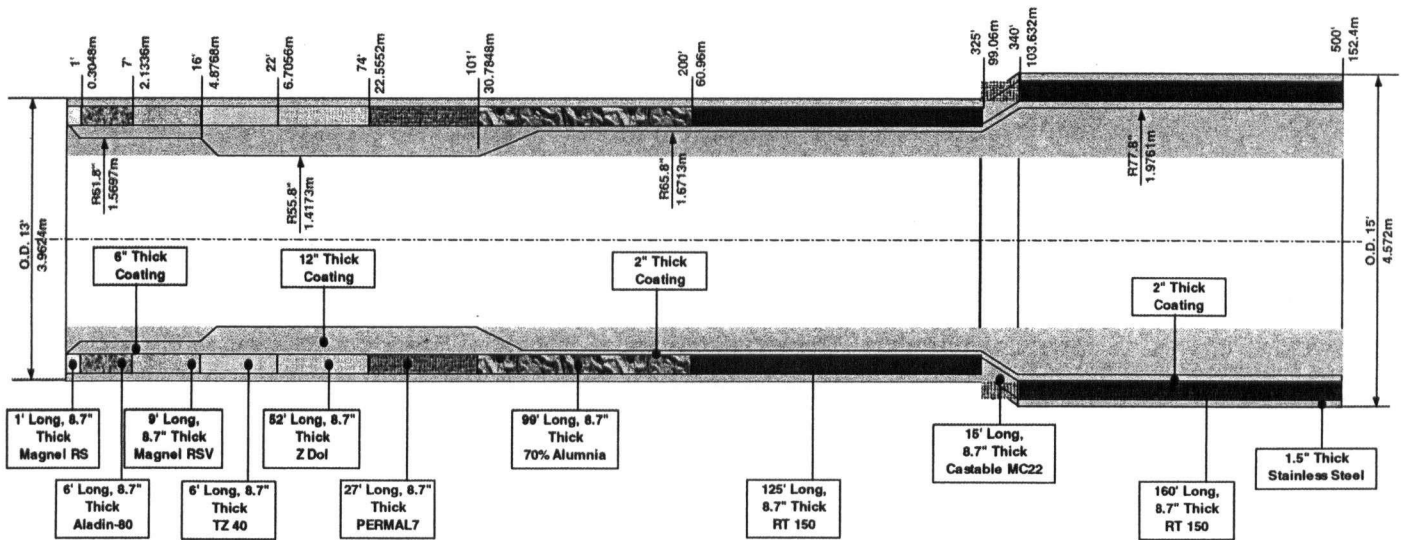


Figure 3-2: Refractory lining details of Kiln #1

3.6.2. Geometry and Refractory Lining Details for Kiln #2

The other kiln, Kiln #2, had a cylindrical section with a length of $L_2=154.82$ m and a diameter of $d_2 = 4.3586$ m . Similar to the other kiln, the dimensions and the detail required for the model were read off AutoCAD files and are depicted in Figure 3-3 and Figure 3-4. Finally, based on the characteristic data of Kiln #1 and considering a bed angle of $\theta = 84^\circ$, its grid was generated.

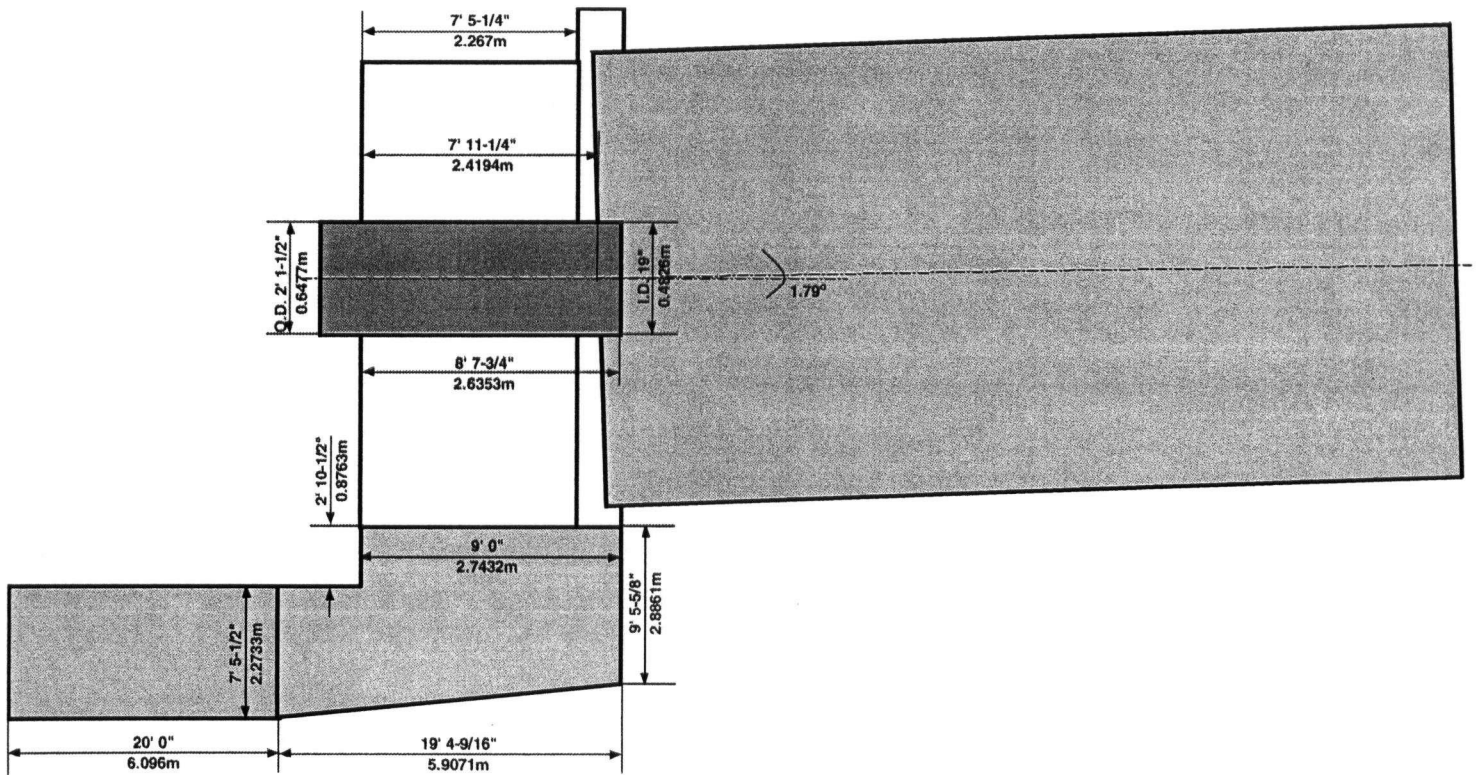


Figure 3-3: Kiln hood details of Kiln #2

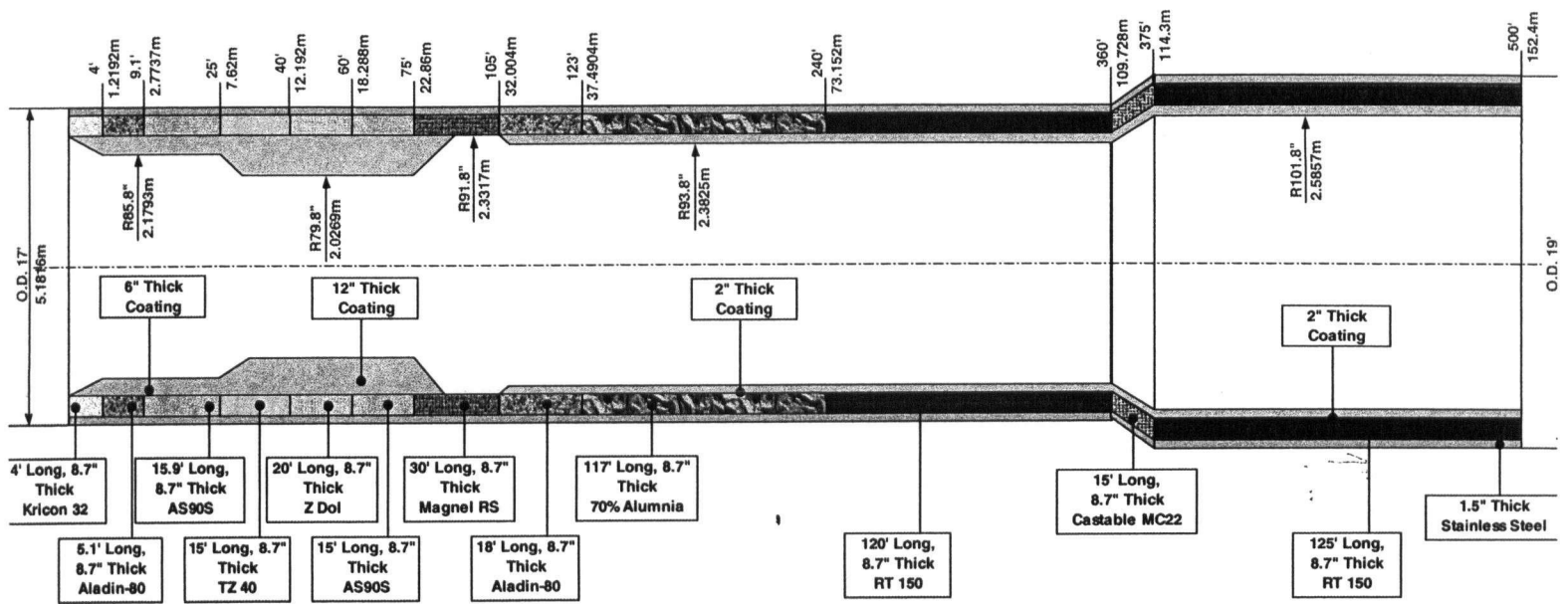


Figure 3-4: Refractory lining details of Kiln #2

After generating the grid, the boundary conditions based on the real conditions of the kilns were applied. The boundary conditions of each model were imposed according to its raw material, fuel, and air input data, and are summarized in the following tables.

3.7. BOUNDARY CONDITIONS

Boundary conditions are needed for the primary and secondary air, fuel, refractory, wall and bed. All the above boundary conditions are schematically depicted in Figure 3-5 and Figure 3-6 and tabulated in the following tables. Two additional conditions were considered for the cylindrical section and are not depicted in these figures: it is assumed that the kiln exit is not affected by the downstream conditions and therefore, zero-gradient boundary condition is imposed for it. It also assumed that the kiln shell loses heat to the ambient air (with $T_{amb} = 30^{\circ}C$) through convection and radiation. Further detail for the above mentioned boundary conditions is available in Chapter 2.

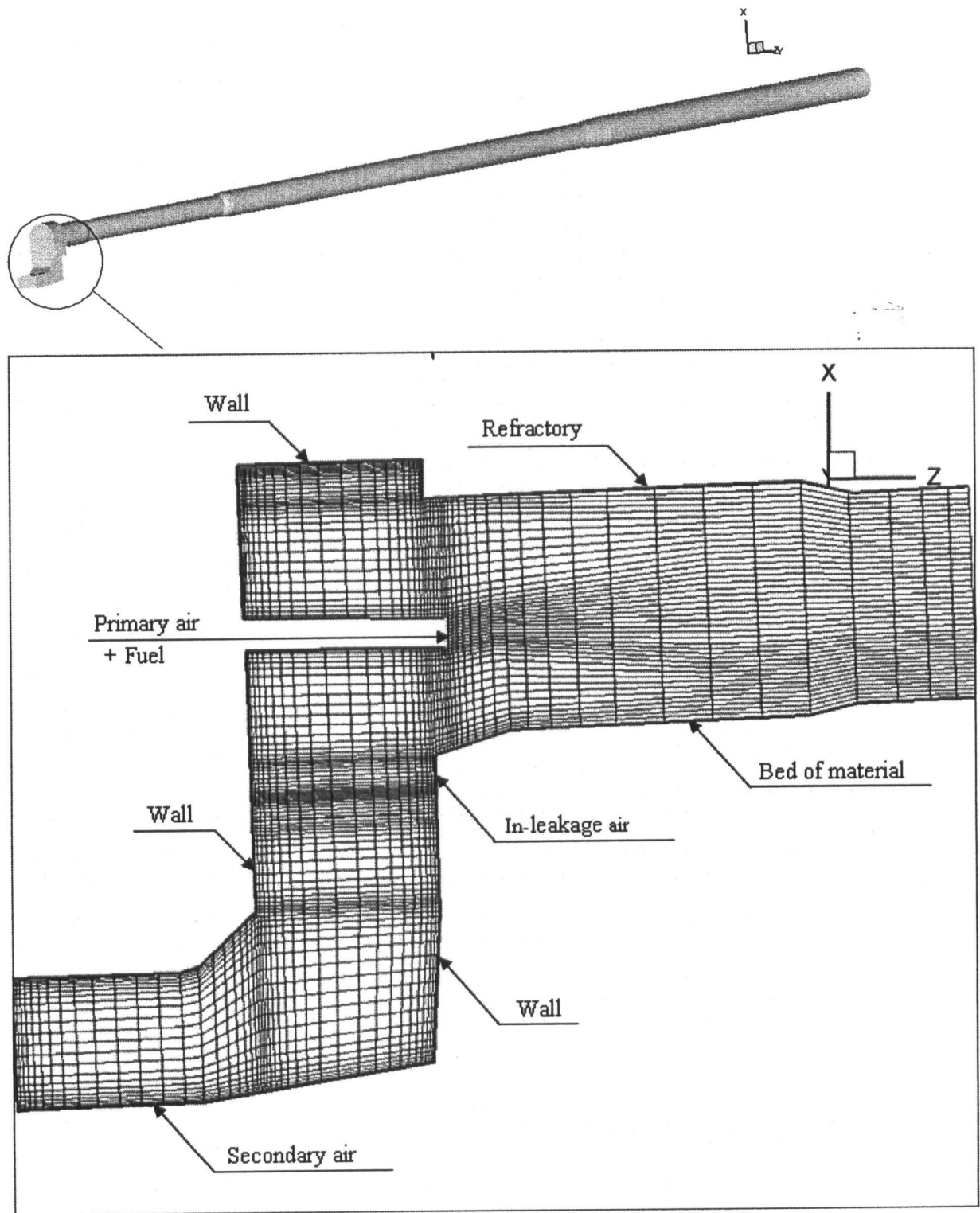


Figure 3-5: Boundary conditions for Kiln #1

Table 3-10: Material information for Kiln #1

Inlet Material Information	
Flow rate [kg/s]	20.788
Temperature [K]	338
Component	Mass Fraction (% wt)
<i>CaCO₃</i>	77.23
<i>CaO</i>	0.00
<i>SiO₂</i>	13.69
<i>Al₂O₃</i>	3.36
<i>Fe₂O₃</i>	1.70
Inert + others	3.85
Moisture	0.17
Total	100
Clinker Information	
Flow rate [kg/s]	13.52
Temperature [K]	1633

Table 3-11: Fuel input information for Kiln #1

Fuel type	Coal/coke
Flow rate [kg/s]	2.7167
Temperature [K]	333
Proximate Analysis (%)	
Moisture	1.24
Volatile	21.86
Fixed Carbon	67.35
Ash	9.55
Total	100
Elemental Analysis (%)	

Moisture	1.24
Carbon	71.81
Hydrogen	3.73
Nitrogen	1.08
Sulphur	5.45
Oxygen	7.14
Chlorine	0.00
Ash	9.55
Total	100
High heating value (HHV) [kJ/kg]	27566
Low heating value (LHV) [kJ/kg]	26720

Table 3-12: Air input information for Kiln #1

Primary Air	
Flow rate [kg/s]	6.516
Temperature [K]	365
Secondary Air	
Flow rate [kg/s]	14.346
Temperature [K]	1122
In-leakage Air	
Flow rate [kg/s]	6.954
Temperature [K]	298
Total air flow rate [kg/s]	27.816

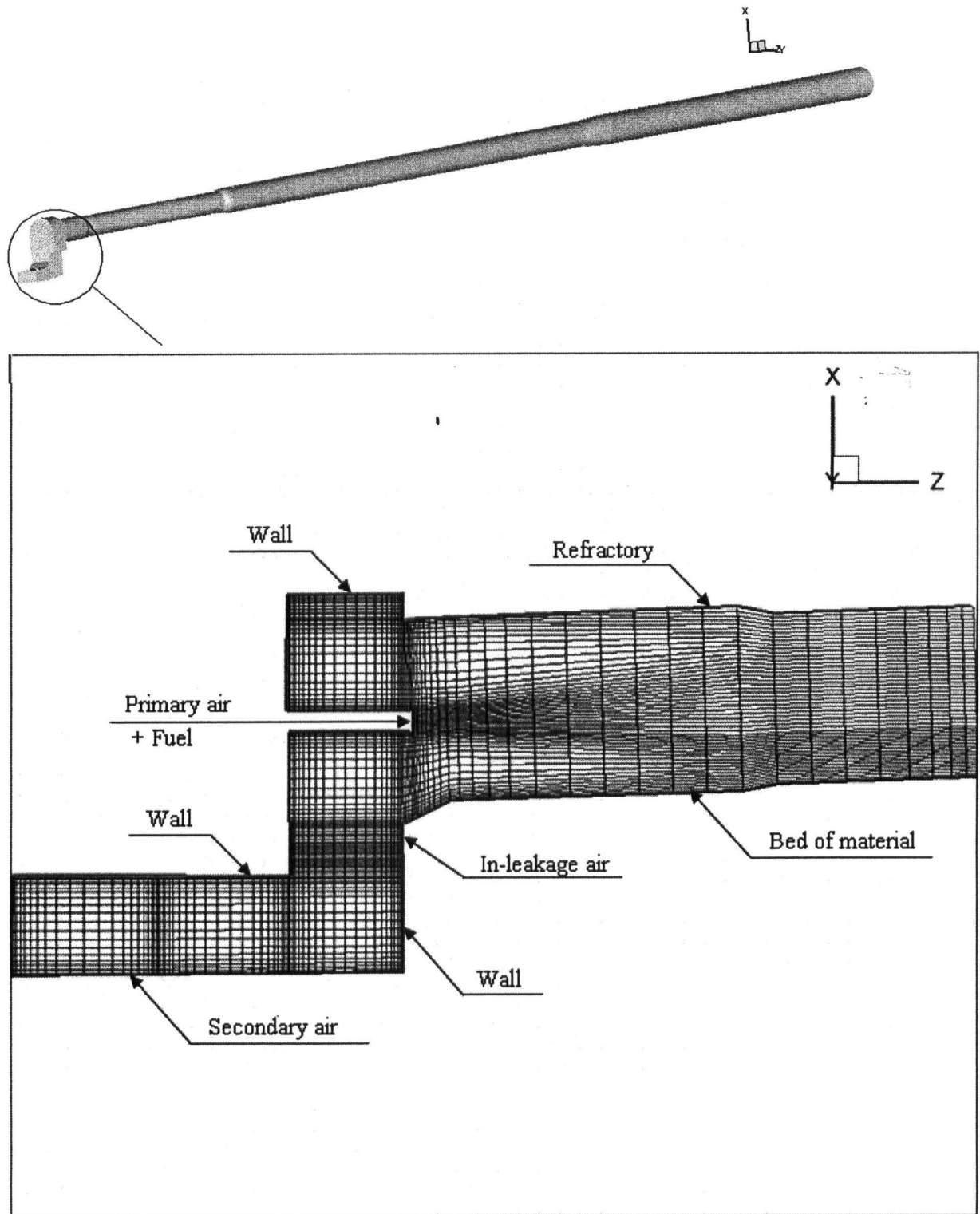


Figure 3-6: Boundary conditions for Kiln #2

Table 3-13: Material information for Kiln #2

Inlet Material Information	
Flow rate [kg/s]	30.60
Temperature [K]	338
Component	Mass Fraction (% wt)
<i>CaCO₃</i>	77.66
<i>CaO</i>	0.00
<i>SiO₂</i>	13.52
<i>Al₂O₃</i>	3.39
<i>Fe₂O₃</i>	1.98
Inert + others	3.45
Moisture	0.17
Total	100
Clinker Information	
Flow rate [kg/s]	20.014
Temperature [K]	1698

Table 3-14: Fuel input information for Kiln #2

Fuel type	Coal/coke
Flow rate [kg/s]	4.1467
Temperature [K]	333
Proximate Analysis (%)	
Moisture	1.09
Volatile	21.36
Fixed Carbon	62.40
Ash	15.15
Total	100
Elemental Analysis (%)	
Moisture	1.09
Carbon	73.51

Hydrogen	3.74
Nitrogen	1.13
Sulphur	5.26
Oxygen	0.13
Chlorine	0.00
Ash	15.15
Total	100
High heating value (HHV) [kJ/kg]	27696
Low heating value (LHV) [kJ/kg]	26858

Table 3-15: Air input information for Kiln #2

Primary Air	
Flow rate [kg/s]	9.7315
Temperature [K]	361
Secondary Air	
Flow rate [kg/s]	24.678
Temperature [K]	1049
In-leakage Air	
Flow rate [kg/s]	11.1661
Temperature [K]	296
Total air flow rate [kg/s]	45.5756

3.8. SOLUTION METHODOLOGY

After finishing the initial set-up of the problem, which consisted of the development of the bed model, its implementation in the parent code, generating the grid, and imposing the boundary conditions, it was time to numerically solve the system of the equations for the whole model. The final code was executed in three steps: first, the cold flow field, in order to get only the velocity contours, was created. Then, the code for the whole model, including all the sub-models, was

executed until a good convergence was achieved. The convergence behaviour was judged by continuous monitoring of the maximum heat flux residual of the refractories, the maximum temperature of the solid material, and the other residuals of the enthalpy, mass, etc. Finally, after simulating the problem, including all the primary parameters, the post-processing was performed to obtain the concentration of secondary species especially NO.

Due to having very small concentrations, it can be assumed that the reactions leading to formation of NO have no practical influence on the aerodynamics/combustion of the model. Therefore, the computations related to the formation of nitrogen oxides can be decoupled from those of the main code and handled in a post-processor. The possibility of having this decoupling will allow us to freeze the whole flow field and execute only the post-processing in order to calculate for the species related to the formation of nitrogen oxides. This, in fact, will save significant amount of computational time.

Due to the strong interactions between the sub-models, an iterative procedure between the predictions for the gas, the wall, and the bed was used. In addition, due to the counter-current flow within cement rotary kilns, a single iteration (in the second step of the code execution) was divided into two sub-iterations. First, the equations related to the gas phase and the wall were solved; then, moving in the opposite direction, the equations related to the bed were solved.

3.9. RESULTS AND DISCUSSION

Two full-scale cement kilns were simulated with the developed code. In order to obtain an estimate on the performance of the developed model and also improve the understanding on the processes taking place inside a cement rotary kiln, the predictions and results were validated, compared and analyzed. Particularly, the clinker temperature at the kiln exit and the flue gas temperature were

compared against limited measurement data provided by the plant. The simulation results are summarized and discussed as follows.

3.9.1. Validation on Clinker Formation Model

One of the main objectives of this chapter was to improve the understanding of the clinker formation process inside cement rotary kilns. The clinker composition from the simulation was validated against the composition calculated by the Bogue formula [26].

3.9.1.1. Bogue Calculation

Bogue calculations are the most important and frequently used indicators of the chemical composition of clinker. For this calculation, it is assumed that the final clinker will be composed only of the four main clinker components (as in Table 3-2). According to the Bogue calculation, the major components of the clinker can be calculated by the following equations:

$$C_3S = 4.07CaO - (7.6SiO_2 + 6.72Al_2O_3 + 1.43Fe_2O_3) \quad (3-21)$$

$$C_2S = 2.87SiO_2 - 0.754C_3S \quad (3-22)$$

$$C_3A = 2.65Al_2O_3 - 1.69Fe_2O_3 \quad (3-23)$$

$$C_4AF = 3.04Fe_2O_3 \quad (3-24)$$

The components calculated by Bogue are only potential compositions and any change in the cooling rate or burning temperature can change the true composition considerably. However, Bogue results become close to the true composition if the un-combined or free lime content of the clinker is considered in the calculations.

3.9.1.2. Modified Kiln Feed Composition

In Bogue calculation, it is assumed that clinker is a composition of the four main components of the kiln feed (CaO , SiO_2 , Al_2O_3 and Fe_2O_3) plus inert (a combination of chemicals such as Na_2O , K_2O , SO_3 , etc.). Therefore, the kiln feed composition was modified such that it consisted only of the above components and all the losses (components that leave the bed such as CO_2 and moisture) were excluded. This re-calculated composition, containing only the major components plus inert, is called the “loss-free composition” (see Table 3-16 and Table 3-17). Loss-free composition is the one used in Bogue calculations.

In addition, clinker analyses usually contain some information regarding un-combined or free lime content. This lime represents the amount of CaO that has not participated in the clinkering reactions and hence its amount should be subtracted from the total lime content in the loss-free composition. As reported from the plant, Kiln #1 and #2 contained 0.89% and 0.95% free lime, respectively.

Table 3-16: Loss-free composition of Kiln #1

Component	Mass Fraction (% wt)
CaO	65.68
SiO_2	20.79
Al_2O_3	5.10
Fe_2O_3	2.58
Inert + others	5.85
Total	100

Table 3-17: Loss-free composition of Kiln #2

Component	Mass Fraction (% wt)
<i>CaO</i>	66.06
<i>SiO₂</i>	20.54
<i>Al₂O₃</i>	5.15
<i>Fe₂O₃</i>	3.01
Inert + others	5.24
Total	100

3.9.1.3. Comparison between Model Prediction and Bogue Calculation

Table 3-18 and Table 3-19 contain a summary of results for both kilns. Table 3-18 shows a fairly good agreement between the model and Bogue calculations for Kiln #1 while for Kiln #2, as seen in Table 3-19, the predictions for the first two components of clinker are not that good.

Table 3-18: Comparison between the model prediction and Bogue calculation for Kiln #1

Component	Model Predictions (% wt)	Calculated by Bogue (% wt)
<i>C₃S</i>	63.65	67.78
<i>C₂S</i>	11.40	8.47
<i>C₃A</i>	9.15	9.15
<i>C₄AF</i>	7.86	7.86
<i>CaCO₃</i>	0.00	0.00
<i>CaO</i>	2.05	0.89
<i>SiO₂</i>	0.06	0.00
<i>Al₂O₃</i>	0.00	0.00
<i>Fe₂O₃</i>	0.00	0.00
Inert + others	5.83	5.85
Total	100	100

Table 3-19: Comparison between the model prediction and Bogue calculation for Kiln #2

Component	Model Predictions (% wt)	Calculated by Bogue (% wt)
<i>C₃S</i>	53.93	70.09
<i>C₂S</i>	18.15	6.00
<i>C₃A</i>	8.55	8.56
<i>C₄AF</i>	9.15	9.15
<i>CaCO₃</i>	0.00	0.00
<i>CaO</i>	4.97	0.95
<i>SiO₂</i>	0.01	0.00
<i>Al₂O₃</i>	0.00	0.00
<i>Fe₂O₃</i>	0.00	0.00
Inert + others	5.24	5.24
Total	100	100

3.9.2. Mass and Energy Balance

Table 3-20 and Table 3-21 contain a summary of the mass and energy balance for both kilns. The balances were performed by considering the main sources of mass and energy. As summarized in Table 3-20 and Table 3-21, the mass and energy are well balanced in both kilns. The acceptable balance indicates that the coupling between the main code and the bed model is correctly established; it also means that the code has reached a satisfactory level of convergence.

The following observations concerning the energy distribution in studied cement rotary kilns can be reported: about 70% of total heat input is provided by fuel combustion and the rest is from the sensible heat in the gas and feed material. About 20% of total energy is consumed by heating the solid material and formation of clinker, and about 4% of it is lost through the refractories to the atmosphere. Approximately 25% of the heat is carried away with the hot clinker leaving the kiln, and most of the remaining energy is lost by exhaust gases (50%).

Table 3-20: Mass and energy balance for Kiln #1

Input	Mass flow rate [kg/s]	Temperature [K]	Enthalpy [MW]	Percent [%]
Sensible heat in air	27.8	1122	23.2	22.18
Sensible heat in feed material	20.788	338	7.645	7.3
Sensible heat in fuel	2.7167	333	1.135	1.12
Fuel combustion			72.59	69.4
<i>Total</i>	<i>51.304</i>		<i>104.57</i>	<i>100</i>
Output	Mass flow rate [kg/s]	Temperature [K]	Enthalpy [MW]	
Exit gas losses	37.1	1224	50	47.55
Clinker discharge	13.691	1661	27.206	25.87
Ash discharge	0.444		0.70	0.67
Heat absorbed by clinkerization			21.273	20.23
Shell heat losses			4.265	4.06
Heat of unburned carbon			1.705	1.62
<i>Total</i>	<i>51.2347</i>		<i>105.149</i>	<i>100</i>

Table 3-21: Mass and energy balance for Kiln #2

Input	Mass flow rate [kg/s]	Temperature [K]	Enthalpy [MW]	Percent [%]
Sensible heat in air	46.2	1049	37.1	22.98
Sensible heat in feed material	30.596	338	11.251	6.97
Sensible heat in fuel	4.1467	333	1.733	1.07
Fuel combustion			111.372	68.98
<i>Total</i>	<i>80.942</i>		<i>161.456</i>	<i>100</i>
Output	Mass flow rate [kg/s]	Temperature [K]	Enthalpy [MW]	
Exit gas losses	59.4	1267	81.1	50.8
Clinker discharge	20.148	1562	37.867	23.72
Ash discharge	0.856		2.06	1.29
Heat absorbed by clinkerization			31.455	19.7
Shell heat losses			6.572	4.12
Heat of unburned carbon			0.528	0.37
<i>Total</i>	<i>80.404</i>		<i>159.582</i>	<i>100</i>

3.9.3. Clinker Temperature and Composition

The beginning zone of the kiln is known as the preheating zone where only the water content of the solid material evaporates. As depicted in Figure 3-7 and Figure 3-8, almost half of the kiln (80 m) is occupied by this zone. The next zone is the calcination zone and is self-explanatory; in this zone, the first step of the clinker formation, the calcination takes place. During calcination, calcium carbonate decomposes into calcium oxide and carbon dioxide; the carbon dioxide will travel from the solid phase to the gas phase. This phenomenon is one of the main losses of the clinker formation process and will result in a decrease in the mass flow rate of the solid material as it moves down. Based on Figure 3-7 and Figure 3-8, about 60 meters of the kiln are occupied by the calcination zone. Since calcination is highly endothermic, we assumed that it is controlled only by heat transfer, and the clinker temperature remains constant at 1089 K during the process. After the completion of calcination, the temperature of the solid phase starts rising again and, as summarized in Table 3-5, the rest of the clinkering reaction, along with the formation of liquid will take place. These reactions consist of formation of the four phases of the clinker (C_2S , C_3S , C_3A and C_4AF); as listed in Table 3-6, each clinkering reaction can take place in a given range of temperature and will either consume or generate heat. The most important of them is the formation of C_2S , due to it being highly exothermic. Referring to Figure 3-7 and Figure 3-8 clinker temperature peaks approximately where the highest flame temperature is attained. After this peak, the clinker cools down and its temperature drops to around 1600 K. The hot clinker leaves the kiln and is transported to the other sections of the cement plant for further processing.

Predicted Axial Profile in Kiln #1

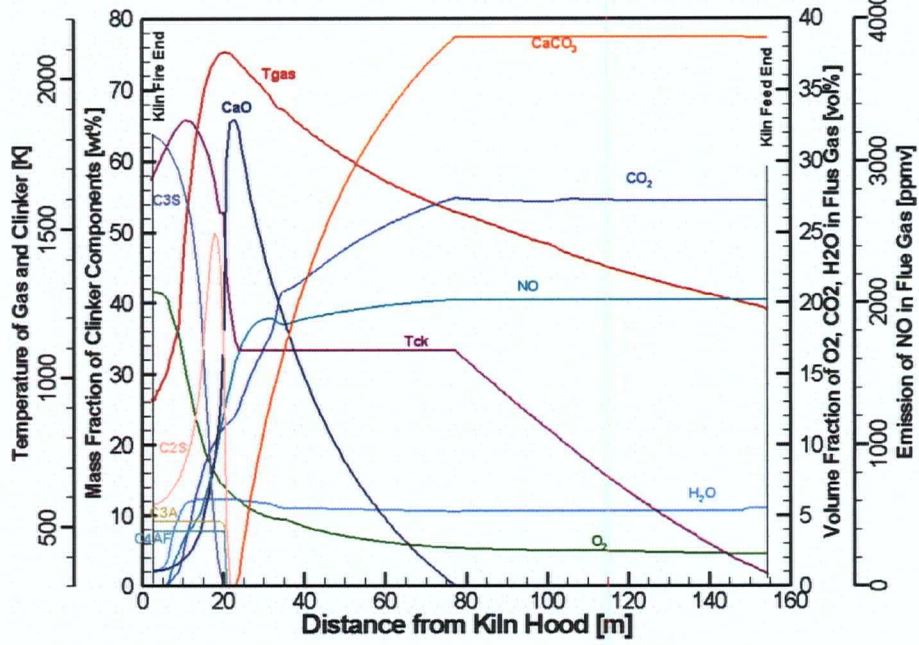


Figure 3-7: Axial profile of species in Kiln #1

Predicted Axial Profile in Kiln #2

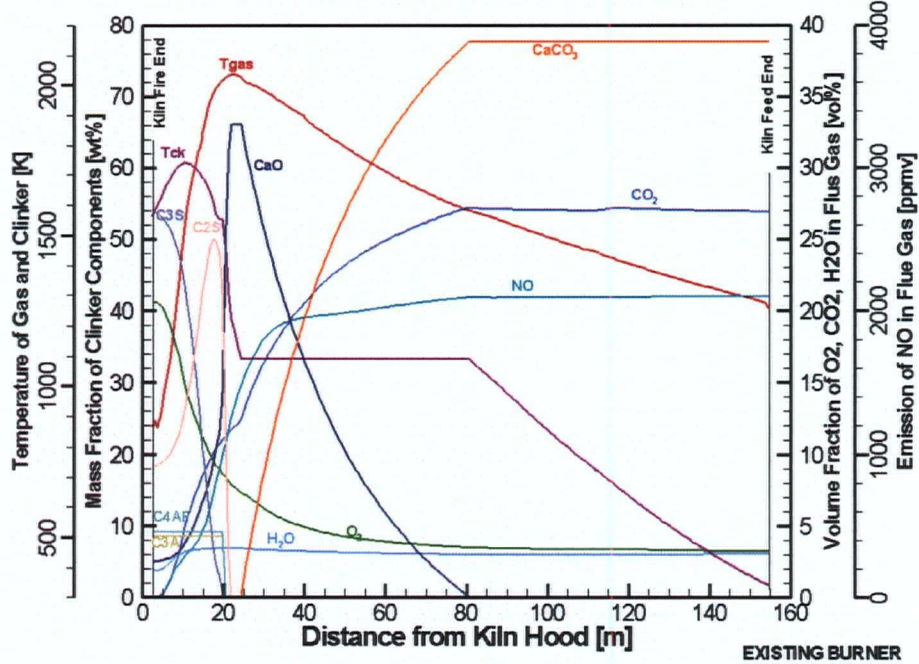


Figure 3-8: Axial profile of species in Kiln #2

3.9.3.1. Validation on Clinker Temperature at the Exit

A comparison between model result and plant measurement showed that the clinker temperature for Kiln #1 was well predicted. However, for Kiln #2 it was poorly predicted. Further investigation revealed that since inadequate heat has been absorbed by the bed of Kiln #2, its clinker temperature is lower than expected, its free-lime content is relatively high and its product quality is poor. Comparing the predicted clinker temperature at the exit with the plant data (Table 3-22) confirms that more heat should have been transferred to the bed of Kiln #2. Two possible modifications are recommended to compensate this matter: the first solution is to build a new grid with a bigger bed angle. This will increase the surface area of the bed and therefore, the heat flow to it. The second one is including the heat transfer between the wall and the bed in the model. In areas where the inner wall temperature is higher than the bed, such as burning zone, the direction of the heat flow will be from the wall to the bed, which results in a clinker with higher temperature in those areas temperature.

Table 3-22: Clinker temperature at the kiln exit

	Model prediction [K]	Reported from plant [K]
Kiln #1	1661	1633
Kiln #2	1562	1698

3.9.4. Gas Temperature Distribution

Figure 3-9 and Figure 3-10 show the contour plot of the temperature within the gas phase. According to these figures, as combustion takes place in the flame area, the flame temperature peaks, 2200 K at $x=25\text{m}$ from the burner. As the hot gas moves downstream, it loses heat and its temperature decreases, reaching around 1250 K at the exit. Elevated gas temperatures, especially in the flame area, indicates the high potential of cement kilns for formation of thermal NO_x .

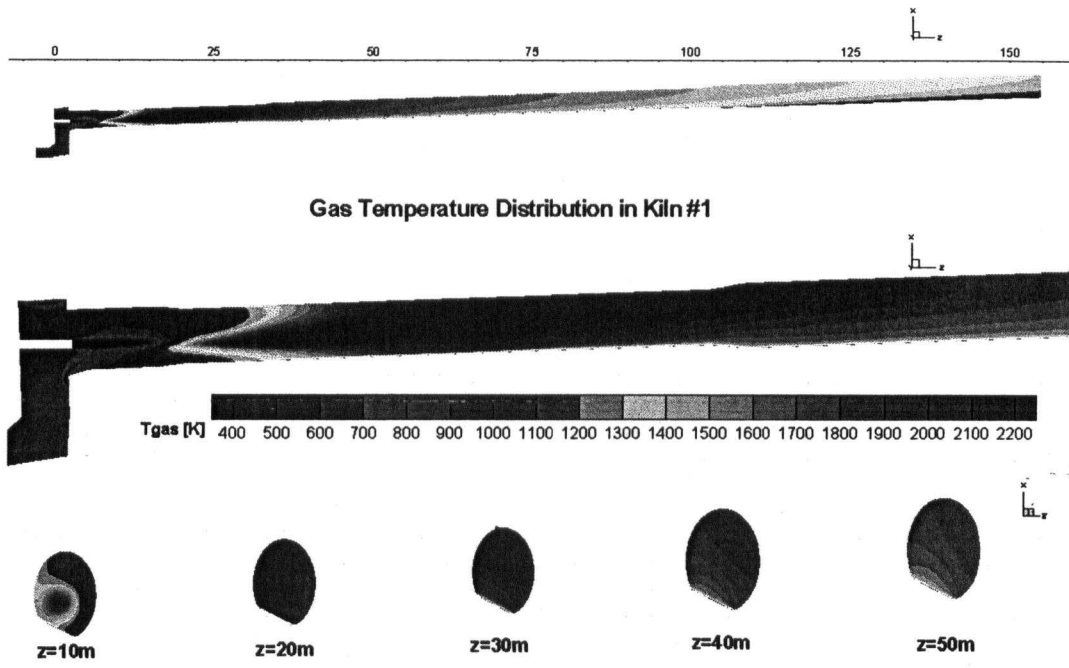


Figure 3-9: Gas temperature distribution in Kiln #1

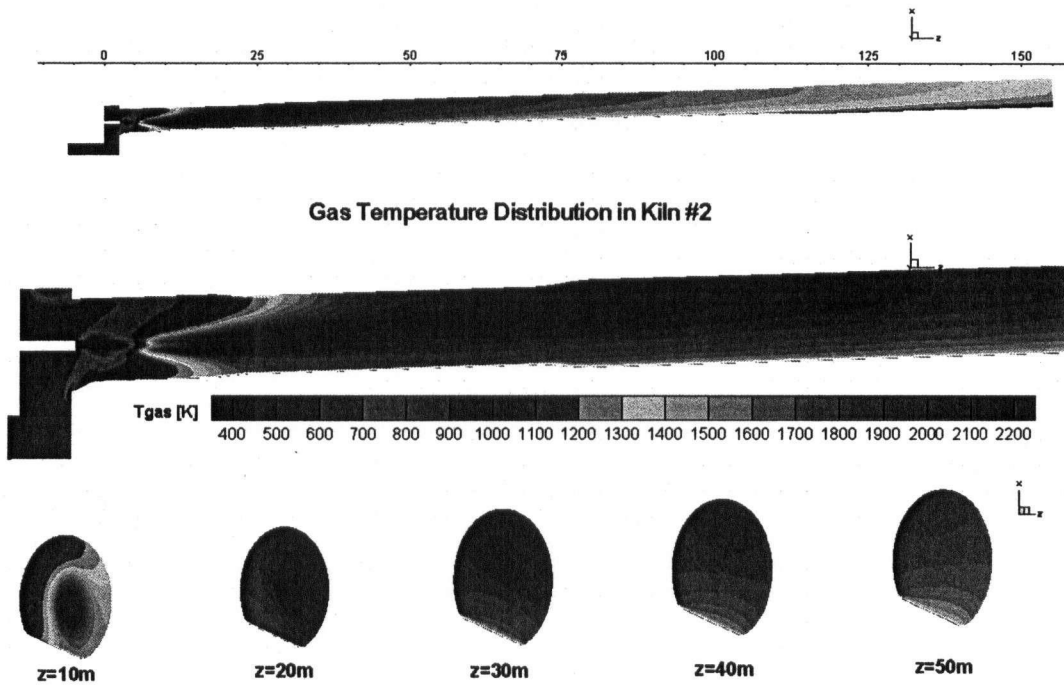


Figure 3-10: Gas temperature distribution in Kiln #2

3.9.4.1. Validation on Gas Temperature at the Exit

Table 3-23 contains a summary of the maximum and exit temperatures of the gas and the bed. As showed in this table, the predicted gas temperature is around 1250 K at the kiln exit while the measured gas temperature was reported to be around 1100 K. After investigation, we concluded that this difference is mainly due to ignoring dust circulation in the system for both kilns. By considering dust in the gas phase, some heat will be absorbed and carried away by these particles. In addition, dust particles contain calcium carbonate and are calcinated as they move downstream. Calcination consumes heat and this will reduce the gas temperature as well. Therefore, by considering dust circulation in the system the gas temperature will be reduced.

The coupling between the gas peak temperature and the clinker temperature is one of the important observations through Table 3-23. As mentioned earlier, we assumed that convection and radiation from the gas are the main heat sources for the bed. Due to very high gas temperatures, it can be concluded that the radiative term is the dominant one. The kiln with the higher gas peak temperature (i.e. Kiln #1) has a higher clinker peak temperature. Another important observation the interaction between the solid phase and the gas at the kiln exit; the kiln with the lower flue gas temperature (i.e. Kiln #1) has a higher clinker temperature at the exit and vice versa.

Table 3-23: Summary of the average gas and clinker temperature at the exit and the peak

	Kiln #1	Kiln #2
Gas temperature at the kiln exit [K]	1224	1260
Gas temperature at its peak [K]	2088	2033
Clinker temperature at the kiln exit [K]	1661	1562
Clinker temperature at its peak [K]	1862	1741

Here is an approximate calculation on how including dust will impact the gas temperature at the exit.

Table 3-24, for instance, contains the dust information for Kiln #1.

There are two energy aspects that have to be considered: difference of sensible heat of dusts, and required heat for dust calcination.

The enthalpy different between the return, material, and exit dust will be:

$$\begin{aligned}\Delta H &= H_2 - H_1 = H_e - H_r - H_m \\ &= (3.944 \text{ kg/s})(1.08 \text{ kJ/kg.K})(1063 \text{ K}) \\ &\quad - (2.639 \text{ kg/s})(1.08 \text{ kJ/kg.K})(367 \text{ K}) \\ &\quad - (1.70 \text{ kg/s})(1.08 \text{ kJ/kg.K})(338 \text{ K}) \\ &= 4.53 - 1.05 - 0.62 \\ &= 2.86 \text{ MW}\end{aligned}$$

In addition to this, dust carries some CaCO_3 . Calcination consumes heat and this heat has to be accounted for as well. The amount of available CO_2 in dust can be calculated based on given loss of ignition (LOI) and mass flow rate of each part. Therefore, the amount of net generated CO_2 due to dust calcination can be calculated:

$$\begin{aligned}\dot{m}_{\text{CO}_2} &= (2.639 \text{ kg/s})(0.097) + (1.70 \text{ kg/s})(0.3434) - (3.944 \text{ kg/s})(0.1132) \\ &= 0.256 + 0.584 - 0.446 = 0.394 \text{ kg/s}\end{aligned}$$

The amount of required heat for dust calcination will be

$$E = (0.394 \text{ kg/s})\left(\frac{100}{44}\right)(1679 \text{ kJ/kg}) = 1.5 \text{ MW}$$

Therefore, a total amount of $2.86+1.5=4.36$ MW of energy will be carried away by dust which has to be subtracted from the total flue gas enthalpy. The equivalent reduction in gas temperature at the exit will be:

$$\Delta T_g = \frac{\Delta H_g}{\dot{m} \cdot C_p} = \frac{4.36 \text{ MW}}{(27.8 \text{ kg/s})(1.08 \text{ kJ/kg.K})} = 145 \text{ K}$$

Considering this, the flue gas temperature will drop to $1224-145=1079$ K. This estimated flue gas temperature is now close to measured flue gas temperature at the plant (1100 K). So it can be concluded that considering kiln dust can bring the gas temperature down to values comparable to plant data. Same calculations can be performed for the other kiln.

Table 3-24: Dust information for Kiln #1

Return Dust Information	
Flow rate [kg/s]	2.639
Temperature [K]	367
LOI	0.097
Exit Dust Information	
Flow rate [kg/s]	3.944
Temperature [K]	1063
LOI	0.1132
Feed Material Dust Information	
Flow rate [kg/s]	1.7
Temperature [K]	338
LOI	0.3434

3.9.5. NO_x Emissions

Nitrogen oxides are hazardous pollutants. Their emissions have to be reduced and controlled as much as possible. Therefore, it is essential to estimate their emissions for any system that emits these pollutants, such as cement kilns, and try to reduce them by applying different technologies. As depicted in Figure 3-11 and Figure 3-12, due to having a very high temperature (over 1800° K), the NO concentrations in the flame area can be very high, 2600 ppm and 3600 ppm for Kiln #1 and #2, respectively. Moving downstream, the gas temperature decreases and hence the NO concentrations reduce and are 2020 and 2100 ppm at the exit of Kiln #1 and #2, respectively.

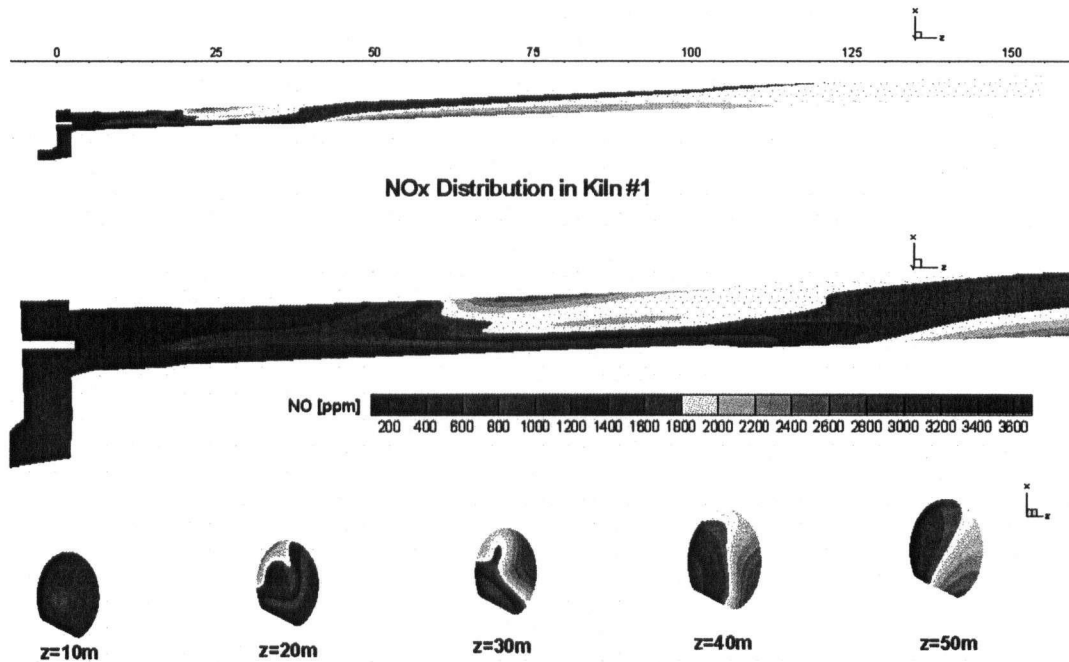


Figure 3-11: NO distribution in Kiln #1

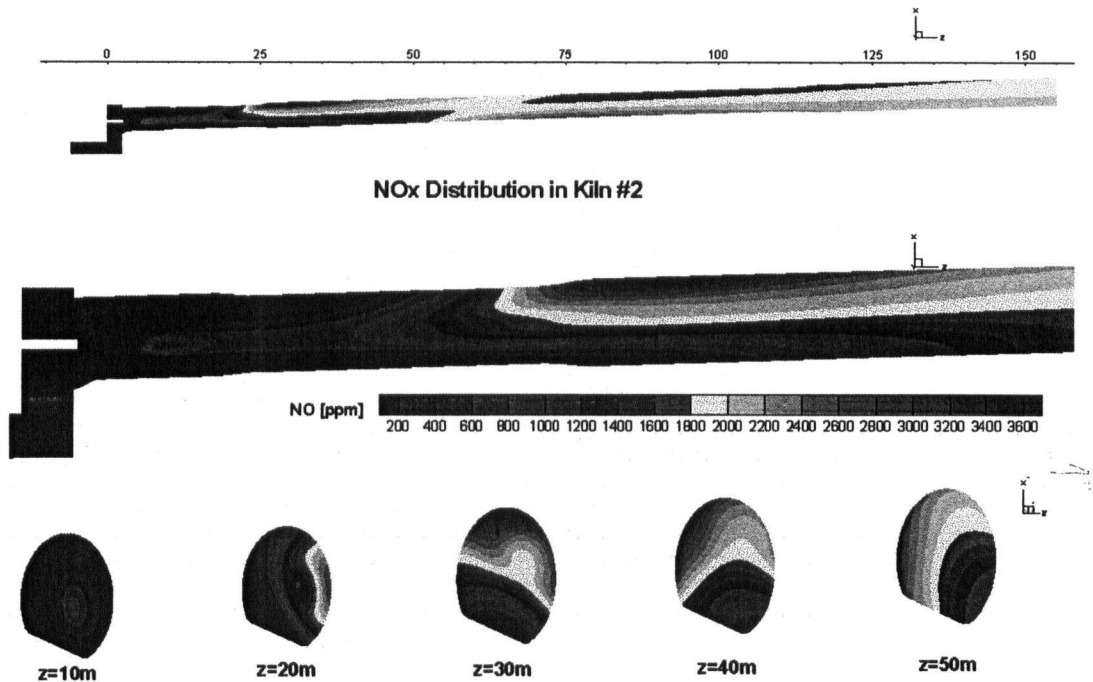


Figure 3-12: NO distribution in Kiln #2

3.9.6. Refractory Temperature Distribution

As explained earlier, the hot gas, the wall, and the bed interact and have impacts on each other. The inner wall temperature receives heat from the gas; some of this heat is absorbed and travels through the shell, and the rest will be reflected. In addition, the inner wall interacts with the bed, which as described before is neglected in this thesis. Due to the close interaction between the hot gas and the inner wall, similar trends can be observed in both of them. This fact can be confirmed by comparing the inner wall temperature distribution of these two kilns, Figure 3-13 and Figure 3-14, with the temperature distribution within the hot gas, Figure 3-9 and Figure 3-10. The inner wall temperature peaks where the maximum gas temperature is attained and will drop as the gas flows downstream. Due to the low ambient temperature, the outer wall loses heat and has a much lower temperature compared to that of the inner wall.

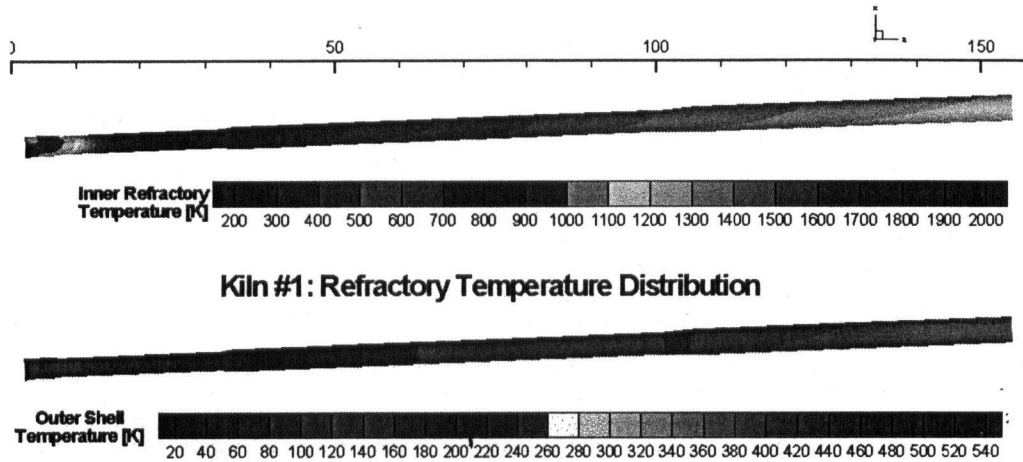


Figure 3-13: Refractory temperature distribution in Kiln #1

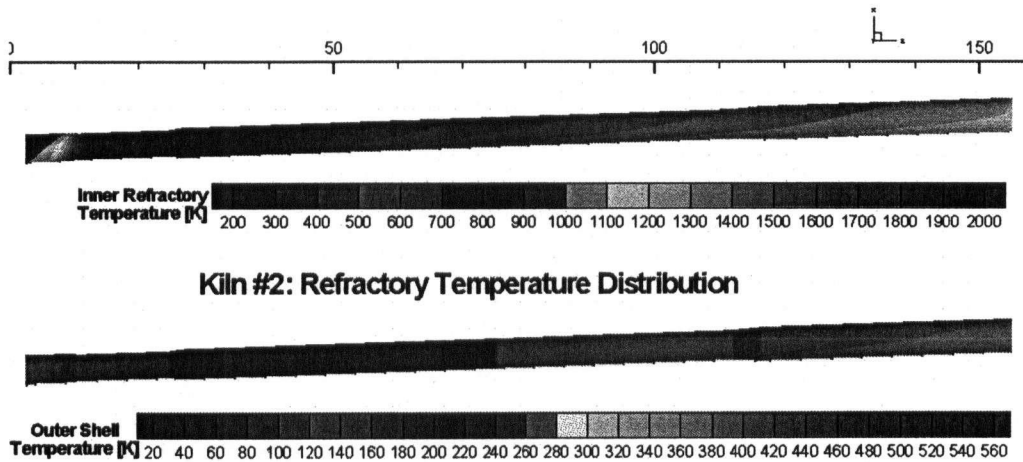


Figure 3-14: Refractory temperature distribution in Kiln #2

3.10. SUMMARY AND CONCLUSIONS

A one-dimensional mathematical model including all the main phenomena associated with the formation of clinker in the bed of material was developed and then implemented in a CFD code. With

the aid of this code, two full-scale cement rotary kilns under realistic operational conditions were targeted and simulated. The modeling results were analyzed and compared against limited available data. Kiln #1 showed good agreement with the experimental evidence of clinker quality; on the other hand, Kiln #2 had low clinker quality and temperature which were not observed in practice. The simulation result indicated a tight coupling between the amount of heat transfer to the bed and the clinker formation process. The likely reason for poor prediction for Kiln #2 is an incorrect evaluation of the heat flux to the bed as a result of an inadequate estimate of the bed angle.

An overall mass and energy balance was performed for both kilns. The analysis of the energy balance revealed that, for the cement kilns studied in this work: the combustion of the fuel accounts for 70 % of the total heat input and the rest is compensated by the sensible heat of the feed material and air. The heat lost via flue gases accounts for 50% of the total heat output, the solid material absorbs about 40-45% of the total energy and around 5% of the heat is lost to the ambient air through refractories.

Moreover, for further investigation of the simulation results, a series of plots were developed. These plots included the contour plots of temperature, NO distribution within the gas phase, and temperature distribution in the wall along with the axial plots of the average concentration of important species in the gas and solid phase.

Finally, it can be concluded that considerable progress has been achieved to develop a predictive tool for simulating the important processes in full-scale cement rotary kilns. By investigating the simulation results of two industrial kilns under realistic operational conditions and quantifying the energy and mass flows in various parts of the system, a better understanding of the cement kiln operation was achieved. It was shown that a reasonable estimate of the bed angle is necessary in order

to obtain good predictions. Also, the developed model can be used for simulating and studying cement kilns with different conditions, such as with a new firing system, a new type of fuel, a new energy distribution layout, or even a combination of them. The subject of the next chapter of this thesis is “Mid-Kiln Firing of Tires in Cement Kilns” in which the combustion of full scrap tires in the middle of the kiln is modeled and its impacts on the kiln operation are studied.

3.11. FUTURE WORK

In this work, some phenomena including dust circulation, heat transfer between the bed and the wall, and rotation of the kiln were neglected. Considering these phenomena can result in a more complete model with improved results and can contribute to a better understanding of the whole process. More specifically, considering dust circulation can lower flue gas temperature. In addition, including the heat transfer between the bed and the wall will have direct impact on the bed temperature and might bring the model predictions closer to the plant data. The kiln rotation is also important and should be implemented when heat transfer between the bed and the wall is considered.

In addition, more plant data are required for the validation of the simulation results such as the gas flow field, temperature distribution of the wall, and the bed height.

Chapter 4. MID-KILN FIRING OF TIRES IN CEMENT KILNS

4.1. INTRODUCTION

Approximately 2.5×10^6 tones of tire are produced in North America each year [27]. Due to an increase in vehicle usage, this rate is increasing. Scrap tires are not easily recycled and traditionally for many years, have been disposed of in stockpiles or landfills. Dumping tires has potential health and environmental hazards. For instance, tire stockpiles can catch fire (which are often hard to extinguish) and emit pollutants. In addition, wet stockpiles of tire can be breeding sites for mosquitoes. Some countries are planning to ban landfilling of tires in the near future. All this brings challenges for thinking of possible ways to reuse them.

Tires are made of rubbery materials and have high carbon content and high heating values. Scrap tires are cheap and available. These factors make tires a good choice for being utilized as fuel. Fuel from tires is also known as tire-derived fuel (TDF). Since for most of the cases, tires are burned as secondary fuel, the term “co-combustion of tire” is also frequently used. Tire-derived fuel is the largest market for scrap tire utilization. It accounts for about 82% of scrap tire recycling [28].

Cement kilns have excellent combustion characteristics for burning scrap tires. They operate at very high temperatures and have long residence times. With an adequate supply of oxygen, complete burnout of tires can be achieved inside them. They also have the potential to use 100% of scrap tire in a completely efficient manner [29]; the ash from tire combustion is combined into clinker and does not require any disposal. In addition, tire combustion in cement kilns seems to be environmentally sound; based on a report [30], co-combustion of scrap tires results in either a decrease or no change in the emissions of the pollutants such as CO, NO_x, SO₂ and particulate matters. Tire-derived fuel in cement kilns is experiencing an increasing trend.

One of the main objectives of this work is to simulate the combustion of tires inside cement kilns (which is also known as “mid-kiln firing of tires”). It should be mentioned that the expression “mid-kiln” does not necessarily mean the middle point of the kiln. In mid-kiln firing of tires in cement kilns, full scrap tires (in one piece without any pre-processing), via a special conveyor, will be elevated and thrown (injected) somewhere inside the kiln. Originally, there is no opening on the kiln shell foreseen for this matter; hence, a special opening will be created at a designated axial location. Through this opening a number of tires will be thrown into the kiln. Tires will fall and rest on top of the solid material and move with it to the downstream of the kiln (where the main fuel is burned). As they move down, they gain heat and burn. In co-combustion, the amount of heat being released from tire combustion will compensate the reduction in the mass flow rate of the original fuel.

It was mentioned that full tires are injected into the middle of the kiln, but it was not explained why tires are in one piece and not shredded, and why in the middle of the kiln rather than in a hot area such as the flame area. The supply of tire for cement kilns can be done in two different ways: whole and chipped. Both have their own advantages and disadvantages [31]. Combustion of chipped tire particles has been employed at many facilities worldwide. Shredded tires can be introduced into the burner zone of the kiln and can be consistently delivered to the fuel system. But the high cost of shredding often makes it uneconomical. On the other hand, burning the whole tire is usually cheap; there is no shredding cost involved. However, in order to inject full tires in the middle of the kiln, a new fuel entry point and a special fuel delivery system will be required. This, in fact, imposes some additional cost. Some kilns have chain curtains (which act as a heat exchanger) at the feed end. The chain section permits only the flow of fine materials and acts as a barrier to the movement of large tires. Therefore, for kilns with chain section, large tires cannot be injected at the feed end and have to be injected somewhere else.

One of the main reasons for burning the tires in the middle of the kiln is its influence on the energy distribution of the system. Before introduction of the tire, the fuel is burned in one zone (flame area). By co-combustion of tires in the middle of the kiln, the energy required for the processes within the kiln will not be concentrated in one spot and will be distributed. This is known as fuel staged-combustion. Staged-combustion is effective in reducing NO_x emissions because it lowers the concentration of oxygen and nitrogen in the primary combustion zone, it reduces the peak flame temperature by allowing for gradual combustion of the fuel, and reduces the amount of time the fuel and air mixture is exposed to at high temperatures. However, the amount of co-combustion of tires is limited (10-20% energy-based) for different reasons. First, as mentioned earlier, tires will be thrown into the middle of the kiln through an opening which is sized based on the size of the tires. Its size is also optimized such that the amount of energy and mass lost through it is minimized. In addition, tires are fed into the kiln discontinuously; whenever the opening meets the end of the conveyor, it will be opened to let the tires in, which takes some time. Based on the size of the opening and the available time for having the entrance open, there will be an upper limit for the number of the tires that can be thrown into the kiln. Thus, the percentage of co-combustion of tires is practically bounded by an upper limit. In addition to this practical obstacle, because of the process and the flow of the cement kilns, at least a certain amount of energy should be released in the flame area to trigger the clinkering reactions. "... Field studies have also confirmed that TDF (Tire-Derived Fuel) can be used successfully as a 10-20% supplementary fuel in properly designed solid-fuel combustors with good combustion control and add-on particulate controls ..."[32].

Another good question is "if the energy distribution is good and can reduce the emissions of pollutants, why not have as many openings as possible?" This is mainly because of their disadvantages. Significant amount of heat and mass can be lost through an opening, and each opening

will need its own conveyor and imposes some costs. In order to maintain a plant at profitable and efficient conditions, it is essential to minimize the losses and operating cost. Also, the location of the opening is important and cannot be at any axial position. Tires should be injected at locations where complete combustion of them can be ensured (where gas temperature is high enough) and is practical. For example, due to excessive gas temperatures and thick coating in the burning zone, placement of the injector in that section would not be practical. Because of the very high temperature within the burning zone, some of the solid material (around 20-30%) will melt and form liquid; as the kiln rotates and the material flows some of this molten material will stick to the inner wall and coat it [25]. In some areas of the burning zone, the coating layers can be thick which will cause practical difficulties in placing the opening. In addition, as mentioned earlier, tires cannot be injected into the chain section either. For these reasons, tires are usually introduced at the beginning of the transition zone, between the burning and calcining zone where high gas temperatures, not excessive, are encountered. Because the transition zone is usually short, it would not be practical to have more than one opening.

This chapter is organized as follows: first the objectives of this work are mentioned which are followed by literature survey. After this, the physical and mathematical model for tire combustion is described. Then, the geometry and boundary conditions for a test kiln are summarized. Later, the results, including a parametric study along with some tables and figures, are presented and analyzed. Finally, summary and conclusions are explained.

4.2. OBJECTIVES

The objectives of this chapter are to develop a tool to simulate scientifically the tire combustion phenomena, improve the understanding of combustion of tire in rotary kilns, study its impacts on the

product quality and process, explore the limitations on the flow rate and axial location of tire injection, and finally quantify the stack emissions mainly nitrogen oxides.

In order to fulfill the above objectives, a simplified one-dimensional model for tire combustion was developed and then implemented in the UBC CFD code developed in our research group [18, 21]. A test cement kiln with different operational conditions was simulated and the final results were compared and analyzed.

4.3. LITERATURE SURVEY

A literature review showed that no investigations regarding the combustion of full tires were done let alone on their combustion in the middle of the cement kilns. The combustion of tire takes place in two steps: the first step is called “devolatization” or “pyrolysis,” during which the volatile content changes phase (from solid to gas); the second step, known as “char combustion,” occurs as the fixed carbon of tire reacts with oxygen and releases heat [33]. The occurrence of devolatization is the key to the availability of the fixed carbon and no char combustion occurs if no volatile matter has been released before. It is also important to mention that in an inert atmosphere (in the absence of oxygen) only pyrolysis without char combustion takes place. The combination of these two processes is known as “tire combustion” phenomenon and any mathematical model proposed for tire combustion should include both of them. Different authors have investigated the pyrolysis and combustion of shredded (small) tire particles [34-37]; however, for our work, literature with emphasis on the devolatization and combustion of large tire particles was required.

To the author’s knowledge, there were no articles on combustion of large tire particles; however, two articles on the pyrolysis of large tire particles were found. The first one was by J. Yang *et al.* [38] in

which a two-dimensional transient pyrolysis model for large tire particles (cylindrical samples with a diameter of 40 mm and a length of 60 mm) was introduced. Their model included a combination of heat transfer, mass transfer, and pyrolysis kinetics. They concluded that the slowest processes are the conduction and mass transfer in the reaction zone. Therefore, the rates of these processes control the overall rate of the tire pyrolysis. Dealing with a large size of tire particle samples with a high content of volatile matters (VM) differentiates their work from other pyrolysis models. The model was tested against experimental data and good agreement was found.

The second article was recently published by M. B. Larsen *et al.* [39]. They performed an experimental study in order to investigate the effects of particle size and surrounding temperature on the devolatilization rate of large tire particles in which cylindrical tire particles with diameters between 7.5 and 22 mm were tested. They found a significant effect of particle size and surrounding temperature on the rate of devolatilization, i.e. larger particles and lower temperatures increase the devolatilization time. They also developed a mathematical model for the devolatilization process including internal and external heat transfer, three parallel devolatilization reactions, and reaction enthalpy effects. They also revealed good agreement with experimental data.

The two latter articles were both on large tire particles; but they both lacked the combustion step, and the particles used by them were still not big enough for our work. Although none of the above literature was giving adequate information and data for our case, their process insight and thermal and kinetics data were inspiring and useful. With the aid of the above articles and a basic knowledge on char combustion, a one-dimensional mathematical model for the tire combustion (including devolatilization and char combustion) was developed and implemented in our CFD code. With this model, co-combustion of full scrap tires inside a test cement kiln with different operational conditions was simulated and investigated.

4.4. PHYSICAL MODEL

In mid-kiln firing of tires, full tires are thrown in the middle of the kiln and burned. This description is rather general and needs more explanation. Further explanation on the whole phenomenon is given as follows: full tires, after being injected through an opening into the kiln, rest on top of the bed and move with it towards the flame area. Meanwhile, the tire gains heat from its vicinity, mainly the hot gas flowing on top of it. When the surface layer becomes hot enough, the devolatilization reactions begin and some volatile matter is released into the atmosphere. As the heat is transferred towards the core of the tire, the devolatilization reactions develop deeper into it. At the same time, the fixed carbon content of the tire reacts with the available oxygen, and some heat will be released; this step is known as "char combustion". This whole process goes on until nothing but ash is left.

4.4.1. Assumptions

For mid-kiln firing, full tires are thrown into the kiln through an opening. Practically, this opening decreases the efficiency of the kiln by allowing the outflow of mass and heat. However, in order to facilitate the modeling, this opening was not included in the physical model. In this work, tire injection part (from the point they are thrown until they rest on top of the bed) was neglected, and tires were introduced on top of the bed. From this point it was assumed that tires move downstream with the same velocity as the bed has until they are completely burned and nothing but ash is left. The remaining ash leaves the kiln at the exit.

It also assumed that the tires are continuously fed to the kiln. The rate is calculated based on the number of tires injected per revolution and kiln angular velocity. Only one heat source for tires is considered and that is the radiative term from the hot gas on top of them.

In addition, the effect of tire on the gas flow field is considered negligible and no physical thickness is accounted for tires. However, the surface area of tires is a key parameter that has a direct impact on the heat flow calculations to tire and is addressed when the heat transfer equation is introduced.

4.5. MATHEMATICAL MODEL

In order to complete the code and include tire combustion in it, two general steps were taken. First, the 1-D model for combustion of tires was developed; then, this model was coupled with the existing code for cement rotary kiln (which was developed in the previous chapter).

4.5.1. Tire Combustion Model

Mathematically, tire combustion consists of two steps: a set of devolatilization reactions and a final step of char combustion. Both steps are governed by internal and external mass and heat transfer, and kinetics of chemical reactions. Modeling tire combustion including all the above mentioned mechanisms would not be possible because of the lack of data and knowledge. Therefore, a simplified model based on the governing mechanisms, that limit the rate for each step, was developed.

4.5.1.1. Heat Transfer

First of all, according to the following formula, the net heat flux absorbed by the tire was calculated.

$$\dot{Q}_{net} = \sigma A_t \varepsilon_t (T_g^4 - T_t^4) \quad (4-1)$$

where \dot{Q}_{net} is the net heat flow rate (W), $\sigma = 5.671 \times 10^{-8} \text{ W}/(\text{m}^2 \cdot \text{K}^4)$ is the Stephan-Boltzmann constant, A_t is the area of tire (m^2), ε_t is the tire emissivity, T_g is the gas average temperature (K) and T_t is the tire temperature (K). Tire surface area was calculated based on the diameter of tire and tire rim. The area was assumed to be constant. It should be mentioned that tires do not necessarily occupy the full surface of the mud; the amount of coverage depends on the ratio of the tire surface and the mud surface in each control volume.

Knowing the net heat flux and tire mass flow rate, the new tire temperature at the exit of each control volume was calculated with the following equation

$$T_{t,new} = T_{t,old} + \dot{Q}_{net} / (\dot{m} \cdot C_p) \quad (4-2)$$

where $T_{t,new}$ is the new tire temperature (at the end of the control volume) in Kelvin, $T_{t,old}$ is the old tire temperature (at the beginning of the control volume) in Kelvin, \dot{Q}_{net} is the net heat flow rate (W), \dot{m} is the tire mass flow rate (kg/s), C_p is the specific heat of tire ($C_p = 2000 \text{ J}/\text{kg} \cdot \text{K}$ [39]).

The tire mass flow rate is calculated as follows

$$\dot{m} = (N_t \cdot W_t \cdot \omega) / 60 \quad (4-3)$$

where N_t is the number of tires injected per revolution of the kiln (tire/rotation), W_t is the weight of one tire (kg/tire) and ω is the rotational speed of the kiln (rotation/min).

It is also assumed that no temperature gradient exists within the tire and the whole particle is at a single average temperature. This average temperature $(\frac{T_{t,new} + T_{t,old}}{2})$ was used for calculating the rate of devolatilization reactions in each control volume.

4.5.1.2. Devolatilization Process

Devolatilization is the process of transformation of volatile matter content into gas. In the present work, inspired by others such as M. B. Larsen *et al.* [39] and J. Yang *et al.* [38], it is assumed that tire devolatilization consists of three independent parallel reactions and takes place in a single step according to the following equation



We assumed that the external heat transfer and chemical reaction kinetics were the controlling parameters for the devolatilization process. Mass transfer and internal heat transfer were neglected. As explained by M. B. Larsen *et al.* [39], these assumptions have been successfully used by other authors in the devolatilization modeling.

Mathematically, the devolatilization process was formulated with a first-order Arrhenius equation as [39]

$$\frac{dx_i}{dt} = -A_i \exp\left(\frac{-E_i}{RT}\right) x_i, i = 1,3 \quad (4-5)$$

where x_i is the mass fraction of the volatile component.

After being initiated, the devolatilization goes on until no volatile matter is left. Table 4-1 contains a summary of the initial mass fraction for each volatile component and the kinetic parameters for each reaction, taken from M. B. Larsen *et al.* [39]. The summation of the initial fractions of three volatile components is equal to 64%, which indicates the total volatile matter content of the sample tire used in this work.

Table 4-1: Composition and kinetic parameters

Parameter		Value	Unit
Initial mass fraction of volatile specie i	$x_{1,0}$	0.15	kg/kg
	$x_{2,0}$	0.13	kg/kg
	$x_{3,0}$	0.36	kg/kg
Pre-exponential factor and activation energies	E_1	49.1	kJ/mol
	A_1	100	1/s
	E_2	207	kJ/mol
	A_2	3.93×10^{14}	1/s
	E_3	212	kJ/mol
	A_3	1.05×10^{13}	1/s

4.5.1.3. Char Combustion

Based on the proximate analysis, the fixed carbon content of tires is usually high. For instance, as indicated in Table 4-2, the sample tire for this work contains 29.7% fixed carbon. This means that char combustion is important and cannot be neglected.

For char combustion, the amount of available char at each control volume was required. As explained earlier, carbon becomes available only if the devolatilization has already happened; in other words, there will be no carbon to burn if no volatile matter has been released before. In order to quantify this,

we assumed that the amount of exposed carbon for combustion, based on the proximate analysis, is proportional to the amount of volatile matter released in each control volume. After being exposed to the air, the carbon reacts with oxygen and burns. The reaction of fixed carbon with oxygen is char combustion. For simplicity, we assumed that oxygen availability is the only controlling parameter for this phenomenon. If enough oxygen is available, all the exposed carbon reacts with the oxygen molecules and CO₂ is formed. This CO₂ is released to the gas. If the amount of available oxygen is not adequate, a portion of it burns and the rest combines with the unburned carbon content (if any) transported from the previous control volumes and is transferred to the next control volume. Char combustion proceeds until no fixed carbon is left. The end of char combustion is the end of tire combustion and after that, nothing but tire ash is left. The char combustion reaction ($C + O_2 \rightarrow CO_2$) is exothermic and as a result, the gas temperature increases in the adjacent area. The heating value of this reaction is 32.79 MJ/kg.

Table 4-2: Proximate, ultimate analysis and lower heating value for the tire rubber [39]

		Truck tire rubber	Unit
Proximate analysis	Volatiles	64.1	wt%
	Fixed C	29.7	wt%
	Moisture	1.2	wt%
	Ash	5.0	wt%
Ultimate analysis	C	82.0	wt%
	H	6.71	wt%
	S	1.35	wt%
	N	0.32	wt%
	O	3.42	wt%
Lower heating value		35.0	MJ/kg

4.5.2. Formation of Thermal NO_x

In the existing code, the formation rate of thermal NO_x was mathematically predicted by the following equation

$$\frac{d[NO]}{dt} = 2[O] \frac{(k_1 k_2 [O_2][N_2] - k_{-1} k_{-2} [NO]^2)}{(k_2 [O_2] + k_{-1} [NO])} \quad (gmol / m^3 .s) \quad (4-6)$$

For the simulations in this chapter, the rate data (k_i) were selected from the work done by Baulch *et al.* and the equilibrium approach was used for determining the concentration of oxygen radicals (see Appendix 1 for more detail). The source term due to thermal NO_x formation is calculated with the following equation

$$S_{th,NO} = M_{w,NO} \frac{d[NO]}{dt} \quad kg / (m^3 .s) \quad (4-7)$$

where $M_{w,NO}$ is the molecular weight of NO, and $\frac{d[NO]}{dt}$, the formation rate, is computed as mentioned above.

4.5.3. Modified Parent Code

In order to simulate the combustion of tire in the middle of the cement kilns, the developed code for modeling cement kilns (as in previous chapter) was modified. The modifications included the interactions between the hot flow and tires and consisted of heat and mass transfer between them.

For including the mass transfer, the gaseous component being released or absorbed due to tire combustion were accounted for. After calculating the extent of devolatilization, based on the

composition of the tire and knowing the tire mass flow rate, the flow rate of each species (O₂, CH₄, CO₂, H₂O, etc.) was calculated.

As seen in Table 4-2, tire composition in elemental form (the mass fractions of elements such as C, H, O, etc.) is given. If this tire composition was going to be considered in the calculations, their own transport equations had to be written and solved. This, in fact, increases the complexity of the problem and requires a significant amount of time for development. Therefore, with a pre-processing code, the elemental analysis of the tire was converted into molecular composition (mass fractions of molecules O₂, CH₄, CO₂, H₂O, etc. as in Table 4-6). Similar to many other CFD codes, this form was suitable for our code and there was no need for considering any additional transport equations.

In addition to the release of gaseous components due to the devolatilization, the mass transfer due to the char combustion was also considered. The amount of consumed oxygen was treated as a sink term in the transport equation of oxygen in the gas flow field; similarly, the formed CO₂ was added as a source term in its transport equation.

The source terms for the conservation equation of the species (S_{m_i}) as in Table 1-1 were calculated with the following equations

$$S_{O_2} = -F_t \cdot m_C \cdot 32/12 \quad (4-8)$$

$$S_{CH_4} = F_t \cdot m_{vol} \cdot x_{CH_4} \quad (4-9)$$

$$S_{CO_2} = F_t (m_{vol} \cdot x_{CO_2} + m_C \cdot 44/12) \quad (4-10)$$

$$S_{CO} = F_t \cdot m_{vol} \cdot x_{CO} \quad (4-11)$$

$$S_{H_2O} = F_t \cdot m_{vol} \cdot x_{H_2O} \quad (4-12)$$

$$S_{H_2} = F_t \cdot m_{vol} \cdot x_{H_2} \quad (4-13)$$

$$S_{C_m H_n} = F_t \cdot m_{vol} \cdot x_{C_m H_n} \quad (4-14)$$

where S_{m_i} is the source term of each component (kg/s), F_t is the tire flow rate (1/s), x_i is the mass fraction of each component (wt%), m_C is the mass of fixed carbon (kg) and m_{vol} is the mass of volatile matter (kg).

In order to conserve energy, in addition to accounting for the heat transfer between tire and the hot gas (which was explained earlier), the enthalpy effects from tire combustion were also included. Equation (4-15) includes all these effects: the first term accounts for the pyrolysis heat, the second term accounts for the heat release due to the char combustion, and the last term accounts for the sensible heat of gaseous components. S_h was treated as a source term for the energy equation of Table 1-1.

$$S_h = F_t (m_{vol} \cdot \Delta H_{pyro} + m_C \cdot \Delta H_{ch} + (m_{vol} + m_C) T_t \cdot C_p) \quad (4-15)$$

where S_h is the additional energy considered as a source term in energy equations of the gas phase (W), F_t is the tire flow rate (1/s), m_C is the mass of carbon (kg), ΔH_{pyro} is the pyrolysis heating value (J/kg), m_{vol} is the mass of volatile matter (kg), ΔH_{ch} is the heat of char combustion (J/kg), T_t is the tire temperature (K) and C_p is the specific heat of tire.

4.6. GRID AND BOUNDARY CONDITIONS

For simulating tire combustion in cement kilns, the grid including the proper boundary conditions for all its sub-models (the hot flow, the wall, the clinker and tire combustion) was required.

4.6.1. Test Kiln

For the simulations in this chapter, the cylindrical section of Kiln #1, referred to as test kiln, was targeted and then proper boundary conditions were prescribed. The developed grid included 23, 37 and 213 nodal points, in r , θ and z direction respectively. The boundary conditions for the hot flow including the primary air, secondary air, fuel and wall conditions are schematically shown in Figure 4-1. In addition, the imposed boundary conditions for the hot flow and the bed model are tabulated in the following tables. It should be stressed that the kiln characteristic data were extracted and supplied by Dr. Jerry Yuan and the grid with the proper boundary conditions was generated with a special software developed by Dr. David Stropky.

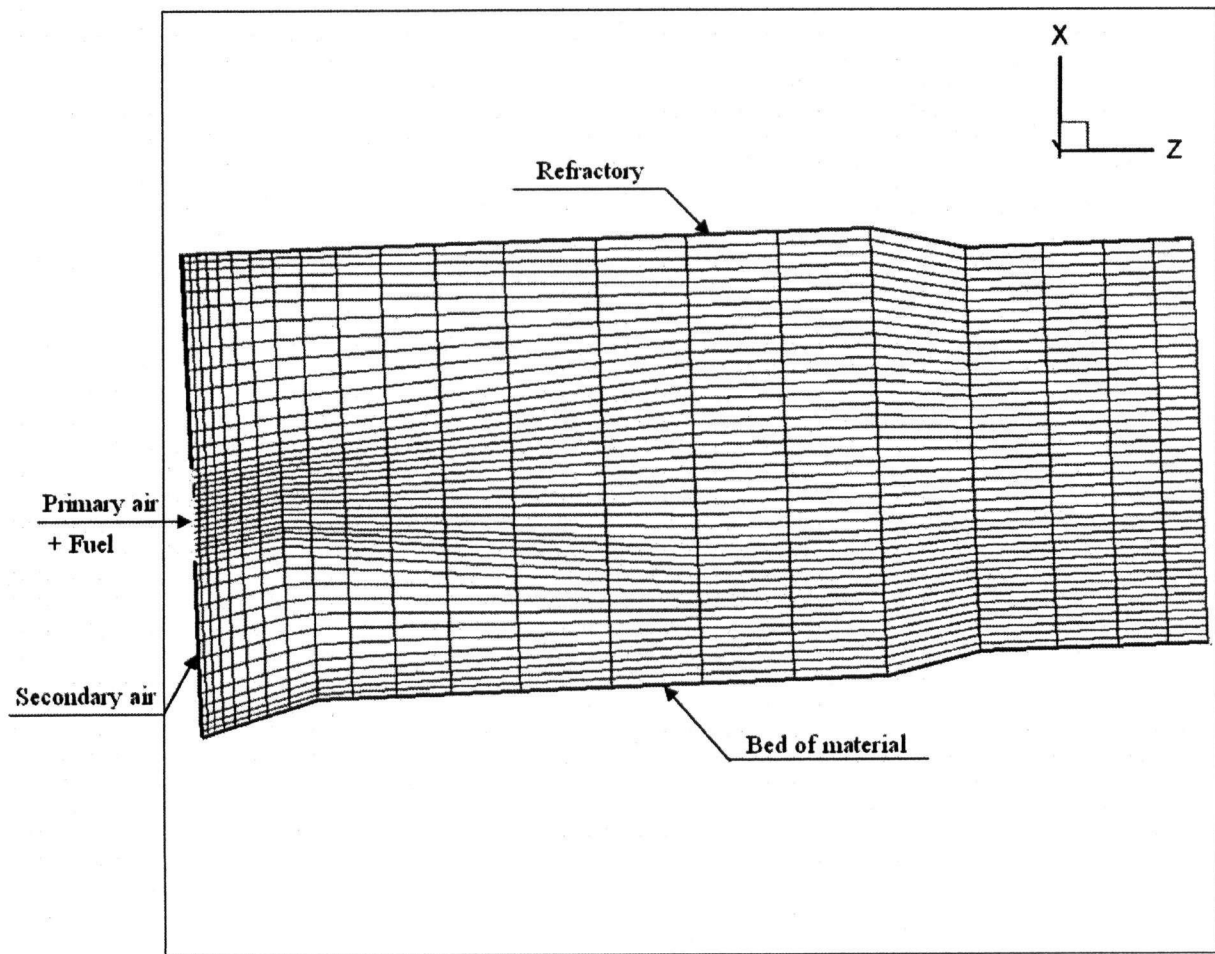
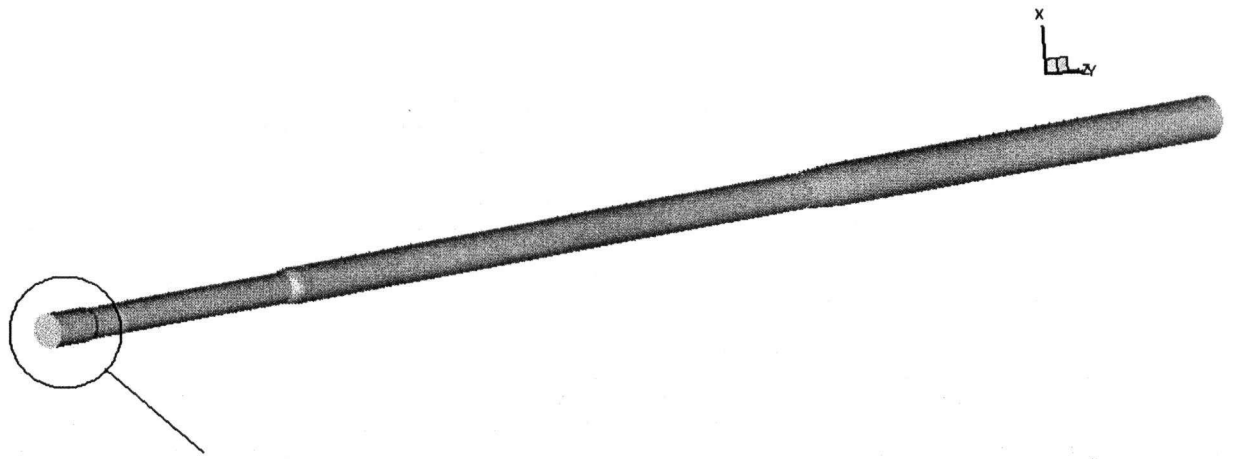


Figure 4-1: Boundary conditions for test kiln

Table 4-3: Material information for test kiln

Inlet Material Information	
Flow rate [kg/s]	20.8
Temperature [K]	338
Component	Mass Fraction (% wt)
<i>CaCO₃</i>	77.23
<i>CaO</i>	0.00
<i>SiO₂</i>	13.69
<i>Al₂O₃</i>	3.36
<i>Fe₂O₃</i>	1.7
Inert + others	3.85
Moisture	0.17
Total	100
Clinker Information	
Flow rate [kg/s]	13.52
Temperature [K]	1633

Table 4-4: Fuel input information for test kiln

Fuel type	Coal/coke
Flow rate [kg/s]	2.72
Temperature [K]	333
Proximate Analysis (%)	
Moisture	1.24
Volatile	21.86
Fixed Carbon	67.35
Ash	9.55
Total	100
Elemental Analysis (%)	
Moisture	1.24
Carbon	71.81

Hydrogen	3.73
Nitrogen	1.08
Sulphur	5.45
Oxygen	7.14
Chlorine	0.00
Ash	9.55
Total	100
High heating value (HHV) [kJ/kg]	27566
Low heating value (LHV) [kJ/kg]	26720

Table 4-5: Air input information for test kiln

Primary Air	
Flow rate [kg/s]	6.52
Temperature [K]	365
Secondary Air	
Flow rate [kg/s]	21.3
Temperature [K]	1122
Total air flow rate [kg/s]	27.82

In addition to the above conditions, it is assumed that the kiln shell loses heat, through natural convection and radiation, to the ambient atmosphere with $T_{amb}=30\text{ }^{\circ}\text{C}$. Moreover, a zero-gradient boundary condition was imposed for the kiln exit. Chapter 2 contains more detail about the boundary conditions.

The above boundary conditions are for test kiln with basic conditions, i.e. without any co-combustion of tire. For simplicity, we assumed that the total amount of heat needed for the whole process within the kiln is constant for all the cases. We also assumed that the airflow and distribution (flow rates,

inlet temperatures, and injection points) would remain unchanged and only the fuel mass flow rate changes for cases with tire combustion. Whenever co-combustion of tire existed, based on the heating values of the original fuel, tire and the amount of co-combustion, the fuel mass flow rate was modified and the rest of boundary conditions remained unaffected. For instance, for the case with 20% co-combustion of tire, the flow rate of the original flow was reduced to $2.72 \times 0.8 = 2.176$ kg/s .

4.6.2. Tire Combustion Model

The boundary conditions for tire combustion model were handled separately. Table 4-6, for instance, contains a summary for the boundary conditions for the case with 20% co-combustion of tire. Similar to the mass flow rate of the original, the tire flow rate was adjusted for different co-combustion percentages. This setting was done by changing proportionally the number of tires dropped per rotation for different co-combustion rates.

Table 4-6: Input data for tire combustion sub-model for the case with 20% co-combustion

Number of tires dropped in a rotation	6
Kiln rotation speed, rpm	1
Axial location of tire drop in, m	50
Tire temperature when dropped in, K	300
Weight of one whole tire, kg	4.15
Tire diameter, m	0.5776
Tire rim diameter, m	0.3556
Tire specific heat, J/kg.K	2000
Chemical composition of the volatile matter content (w_i)	
CH ₄ content, wt%	0
CO ₂ content, wt%	0
CO content, wt%	9.34

H ₂ O content, wt%	0
H ₂ content, wt%	3.99
C _m H _n content, wt%	83.63
Lower heating value of C _m H _n , MJ/kg	40.217

4.7. SOLUTION METHODOLOGY

After finishing the initial set-up of the problem, which consisted of the development of the tire combustion model, its implementation in the existing code, and grid generation along with the assignment of the appropriate boundary conditions, the system of the equations for the whole model was solved. The final code was executed in three steps: first, the cold flow field was created. Then, the code including all the sub-models was executed until a good convergence was achieved. After simulating the problem, including all the primary parameters, in order to get the concentration of secondary species (such as NO), the post-processing code was used. The computations related to formation of nitrogen oxides were decoupled from those of the main code and handled in a post-processor. We stress again that the decoupling allows freezing the whole flow field and only executing the post-processing in order to calculate for the species related to the formation of nitrogen oxides. This, in fact, will save a lot of computational time.

4.8. RESULTS AND DISCUSSION

Originally, three different test cases were simulated: the first case had no tire combustion, and the second and third cases were with 10% and 20% co-combustion of tire, respectively. In all the above simulations, tires were injected at $x=50$ m; this distance is measured from the burner end.

4.8.1. Mass and Energy Balance

Table 4-7 to Table 4-9 contain a summary of the mass and energy balance for the above mentioned cases. Both terms are well balanced for all cases. This indicates that the coupling between the main code and tire combustion model is properly done; it also indicates that the code has reached a satisfactory level of convergence. A detailed discussion on the important parameters is presented later.

Table 4-7: Mass and energy balance: without co-combustion of tire

Input	Mass flow rate [kg/s]	Average temperature [K]	Enthalpy [MW]	Percent [%]
Sensible heat in air	27.8		28.0	25.60
Sensible heat in feed material	20.788	338	7.645	6.99
Sensible heat in fuel	2.717	333	1.135	1.04
Sensible heat in tire	-	-	-	-
Heat form fuel combustion			72.59	69.4
Heat from tire combustion			-	-
<i>Total</i>	<i>51.305</i>		<i>109.37</i>	<i>100</i>
Output	Mass flow rate [kg/s]	Average temperature [K]	Enthalpy [MW]	
Exit gas losses	37.1	1225	50.1	45.50
Clinker discharge	13.691	1811	29.441	26.72
Fuel ash discharge	0.448		0.68	0.62
Tire ash discharge	-	-	-	-
Heat absorbed by clinkerization			21.291	19.34
Shell heat losses			7.20	6.54
Heat of unburned carbon			1.328	1.21
Heat of water evaporation			0.076	0.07
<i>Total</i>	<i>51.239</i>		<i>110.116</i>	<i>100</i>
Imbalance	<i>0.066</i>		<i>-0.746</i>	

Table 4-8: Mass and energy balance: with 10% co-combustion of tire

Input	Mass flow rate [kg/s]	Average temperature [K]	Enthalpy [MW]	Percent [%]
Sensible heat in air	27.8		28.0	25.60
Sensible heat in feed material	20.788	338	7.645	6.99
Sensible heat in fuel	2.445	333	1.022	0.93
Sensible heat in tire	0.208	300	0.125	0.11
Heat form fuel combustion			65.33	59.73
Heat from tire combustion			7.263	6.64
<i>Total</i>	<i>51.241</i>		<i>109.384</i>	<i>100</i>
Output	Mass flow rate [kg/s]	Average temperature [K]	Enthalpy [MW]	
Exit gas losses	37.1	1228	50.1	45.37
Clinker discharge	13.691	1740	28.383	25.69
Fuel ash discharge	0.401		0.600	0.54
Tire ash discharge	0.01	1210	0.025	0.02
Heat absorbed by clinkerization			22.943	20.77
Shell heat losses			7.205	6.52
Heat of unburned carbon			1.141	1.03
Heat of water evaporation			0.068	0.06
<i>Total</i>	<i>51.202</i>		<i>110.466</i>	<i>100</i>
Imbalance	<i>0.039</i>		<i>-1.082</i>	

Table 4-9: Mass and energy balance: with 20% co-combustion of tire

Input	Mass flow rate [kg/s]	Average temperature [K]	Enthalpy [MW]	Percent [%]
Sensible heat in air	27.8		28.0	25.59
Sensible heat in feed material	20.788	338	7.645	6.99
Sensible heat in fuel	2.173	333	0.908	0.83
Sensible heat in tire	0.415	300	0.249	0.23
Heat form fuel combustion			58.071	53.08
Heat from tire combustion			14.525	13.28
<i>Total</i>	<i>51.176</i>		<i>109.397</i>	<i>100</i>
Output	Mass flow rate [kg/s]	Average temperature [K]	Enthalpy [MW]	

Exit gas losses	37.1	1239	50.7	45.82
Clinker discharge	13.691	1740	28.383	25.65
Fuel ash discharge	0.351		0.537	0.49
Tire ash discharge	0.021	1095	0.045	0.04
Heat absorbed by clinkerization			22.943	20.73
Shell heat losses			7.200	6.51
Heat of unburned carbon			0.79	0.71
Heat of water evaporation			0.061	0.05
<i>Total</i>	<i>51.163</i>		<i>110.66</i>	<i>100</i>
Imbalance	<i>0.13</i>		<i>-1.263</i>	

4.8.2. Clinker Temperature and Composition

Comparing Figure 4-2 to Figure 4-4, it is observed that co-combustion of tires has no effect on the clinker formation process. This conclusion is based on the fact that the species evolutions in the bed are the same for all three cases. This is the key to tire utilization in cement kilns because the main function of a cement kiln is clinker production. As long as the clinker composition is maintained, the co-combustion of tire is assumed to be successful. Another important factor is the production rate, which may slightly decrease due to tire firing [40]; based on this report, the reduction in the kiln production rate is because of the increased dust pickup and the loss in the stability of the kiln. However, possible production rates that can occur with tire injection were not considered and the production rate for all cases was assumed to be unchanging.

In the area close to the tire injector ($x=50$ m), a slight increase in the gas temperature is observed (see Figure 4-3 and Figure 4-4). This is mainly because the tire devolatilization process is exothermic and some heat will be released to the gas in its vicinity. The higher the tire feed rate, the bigger this increase will be. A quantitative discussion on all the important parameters is presented later on.

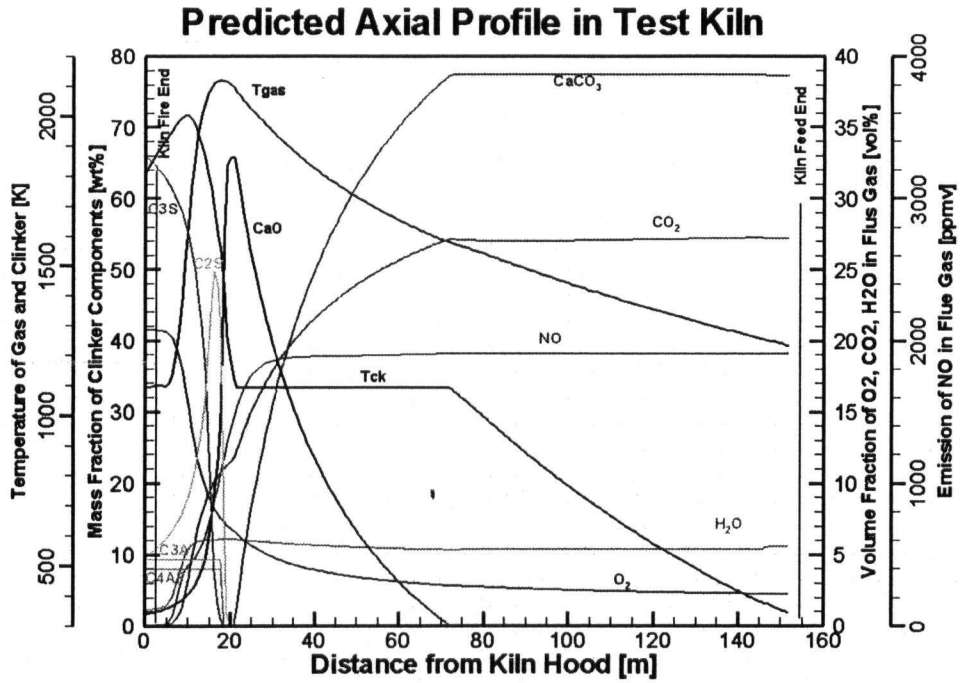


Figure 4-2: Axial profile of species: without co-combustion of tire

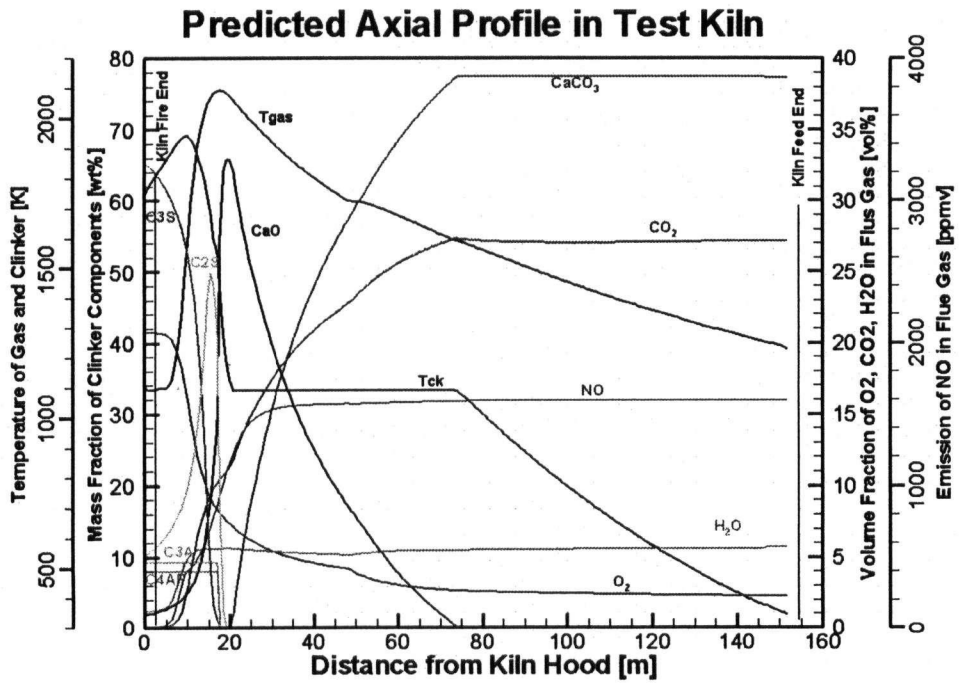


Figure 4-3: Axial profile of species: with 10% co-combustion of tire

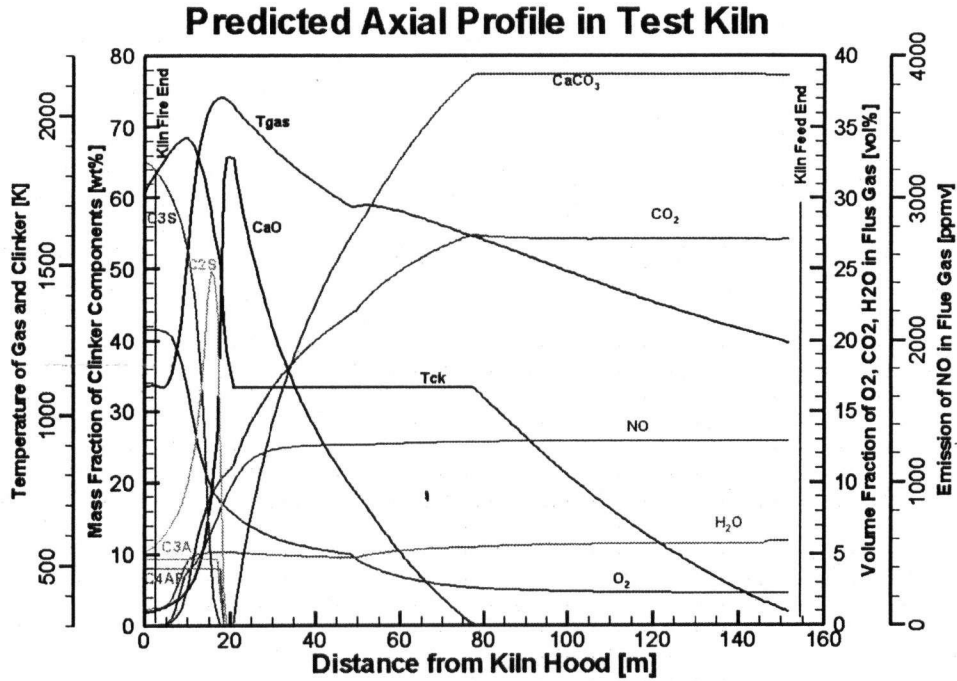


Figure 4-4: Axial profile of species: with 20% co-combustion of tire

4.8.3. Gas Temperature Distribution

The contour plots for the gas temperature for all three cases were similar but not completely the same; as tire was burned in the middle of the kiln, there was a slight decrease in its temperature in the flame area (see Table 4-10) and a slight increase in the area close to the surface of the tire. According to Table 4-10, the more co-combustion of tire, the bigger the reduction in the peak temperature will be. However, this difference was not noticeable in the contour plots of temperature of these three cases; therefore, only one of the contour plots (that of without tire combustion) is depicted as in Figure 4-5.

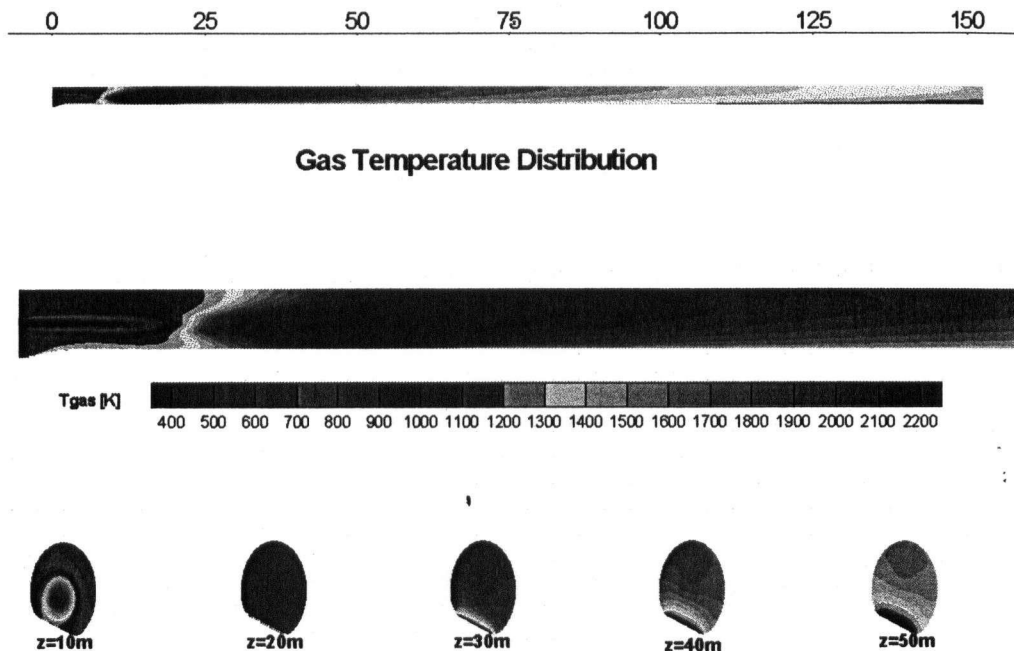


Figure 4-5: Gas temperature distribution

4.8.4. Refractory Temperature Distribution

It was also observed that the mid-kiln firing of tires had no effect on refractory temperature distribution and therefore only the case without any co-combustion of tire is represented in Figure 4-6.

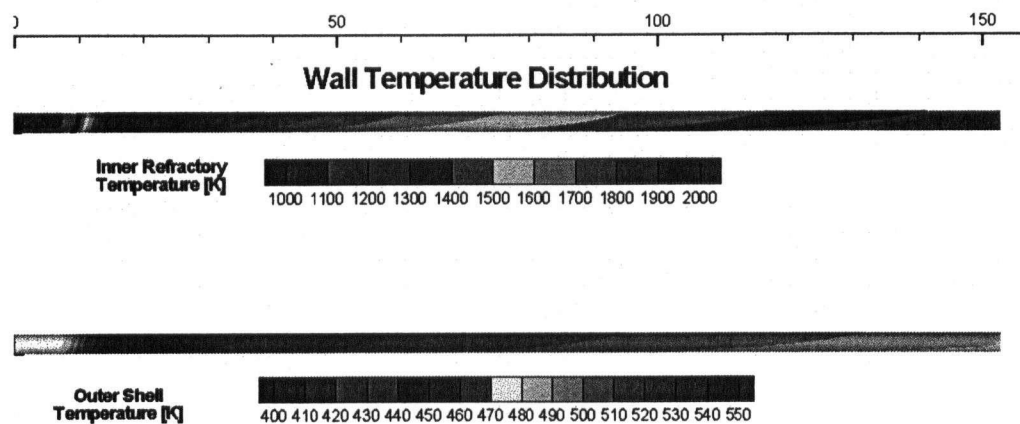


Figure 4-6: Refractory temperature distribution

4.8.5. NO_x Emissions

Any change in the gas temperature, specifically for temperatures beyond 1800 K, has a direct impact on NO formation rate [41]. As mentioned earlier, one of the desired impacts of the mid-kiln firing of tires is the reduction in the flame temperature and consequently a decrease in NO_x concentrations throughout the whole kiln. More specifically, for the case without tire combustion (Figure 4-7a), NO concentration reaches a peak around 2500 ppm in the flame area and goes down to 1908 ppm at the exit. For the case with 10% tire (Figure 4-7.b), the maximum NO concentration goes down to around 1900 ppm in the flame area and reduces to 1591 ppm (17% reduction) at the exit. Similarly, with 20% co-combustion of tire, the peak and the exit concentrations are around 1600 and 1283 ppm (33% decrease), respectively.

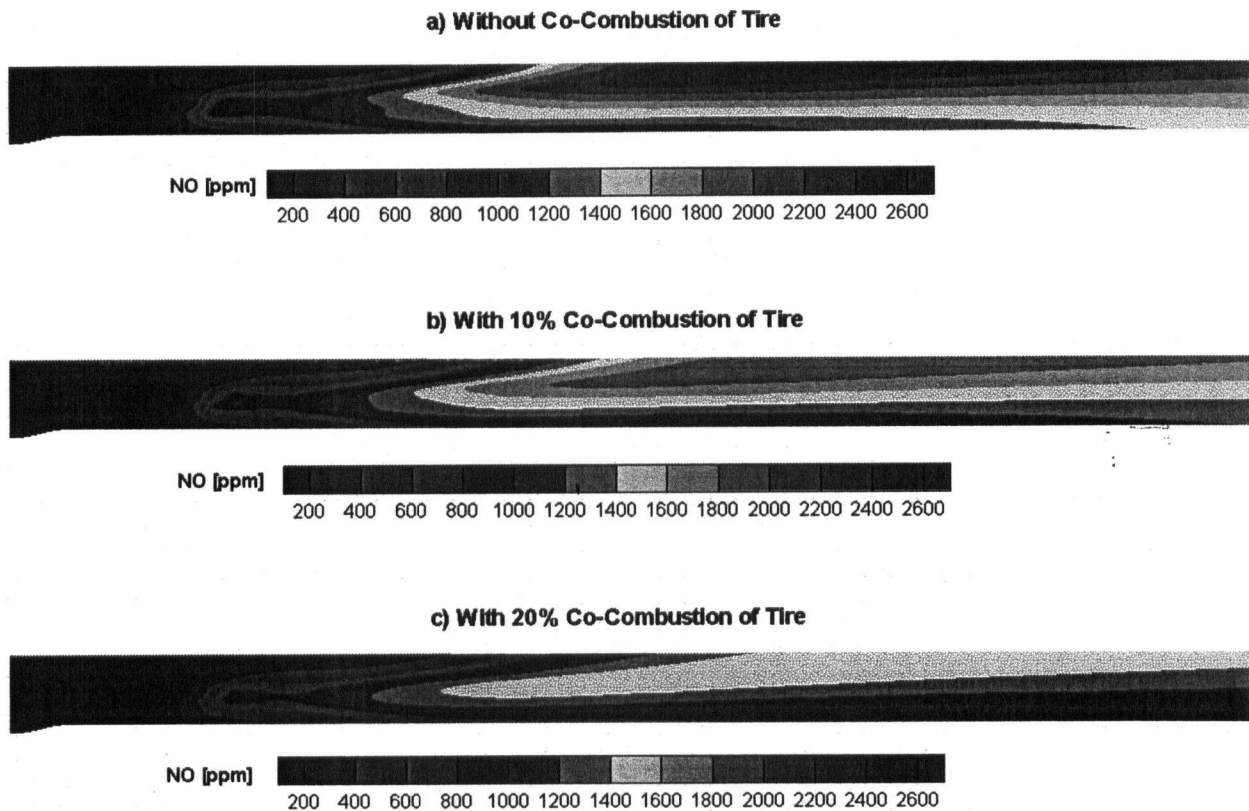


Figure 4-7: NO concentration distribution

4.8.6. Overall Impact of Mid-Kiln Firing of Tires on Kiln Performance

Table 4-10 contains a summary of all the important parameters that are used to analyze the overall impact of tire utilization on test kiln.

As tire is burned, the maximum gas average-temperature drops in the flame area. It has decreases from 2118 K to 2091 and 2059, respectively, for 10% and 20% co-combustion of tire. This finally contributes to a reduction in NO concentrations at the kiln exit (17% and 33%, for 10% and 20% tire

combustion). The maximum clinker temperature and the clinker temperature at the kiln exit decrease as the maximum gas temperature reduces (see Table 4-10).

Because of tire combustion, the gas average-temperature at the kiln exit increases. The gas temperature at the kiln exit directly indicates the exit gas losses. The higher this temperature, the more these losses will be. Therefore, this parameter is important and should be investigated to make sure that the heat losses are still within a reasonable range. More specifically, the energy distribution within the kiln should be such that all the necessary processes and reactions are successfully achieved and not too much heat is lost via flue gasses. Referring to the energy balance tables (Table 4-7 to Table 4-9), it is observed that the enthalpy lost through the exit gas is slightly increased (for the worst case, it has increased from 50.1 MW to 50.7). On the other hand, since the clinker composition at the exit for all three cases was the same, it is concluded that the additional heat loss via flue gases is acceptable. More detailed discussion on this issue is presented in the sensitivity analysis section.

Table 4-10: Summary of important parameters with tire injection at x=50 m and different tire flow rates

	Kiln without co-combustion of tire	Kiln with 10% co-combustion of tire	Kiln with 20% co-combustion of tire
Gas average temperature at kiln exit [K]	1225	1228	1239
Maximum gas average temperature [K]	2118	2091	2059
NO concentration at kiln exit [ppm]	1908	1591	1283
Relative NO reduction [%]	-	17	33
Maximum clinker average temperature [K]	2008	1939	1925
Clinker average temperature at kiln exit [K]	1811	1740	1740

4.8.7. Sensitivity Analysis

So far we have learned that co-combustion of tires (up to 20%) significantly reduces NO_x emissions. It was also shown that mid-kiln firing (up to 20%) of tires had no negative impact on clinker quality. It was highlighted that the total enthalpy carried out by the exit flue gasses is an important parameter and should be investigated to ensure that not too much heat is lost via exit gases. This parameter is tightly coupled with the bed processes. If the total enthalpy of exit flue gasses, for example, increases, the total heat absorbed by the bed reduces. An excessive reduction results in clinker with poor composition. So not all mid-kiln firing of tires can be successful and each kiln has proper rates, for a specific injection point. The whole process is successful as long as NO_x emissions at the kiln exit are reduced, while clinker quality at the exit is still acceptable. There are mainly two parameters that can be investigated: the tire feed rate and the location of the tire injector.

4.8.7.1. *Tire Feed Rate*

So far it has been shown that for test kiln co-combustion of tires up to 20% is successful and NO_x concentration at the kiln exit reduces without any negative impact on the product quality. More reduction might be achieved if more tires are burned. So limits of the tire flow rate have to be explored. Despite the existence of practical barriers, such as opening size and the available time for throwing tires in the kiln, a case with higher flow rates in order to improve our understanding regarding this issue was simulated.

We simulated a rather extreme case with 50% co-combustion where tires were still injected at x=50 m. We found that the gas average temperature in the flame area was reduced and the NO_x emission at the kiln exit was reduced as well, a 70% reduction was observed. However, since not enough heat was available in the flame area, the clinker temperature was significantly reduced (see Figure 4-8)

and clinker composition at the kiln exit was poor and not acceptable. The fact that the total heat lost by the exit flue gasses was increased from 50.1 MW to 54.3 MW confirms that more heat should have been absorbed by the bed.

Because of the high tire flow rates, an excessive amount of heat was released in the tire burning area, and as a result the gas temperature in that area was even higher than that of the flame area (see Figure 4-9). Accordingly, more NO_x was formed in that area than in the flame area (see Figure 4-10); however, the NO concentration in that area was still low and NO concentration at the kiln exit was low too.

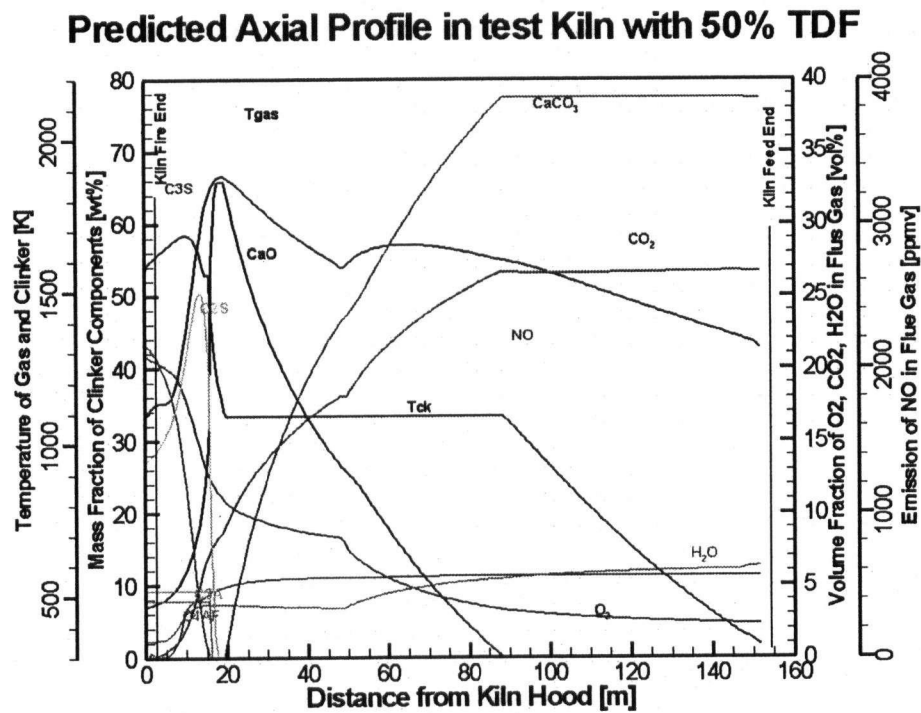


Figure 4-8: Axial profile of species: with 50% co-combustion of tire

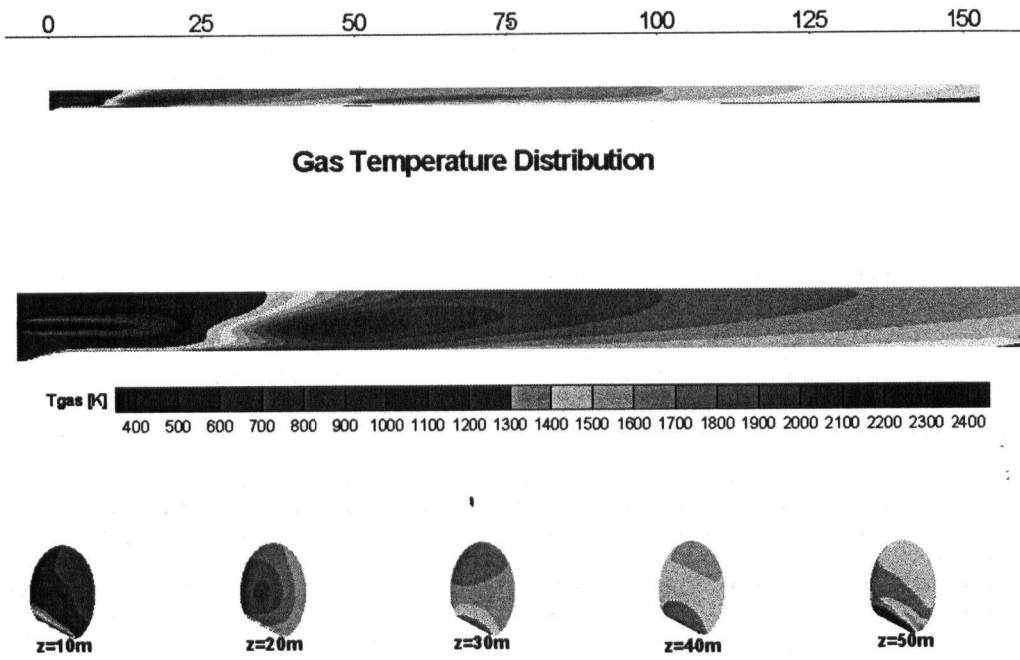


Figure 4-9: Gas temperature distribution: with 50% co-combustion of tire

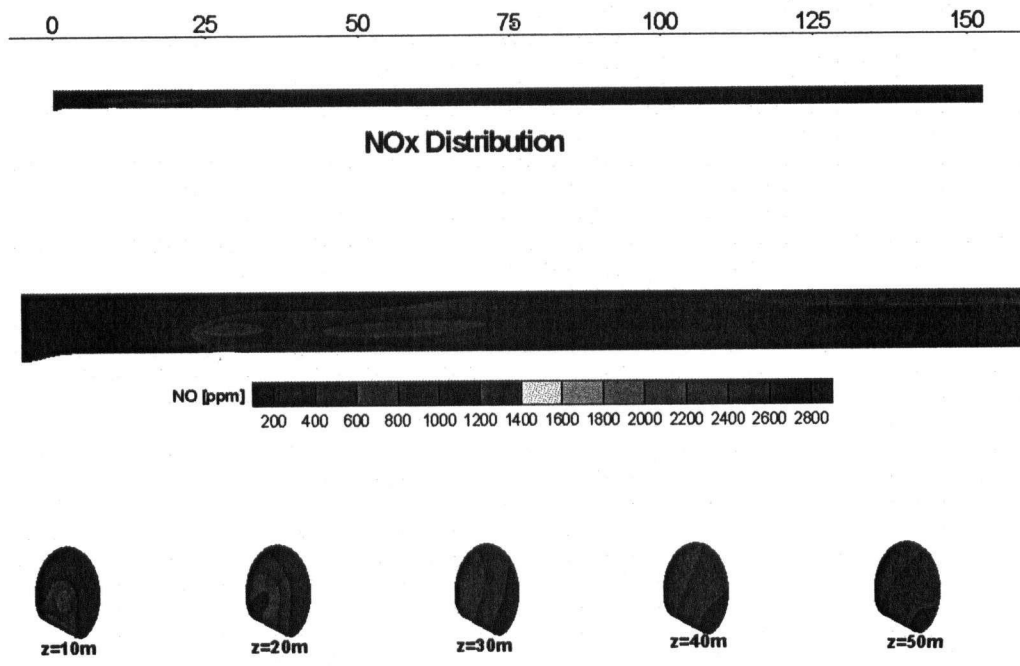


Figure 4-10: NO distribution: with 50% co-combustion of tire

4.8.7.2. *Location of Tire Injector*

In order to optimize the location of the injection point, the thermal profile and the production rate (provided that the clinker quality is satisfactory) should be simulated as a function of injector location. The injection point should be such that the heat losses via flue gasses are minimized while complete combustion of tires can be ensured.

In order to investigate the impact of the injection point, the test kiln with three new injection points, $x=30$, 40, and 80 m, was simulated. For all these simulations, the tire rate was fixed at 20%. Table 4-11 contains a summary of important parameters for these three cases. The original case (with tire injector at $x=50$ m) is included in this table as well.

As the tire injector is placed closer to the flame area, less heat is lost via the flue gasses at the exit. This is actually good, and means that considering a constant heat loss through the wall, more heat is absorbed by the bed. The more heat absorbed by the bed, the higher its temperature will be (see Table 4-11). This guarantees that, if a clinker with an acceptable composition has been produced by throwing tire at $x=50$, for cases with injection points less than 50 (here, $x=30$ and 40 m) acceptable product quality will be obtained as well. This was confirmed by comparing the axial concentration profiles of clinker components of these cases with the original case. However, for the case of $x=80$ m, the heat lost by the flue gasses was too high (see the gas temperature at the exit) and not enough heat was absorbed by the bed. Therefore, the product quality was poor (see Figure 4-11).

For the first three cases ($x=30, 40,$ and 50 m), the maximum gas temperature is almost the same, and as a result, NO concentration at the kiln exit was the same. On the other hand, for the last case ($x=80$), the maximum flame temperature was low and NO concentrations at the exit were significantly reduced.

Based on the above observation, one can conclude that varying the injection point from 50 to 30 m would result in acceptable clinker quality and unchanged NO emissions while putting the injection point somewhere farther downstream, e.g. at a distance of 80 m, would result in a poor quality product and reduced NO emissions.

Table 4-11: Summary of important parameters with 20% co-combustion of tire and different tire injection points

	Injection point x=30	Injection point x=40	Injection point x=50	Injection point x=80
Tire combustion finished at $x = \dots$ [m]	2.7	4.2	6.5	10.9
Gas average temperature at kiln exit [K]	1232	1235	1239	1278
Maximum gas average temperature [K]	2058	2059	2059	2047
NO concentration at kiln exit [ppm]	1281	1280	1283	1217
Maximum clinker average temperature [K]	1912	1921	1925	1801
Clinker average temperature at kiln exit [K]	1756	1751	1740	1591

Predicted Axial Profile in test kiln

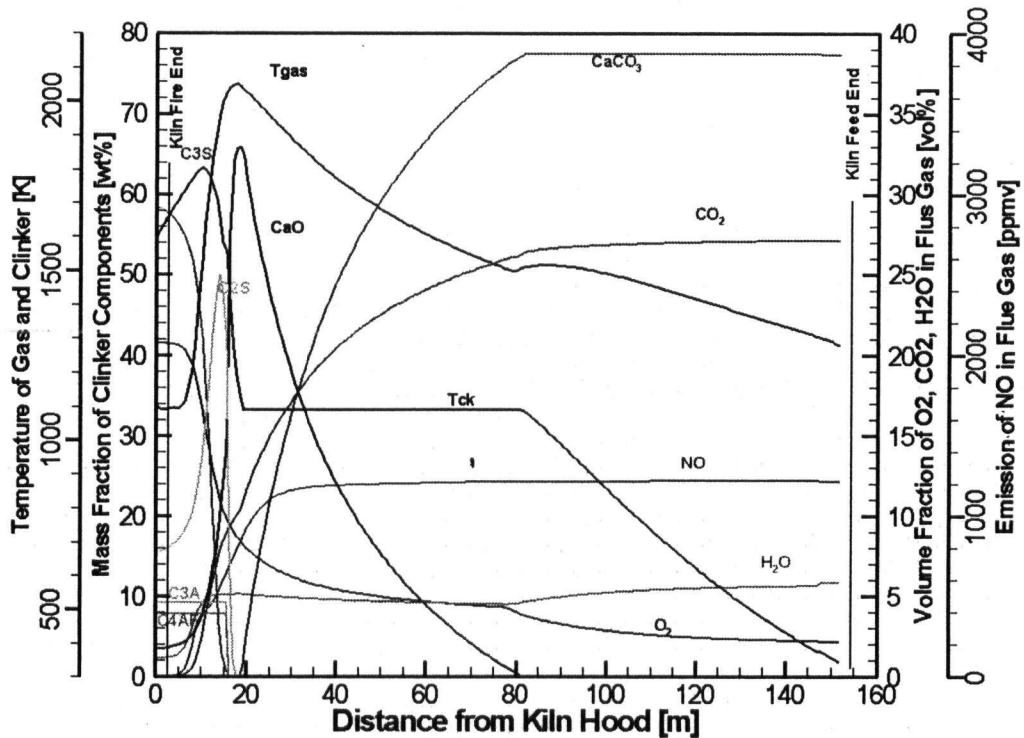


Figure 4-11: Axial profile of species: 20% co-combustion of tire with tire injection point $x=80$ m

4.8.7.3. Grid Sensitivity Analysis

The original grid was compared against two finer grids, one 50% finer and the other one 100% finer. For this comparison, the test kiln with the same geometry and boundary conditions without any tire combustion was simulated. Referring to the trend in Figure 4-12 and the data in Table 4-12, as the nodal points increase, the gas temperature profiles tend to become the same and it is concluded that the grid convergence is achieved. Based on the results of this simulation it seems that the second grid should be chosen for our simulations; however, due to having significantly smaller computational times and showing a better convergence behavior especially on enthalpy imbalance, the original grid (the coarsest one in Table 4-12) was preferred to the other two.

Table 4-12: Summary of results for three different grids

	Case 1	Case 2	Case 2
Grid points in r, θ and z direction	23 x 37 x 213	29 x 37 x 249	29 x 49 x 249
Number of nodes	181263	267177	353829
Nodes ratio (N_i/N_1)	1.0	~1.5	~2.0
Maximum local temperature of the gas[K]	2190	2163	2159
Maximum axial temperature of the gas [K]	2064	2042	2033
Enthalpy imbalance	0.80e+04	-.19e+06	-.10e+06
Mass imbalance	-.86e-04	0.27e-04	0.14e-04

Grid Sensitivity Analysis

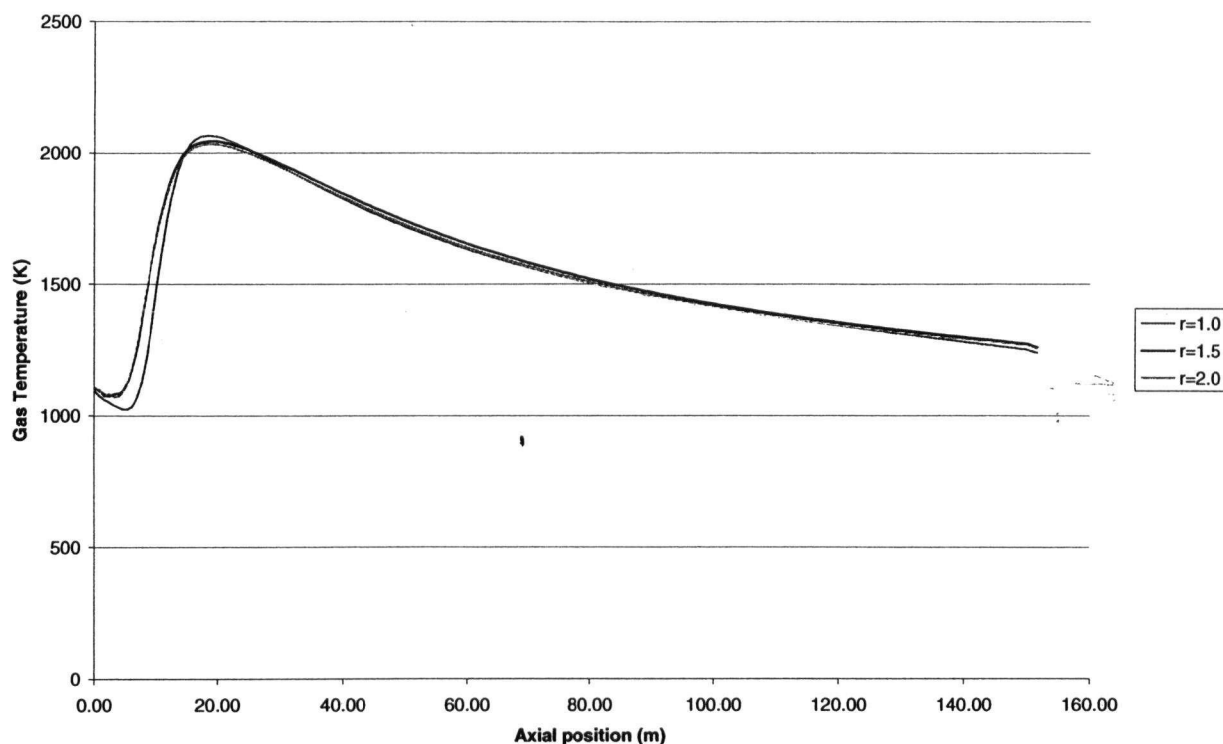


Figure 4-12: Axial gas temperature profile for three different grids

4.9. SUMMARY AND CONCLUSIONS

A one-dimensional mathematical model for tire combustion was developed and implemented in an existing code. With the aid of this code, three different cases (one without tire combustion and the other two with co-combustion of tire, 10% and 20% respectively) were simulated and analyzed through a series of contour plots and tables.

The primary results of these simulations revealed that the co-combustion of tire, up to 20% at $x=50$ m for the text kiln, has no negative impact on the product quality and causes significant reductions in

NO_x emissions at the exit (up to 33% for the case with 20% co-combustion). Finally, it is concluded that for this kiln co-combustion of tires up to 20% at $x=50$ is successfully utilized. Therefore, tire combustion can contribute to a cement kiln with less pollutant and less operational costs.

In order to explore the limits and possibilities of tire combustion, in addition to above operational conditions, test kiln with different tire flow rates and injector locations was simulated. We particularly investigated their impact on two important parameters: the clinker composition and NO_x emissions at the exit. The summary of our observations along with conclusions is presented in the following:

For studying the impact of tire flow rate, we increased the co-combustion rate up to 50%. The simulation results revealed that NO_x emissions were significantly reduced (70%), but the clinker composition was not acceptable. Based on this observation, we concluded that the high tire flow rates, in addition to having practical limitations, may also impair the clinker quality. Therefore, an upper limit should be prescribed for the amount of co-combustion in the middle of the kiln. Based on our analysis, we recommend 20% co-combustion of tires.

On other hand, the test kiln with three new tire injection points was simulated. The results showed that whenever the tire injection point was less than 50 m, the clinker composition was still acceptable and NO emissions were almost the same. This means that for this kiln, there is actually more than one suitable point for injecting tires, although some of these points may not be practically accessible (they may be in the burning zone). We also simulated a test case with tire injector at $x=80$ m. For this case, because of injecting the tire in an inappropriate area, too much heat was lost through the exit flue gasses and the clinker did not absorb adequate heat; therefore, its quality was poor. It also did not

have that much of an effect on NO emissions at the exit. Therefore, we concluded that placing the tire injector somewhere far from the burner can result in a kiln operation with unacceptable product. We recommend a tire injector at around $x=50$ m.

Chapter 5. SUMMARY, CONCLUSIONS, AND RECOMMENDATIONS

A fully-coupled mathematical model, including the hot flow, the bed, and the wall of rotary kilns, was developed. With the aid of this model, full-scale industrial cement kilns under steady-state and realistic operational conditions were simulated. The results were analyzed and validated against limited measurement data. In addition, a 1-D model for tire combustion was added to the existing code. This new code was used for modeling cement rotary kilns with combustion of full scrap tires in the middle of them.

The visualized solutions such as the temperature distribution and species concentrations in the gas flow-field, the temperature distribution within the wall, and the material and temperature evolution in the bed were analyzed and compared. The results indicated that significant progress has been made to create a predictive tool for cement rotary kilns. In addition, with the aid of the developed model, a better understanding of cement kilns with various operational conditions, kiln geometries, and burner designs can be obtained. The model can be used to diagnose the operational problems associated with this complex equipment.

A brief summary of the present work, some concluding remarks, and recommendations for future work, are given as follows.

Summary and Contributions:

- An existing CFD code, which has the capability of simulating rotary furnaces including the hot gas and the wall, was used for further development.

- A 1-D model for the transport phenomena in the bed, including the species and thermal evolution, was developed. This model included ten elements and five chemical reactions between them.
- For simulating cement rotary kilns, the bed model was implemented into the existing CFD code; coupling was achieved by implementing the heat and mass transfer between the gaseous phase and the bed.
- A new 1-D model for combustion of full tires in the middle of rotary kilns was developed and implemented in a cement kiln model.
- The implementation of tire combustion model was achieved by including the mass and heat transfer between different sub-models. With the aid of this code, cement kilns with different tire combustion conditions (different rates and different injector locations) were simulated and analyzed.
- The tire combustion model consisted of two sub-models: devolatilization and char combustion. Attempts were made to include all the important physical and chemical phenomena associated with the combustion of tire in this model. For devolatilization, the external heat transfer and chemical reaction kinetics were assumed to be dominant. Char combustion was assumed to be controlled by oxygen availability.
- A mathematical model for mid-kiln firing of tires was developed. The newly developed model was applied to a test cement kiln with different tire combustion rates and different locations of tire injector and the results of the simulations were analyzed. These simulations were performed to investigate and explore the limitations and feasibility of tire combustion in cement rotary kilns.
- The product quality and NO_x concentration at the kiln exit were chosen as the main performance indicators of co-combustion of tires in the middle of cement kilns.

- It was shown that 20% co-combustion of tire can reduce the NO_x emissions of test kiln substantially without any negative impact on its product quality.

Conclusions:

- Analysis and investigation of simulation results revealed that a useful tool in advancing the understanding of cement kilns has been developed. The developed model can be used to address operational problems and improve kiln design.
- The simulation result indicated that the clinker formation process is very sensitive to the heat transfer to the bed, and a good estimate of the bed angle is a key step for gaining high quality products.
- The results indicated that almost half of a wet process kiln is dedicated to the preheating of the raw material. This means that by introducing a drying system before the kiln system, the kiln length can be significantly reduced. That proves again the usefulness of the modern practice of using preheaters.
- A heat balance of the kiln indicated that for a wet process kiln, the combustion of the fuel accounts for 70% of the inlet heat and the rest (30%) is accounted for by the sensible heat of the air, the raw material, and the fuel. About 50% of the total heat is lost by flue gases; the bed material absorbs 40-45% of this heat and the rest of it (5-10%) is lost through the refractory wall to the ambient air. The fact that almost half of the kiln energy is lost through the flue gasses is one the major reasons for low thermal efficiency of cement kilns.
- Tire combustion simulations have shown that tires were completely burned. However, for certain firing rates and axial locations the product quality deteriorated. The model can be used to establish the desired firing rate and axial location for tire burning.

- For the cases without any negative impact on the product quality, a significant reduction in NO_x emissions at the exit was observed. This, in fact, was one of the desired impacts from tire combustion.
- Based on the simulation results, it was concluded that the best performance can be achieved when 20% of the primary fuel is replaced with tires somewhere in the middle of the calcination zone.
- It was concluded that successful utilization of tires, as expected, can save energy and money, and lower the emissions of pollutants such as NO_x . It is also likely to expand refractory lifetime because of the lower gas temperature especially in the burner area.
- By burning tires with different rates and different axial location, it was confirmed that a certain flame temperature is required for the clinker formation process. Low flame temperatures or inappropriate energy distributions (by burning too much tire inside the kiln) can result in poor product quality. Therefore, the energy distribution within the system has to be chosen carefully. This is one of the main reasons for limiting the amount of tire co-combustion.

Recommendations:

- Including the heat transfer between the wall and the bed of material would lead to more accurate model predictions
- Modeling the dust circulation in the system would contribute to a more complete model and is expected to bring the gas temperature closer to plant measurement data.
- Considering the rotational term in the wall model would result in better temperature predictions.

- Improving the bed model, for example expanding the computational domain to three dimensions could be pursued. However, this would increase the complexity of the model and computational time. Also the bed physics is very complex and not well understood. Therefore, it is possible that the increase in complexity might not result in commensurate model improvement.
- Validating the simulation results for cases with tire combustion inside the kiln against some measurement data would be very useful.

REFERENCES

- [1] Choate, W.T., 2003, "Energy and Emission Reduction Opportunities for the Cement Industry," US Department of Energy, Energy Efficiency and Renewable Energy.
- [2] Mike Georgallis, 2004, "Mathematical Modelling of Lime Kilns," The University of British Columbia.
- [3] Locher, G., 2002, "Mathematical Models for the Cement Clinker Burning Process- Part 1: Reactions and Unit Operations," ZKG International, **55**pp. 29-38.
- [4] Peray, K.E., 1979, "Cement Manufacturer's Handbook," Chemical Publishing Co. Inc.
- [5] Brimacombe, J. K., and Watkinson, A. P., 1978, "Heat Transfer in a Direct Fired Rotary Kiln-I. Pilot Plant and Experimentation," Met. Trans. B, **9B**pp. 201-208.
- [6] Watkinson, A. P., and Brimacombe, J. K., 1978, "Heat Transfer in a Direct Fired Rotary Kiln-II. Heat Flow Results and their Interpretation," Met. Trans. B, **9B**pp. 209-219.
- [7] Gorog, J. P., Adams, T. N., and Brimacombe, J. K., 1983, "Heat Transfer from Flames in a Rotary Kiln," Met. Trans. B, **14B**pp. 411-424.
- [8] Boateng, A. A., and Barr, P. V., 1996/7, "A Thermal Model for the Rotary Kiln Including Heat Transfer within the Bed," International Journal of Heat and Mass Transfer, **39**(10) pp. 2131-2143.
- [9] Mellmann, J., 2001/8/28, "The Transverse Motion of Solids in Rotating Cylinders--Forms of Motion and Transition Behaviour," Powder Technology, **118**(3) pp. 251-270.

- [10] Ding, Y. L., Seville, J. P. K., and Forster, R., 2001/3, "Solids Motion in Rolling Mode Rotating Drums Operated at Low to Medium Rotational Speeds," *Chemical Engineering Science*, **56**(5) pp. 1769-1780.
- [11] Ding, Y. L., Forster, R., and Seville, J. P. K., 2002/4, "Segregation of Granular Flow in the Transverse Plane of a Rolling Mode Rotating Drum," *International Journal of Multiphase Flow*, **28**(4) pp. 635-663.
- [12] Van Puyvelde, D. R., 2006/7, "Comparison of Discrete Elemental Modelling to Experimental Data Regarding Mixing of Solids in the Transverse Direction of a Rotating Kiln", *Chemical Engineering Science*, **61**(13) pp. 4462-4465.
- [13] Martins, M. A., Oliveira, L. S., and Franca, A. S., 2001/9, "Modeling and Simulation of Petroleum Coke Calcination in Rotary Kilns," *Fuel*, **80**(11) pp. 1611-1622.
- [14] Spang, H. A., 1972, "A Dynamic Model of a Cement Kiln," *Automatica*, **8**pp. 309.
- [15] Marias, F., 2003/6/15, "A Model of a Rotary Kiln Incinerator Including Processes Occurring within the Solid and the Gaseous Phases," *Computers & Chemical Engineering*, **27**(6) pp. 813-825.
- [16] R.T. Bui, G. Simard, A. Charette, Y. Kocaefe, and J. Perron, 1995, "Mathematical Modeling of the Rotary Coke Calcining Kiln," *Canadian Journal of Chemical Engineering*, **73**pp. 534-544.
- [17] Mastorakos, E., Massias, A., and Tsakiroglou, C. D., 1999/1/1, "CFD Predictions for Cement Kilns Including Flame Modelling, Heat Transfer and Clinker Chemistry," *Applied Mathematical Modelling*, **23**(1) pp. 55-76.

- [18] Nowak, Z. P. and Salcudean, M., 1996, "Turbulent Flow Calculations by the Nonlinear Multi-Grid Method," *Journal of Applied Mathematics and Mechanics*, **76**pp. 463.
- [19] Yuan J., Stropky D., Bibeau E.L., 2003, "Using Process Modelling to Improve Lime Kiln Operations," *Pulp and Paper Canada*, **104**(11) pp. 41-44.
- [20] Patankar, S.V., 1980, "Numerical Heat Transfer and Fluid Flow," Hemisphere Publishing Corp.
- [21] He, P., Salcudean, M., and Gartshore, I. S., 1996/5, "Multigrid Calculation of Fluid Flows in Complex 3D Geometries using Curvilinear Grids," *Computers & Fluids*, **25**(4) pp. 395-419.
- [22] HE, P., 1995, "Numerical Simulation of Film Cooling of a Turbine Blade using Block-Structured Curvilinear Grids," University of British Columbia.
- [23] B.E. Launder and D.B. Spalding, 1974, "The Numerical Computation of Turbulent Flows," *Computer Methods in Applied Mechanics and Engineering*, **3**pp. 269-289.
- [24] Holman, J.P., 2002, "Heat transfer," McGraw-Hill, Boston.
- [25] Peray, K.E. and Waddell, J.J., 1972, "The Rotary Cement Kiln," Chemical Publishing Co., Inc., New York, pp. 194.
- [26] Bogue, R. H., 1929, "Calculation of the Compounds in Portland Cement," *Ind. Eng. Chem. Anal. Ed.*, **1**pp. 192-197.
- [27] de Marco Rodriguez, I., Laresgoiti, M. F., and Cabrero, M. A., 2001/8, "Pyrolysis of Scrap Tyres," *Fuel Processing Technology*, **72**(1) pp. 9-22.

- [28] Yamaguchi, E., 2000, "Waste Tire Recycling," **2006**(June/29) available from:
<http://www.p2pays.org/ref/11/10504/> .
- [29] Barlaz, M. A., Eleazer, I., William E., and Whittle, D. J., 1993/12, "Potential to use Waste Tires as Supplemental Fuel in Pulp and Paper Mill Boilers, Cement Kilns and in Road Pavement," *Waste Management & Research*, **11**(6) pp. 463-480.
- [30] Karell, M., 2000, "Regulation Impacts on Scrap Tire Combustion: Part II," **2006**(June/29), available from: http://www.pirnie.com/resources_pubs_air_feb00_3.html..
- [31] Stillwagon, M. A., and Wahlquist, C. J., 1999, "Building A Successful Tire-Derived Fuel Program," **2006**(June/29), available from:
http://cementamericas.com/mag/cement_building_successful_tirederived/.
- [32] Reisman, J. I., October 1997, "Air Emissions from Scrap Tire Combustion," **2006**(June/29) pp. 117, available from: http://www.epa.gov/ttn/catc/dir1/tire_eng.pdf.
- [33] Conesa, J. A., Font, R., and Fullana, A., 1998/10, "Kinetic Model for the Combustion of Tyre Wastes," *Fuel*, **77**(13) pp. 1469-1475.
- [34] Williams, P. T., Besler, S., and Taylor, D. T., 1990/12, "The Pyrolysis of Scrap Automotive Tyres: The Influence of Temperature and Heating Rate on Product Composition," *Fuel*, **69**(12) pp. 1474-1482.
- [35] Conesa, J. A., and Marcilla, A., 1996/8, "Kinetic Study of the Thermogravimetric Behavior of Different Rubbers," *Journal of Analytical and Applied Pyrolysis*, **37**(1) pp. 95-110.

- [36] Conesa, J. A., Font, R., and Marcilla, A., 1997/8, "Mass Spectrometry Validation of a Kinetic Model for the Thermal Decomposition of Tyre Wastes," *Journal of Analytical and Applied Pyrolysis*, **43**(1) pp. 83-96.
- [37] Leung, D. Y. C., and Wang, C. L., 1998/5, "Kinetic Study of Scrap Tyre Pyrolysis and Combustion," *Journal of Analytical and Applied Pyrolysis*, **45**(2) pp. 153-169.
- [38] Yang, J., Tanguy, P. A., and Roy, C., 1995/6, "Heat Transfer, Mass Transfer and Kinetics Study of the Vacuum Pyrolysis of a Large used Tire Particle," *Chemical Engineering Science*, **50**(12) pp. 1909-1922.
- [39] Larsen, M. B., Schultz, L., and Glarborg, P., 2006/0, "Devolatilization Characteristics of Large Particles of Tyre Rubber under Combustion Conditions," *Fuel*, **85**(10-11) pp. 1335-1345.
- [40] Ukrainetz, P. and Denizeau, P., 1995, "Mid-Kiln Injection of Tire-Derived Fuel (TDF) at the Lafarge Canada Inc. Cement Plant at St. Constant, Quebec".
- [41] Fluent Inc., 2003, "User's Guide Index," *Fluent Inc.*, Chap. 18.
- [42] Westenberg, A., 1971, *Combustion Science and Technology*, 4pp. 59-64.
- [43] Warnatz, J., 1991, "NO_x Formation in High Temperature Processes," *Proc. European Gas Conference*, Anonymous pp. 303-320.
- [44] Baulch, D. L. et al., 1992, "Evaluated Kinetic Data for Combustion Modelling," *Journal of Physical and Chemical Reference Data*, **21**(3) pp. 411-734.

[45] Flower, W. L., Hanson, R.K., and Kruger, C.H. In 15th Symp. (Int'l.) on Combustion, pp. 823.
The Combustion Institute, 1975.

[46] Baulch, D.L., Drysdall, D.D., and Horne, D.G., 1973, "Evaluated Kinetic Data for High
Temperature Reactions," Butterworth.

Appendix A. FORMATION OF THERMAL NO_x

The principal reactions governing the formation of thermal NO_x, known as the extended Zeldovich mechanism, are as follows:



Based on the above reactions, the formation rate of NO can be calculated [41]

$$\frac{d[NO]}{dt} = k_1[O][N_2] + k_2[N][O_2] + k_3[N][OH] - k_{-1}[N][NO] - k_{-2}[O][NO] - k_{-3}[H][NO] \quad (\text{A-4})$$

where all concentrations are in gmol/m³.

In order to calculate the formation rates of NO, the concentrations of N, N₂, O, H, and OH are required.

A.1. THE QUASI-STEADY ASSUMPTION FOR [N]

When sufficient oxygen is available, the rate of consumption of nitrogen atoms will be equal to the rate of its formation, and a quasi-steady state can be assumed. Therefore, the NO formation rate can be modified to [41]

$$\frac{d[NO]}{dt} = 2[O] \frac{\left(k_1[N_2] - \frac{k_{-1}k_{-2}[NO]^2}{k_2[O_2]} \right)}{\left(1 + \frac{k_{-1}[NO]}{k_2[O_2] + k_3[OH]} \right)} \quad (gmol / m^3 .s) \quad (A-5)$$

A.2. DETERMINING O RADICAL CONCENTRATION

There are three approaches used by FLUENT [41] to determine the concentration of oxygen radicals: the equilibrium approach, the partial equilibrium approach, and the predicted concentration approach.

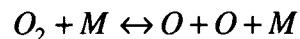
A.2.1. Method 1: Equilibrium Approach

The thermal NO_x formation rate is much slower than the main hydrocarbon oxidation rate; therefore, the formation process of thermal NO_x can often be decoupled from the main combustion reactions. Using this approach, according to Westenberg [42], the equilibrium oxygen atom concentration can be calculated from the following expression:

$$[O] = 3.97 \times 10^5 T^{-1/2} e^{(-31090/T)} [O_2]^{1/2} \quad (gmol / m^3) \quad (A-6)$$

A.2.2. Method 2: Partial Equilibrium Approach

The first method can be improved by accounting for third-body reactions as



Considering this reaction, the oxygen atom concentration can be calculated by the following expression [43]:

$$[O] = 36.64 T^{1/2} e^{(-27123/T)} [O_2]^{1/2} \quad (gmol / m^3) \quad (A-7)$$

This method generally leads to a higher oxygen atom concentration compared to Method 1.

A.2.3. Method 3: Predicted O Approach

When the concentration of the oxygen atom is calculated using an advanced chemistry model, [O] can be taken simply from it.

A.3. DETERMINING OH RADICAL CONCENTRATION

There are three approaches used by FLUENT [41] to determine the OH radical concentration: exclusion of OH approach, the partial approach, and the predicted OH concentration approach.

A.3.1. Method 1: Exclusion of OH Approach

In this approach, it is assumed that the $k_2[O_2]_{eq} \gg k_3[OH]_{eq}$ and therefore the third reaction in the extended Zeldovich mechanism is neglected.

A.3.2. Method 2: Partial Equilibrium Approach

In this approach, the OH radicals are not ignored anymore and their concentration is calculated with the following expression [44]:

$$[OH] = 212.9T^{-0.57} e^{(-4595/T)} [O]^{1/2} [H_2O]^{1/2} \text{ (gmol/m}^3\text{)} \quad (\text{A-8})$$

A.3.3. Method 3: Predicted OH Approach

Similar to the predicted O approach, when the OH radical concentration is calculated using an advanced chemistry model, [OH] can be taken from the local OH mass fraction.

A.4. THERMAL NO_x REACTION RATES

The expressions for the rate coefficients for the extended Zeldovich mechanism based on the evaluation of Hanson and Salimian [45] and Baulch et al. [46] are summarized in the following table.

Table A-1: Rate data (m³/gmol.s) for NO kinetics

Rate constant	Reaction	Baulch <i>et al.</i>			Hanson and Salimian		
		A [m ³ gmol ⁻¹ s ⁻¹ K ^{-β}]	β	E/R [K]	A [m ³ gmol ⁻¹ s ⁻¹ K ^{-β}]	β	E/R [K]
k_1	$O + N_2 \rightarrow N + NO$	7.6E+7	0	38000	1.82E+8	0	38370
k_{-1}	$N + NO \rightarrow O + N_2$	1.6E+7	0		3.8E+7	0	425
k_2	$N + O_2 \rightarrow O + NO$	6.4E+3	1	3150	1.8E+4	1	4680
k_{-2}	$O + NO \rightarrow N + O_2$	1.5E+3	1	19500	3.8E+3	1	20820
k_3	$N + OH \rightarrow H + NO$	4.1E+7	0		7.1E+7	0	450
k_{-3}	$H + NO \rightarrow N + OH$	2.0E+8	0	23650	1.7E+8	0	24560

Note: reaction rate constants (k_i) are in the form $k = AT^\beta \exp(-E/RT)$.

A.5. SUMMARY

The thermal NO_x formation rate can be predicted by equation (A-5). The expressions for the rate coefficients for the extended Zeldovich mechanism are often selected based on the evaluation of Baulch *et al.* [46]. The O-atom concentration needed in equation (A-5) is often computed according to equation (A-6), the equilibrium assumption. With the exclusion of the OH approach, equation (A-5) will be simplified to:

$$\frac{d[NO]}{dt} = 2[O] \frac{(k_1 k_2 [O_2][N_2] - k_{-1} k_{-2} [NO]^2)}{(k_2 [O_2] + k_{-1} [NO])} \quad (\text{gmol} / \text{m}^3 \cdot \text{s}) \quad (\text{A-9})$$

Finally, the NO source term due to formation of thermal NO_x can be calculated

$$S_{th,NO} = M_{w,NO} \frac{d[NO]}{dt} \quad \text{kg l(m}^3 \cdot \text{s)} \quad (\text{A-10})$$

where $M_{w,NO}$ is the molecular weight of NO, and $\frac{d[NO]}{dt}$ is computed from equation (A-9).